FRACTURE TOUGHNESS OF RESIN BASED COMPOSITES

by

HEMAGUPTHA DHARMARAJ GOONETILLEKE

B.Sc.(Eng), The University of Sri Lanka, 1973

A THESIS SUBMITTED IN PARTIAL FULFILMENT OF

THE REQUIREMENTS FOR THE DEGREE OF

MASTER OF APPLIED SCIENCE

in

THE FACULTY OF GRADUATE STUDIES

Department of Metallurgical Engineering

We accept this thesis as conforming

to the required standard

THE UNIVERSITY OF BRITISH COLUMBIA

October 1982

Department of Metallurgical Engineering

The University of British Columbia
1956 Main Mall
Vancouver, Canada
V6T 1Y3

Date October 15, 1982.

ABSTRACT

A study has been made of several composite systems based on polyester resin matrix, investigating the influence of various parameters on their fracture behaviour. This included the effects of such variables as the specimen geometry, fibre and filler volume fractions and the particle size of heavy metal dispersions within the resin itself or the resin reinforced with glass fibres. Different methods of fabrication have been attempted and tests were carried out on each polyester particle and/or fibre dispersion combination in order to examine their fracture resistance.

In two phase composite systems, the powder dispersions showed less influence on the resulting fracture toughness than the fibre reinforcement. The toughness of three phase particle filled fibre reinforced composites were also primarily governed by the fibre reinforcement.

Mechanisms which may have contributed to the fracture behaviour of these composites have been considered. The formation of microcracks due to residual shrinkage stresses and the interactions of the crack front with dispersed particles may lead to increased fracture toughness in particle filled composites. The creation of new fracture surfaces which includes fibre debonding was found to be mainly responsible for the fracture behaviour of fibre reinforced composites. Although

these mechanisms have their individual contributions to the fracture toughness of three phase composites, the addition of particles at high volume fractions may have a detrimental effect on the toughening character of fibre reinforcement.

TABLE OF CONTENTS.

LIST OF FIGURES

LIST OF TABLES

ACKNOWLEDGEMENT

I wish to express my sincere gratitude to Professor E.Teghtsoonian for his useful advice and guidance throughout the course of this study.

My thanks are also due to Professor J.S.Nadeau for his helpful advice and encouragement.

I would also like to extend a personal note of thanks to Mr. Jim Hogan for his assistance in setting up the injection moulding unit.

Thanks are also extended to my fellow graduate students and faculty members in the Department of Metallurgical Engineering. The assistance of the technical staff of this department, in particular Mr. Roger C Bennett, is greatly appreciated.

I am also grateful to the Department of Metallurgical Engineering, University of British Columbia., for providing financial support in the form of a research assistantship.

I. INTRODUCTION

1.1 GENERAL BACKGROUND:-

Fibre reinforced composites have many advantages over the conventional materials. The high strength attainable in fine fibres of some materials provided the necessary technological background for early development of composite materials. Large numbers of these fibres are bonded together in suitable matrix materials to form useful structural materials. In addition to being useful in holding the fibres together the matrix protects them from corrosive environments and assists in transfering the stresses from the matrix to the fibre. Applications of these fibre reinforced materials, in particular the resin matrix composites, are very common in the pipeline and building industries as well as in air, ground and sea transportation industries.[1]

Rigid particulate fillers are also often added to matrix materials to increase stiffness and abrasion resistance as well as to reduce cost and shrinkage. The mechanical behaviour of the resulting composites have been studied by a number of researchers over the past 10 years.[2-6] This interest is due mainly to the increasing use of these materials in such diverse applications as furniture, high speed cutting/grinding

tools, high-temperature structural materials and in deep submergence vessels.[7-8] The concept of strengthening of a matrix by the introduction of particles of a less compliant phase is of very general application and used extensively in plastics to achieve an increase in strength and an increase in elastic modulus and wear resistance.

Interest has been shown recently in the use of three phase composites containing both fibres and particles together in suitable matrix materials. Particles of a dense material are often added to fibre reinforced matrices in order to control the weight distribution or increase the density and stiffness of the composite.

A classical application of this type of composites is in the multirim superflywheels designed for high specific inertial energy storage.[9] As suggested by Rabenhorst[10] a multirim composite flywheel capable of storing very large amounts of energy per unit of mass can be constructed by adding increasing amounts of a dense filler, such as lead powder, to the filament wound inner rings. A brief account of the development of this idea is given in Appendix A.

A large fraction of low cost filler (40% by weight) is sometimes used to reduce the overall cost of automotive type sheet moulding compounds which are premixtures of short length fibres and partly cured resins.[11] A widely used filler material for these compounds is calcium carbonate. A variety of other additives, comprising only a small volume fraction of the

composite, help control the chemical reaction, improve the face smoothness and fire resistance of many other reinforced polymers which are used for the manufacture of building materials.[1]

The mechanical properties of a composite may bear little relation to those of the components, even though the components retain their integrity within the composite. In order to appreciate the potential benefits to be gained from three phase composites, it is necessary to be aware of the resulting properties which account for their use in load-bearing applications. Despite the published results of analytical and experimental work on several commercial systems, investigating the effects of various components, three phase composites have received much less attention than other composite materials. There is clearly a need for further study of the influence of fillers and fibres on the mechanical behaviour of these materials, in particular the resin based composites. The present work is an attempt to develop such a composite containing a dense material, and help clarify the relative influence of filler and fibres on fracture behaviour of these composites.

In the present work, a study has been made of several composite systems based on polyester resin matrix, investigating the influence of various parameters on their fracture behaviour. This included the effects of such variables as the distribution, volume fraction and the particle size of

heavy metal dispersions within the resin itself or the resin reinforced with glass fibres. Various methods of fabrication have been attempted and tests were carried out on each polyester particle and/or fibre dispersion combination in order to examine their fracture resistance. The fracture toughness, which is considered to be one of the most characteristic properties that influence the behaviour of these brittle composite systems in service, was determined.

1.2 PREVIOUS WORK:-

It has long been recognized that composite materials possess many attractive properties which make them very promising in a large number of present-day applications. Lighter but much stronger components for aircraft, automobiles, buildings, pipe lines and machinery are widely produced nowadays with fibre reinforced composite materials. These materials vary significantly in terms of their structure and the properties derived through them. With the development of type E glass fibres, the interest in modern resin matrix composites has increased rapidly over the past 40 years and significant progress has been made in this area of composite technology. Plastics, being low in density,[16] appear to be one of the useful matrix materials suitable for lightweight composites. The incorporation of reinforcing materials such as

particles and/or fibres of a different phase can enhance the resistance of these materials to crack propagation. In the following sections, a review of the work done on these materials is presented with reference to many other brittle systems of similar kind. Two phase systems containing either particles or the fibres in a continuous brittle matrix, and three phase systems in which both the particles and fibres are incorporated together are discussed separately.

1.2.1 Particle Reinforced Composites:-

Many publications have appeared during the past few years, on the effect of particulate fillers on the mechanical properties of brittle materials.[2-8] The addition of particles very often enhances the mechanical properties, in particular the resistance to crack propagation, strength and modulus. Table I lists typical mechanical properties of two matrix materials and their properties after the addition of fine particles of another material.[17-19] The extent of the influence depends upon the particular composite system being considered and the nature of the dispersion, viz; the average particle size, interparticle spacing and the volume fraction, which in turn are inter-related through an equation given by Fullman[20]

$$d = \frac{2D(1-\phi)}{3\phi} \tag{1.1}$$

where,

d = average interparticle spacing

D = average particle size

ϕ = volume fraction of particles

Although this relationship holds true for any particulate system, the effects of these variables on the properties mentioned above depend primarily upon the particular composite system being considered.

Systems containing rigid particle dispersions in a glass matrix have been the object of special consideration as model systems to understand the fracture behaviour of particle filled composites. Fracture energies and critical stress intensity factor values have been determined experimentally for several model systems using standard specimen configurations. It has been shown[17] that the fracture energy, which is the amount of energy required at the moment of crack initiation to form a unit area of fracture surface, could be increased significantly by the addition of particles. This increase is shown to be dependent upon both the volume fraction and the average

Table I Mechanical Properties of Some Particulate Composite systems:-

Material	Fracture energy J/m^2	Strength (MPa)	Elastic Modulus (GPa)	Ref. No.
Glass(Matrix)	6.28	93.8	80.6	17,18
Glass+40 vol% 3.5 μm Al_2O_3 particles	12.80	167.5	144.0	
Si_3N_4(Matrix)	69.20	654.3	306.8	19
Si_3N_4+10 vol% 5.0 μm SiC particles	51.00	577.9	317.8	
Si_3N_4+40 vol% 5.0 μm SiC particles	18.60	390.3	352.3	
Si_3N_4+10 vol% 32.0 μm SiC particles	94.70	390.3	317.8	

particle size for a glass-Al_2O_3 system.[17] The effect of increasing the volume fraction or the particle size of Al_2O_3 powder is to increase the fracture energy. For another system containing nickel spheres in a glass matrix,[21-22] a marked increase in fracture energy has been

observed as the nickel volume fraction is increased.

Fractographic observation of the glass-Al_2O_3 samples indicated a difference in fracture surface topography for low and high volume fraction composites. At low volume fractions, steps associated with most of the particles, indicating interaction of the crack front with the particles, have been observed. These steps become less distinct at high volume fractions.

A concept of crack front interaction with the second phase dispersion, which is consistent with the fracture behaviour of these systems has been developed by Lange[23] and Evans.[24-25] As the crack front meets an array of particles present on the crack plane it bows out between each pair of particles increasing its total length before being driven through. The fractional increase in crack front length per unit crack extension was shown to increase with decreasing interparticle spacing, consistent with either an increase in volume fraction or a decrease in particle size (see Equation 1.1). This leads to an increase in fracture toughness, as additional energy is required to increase the length of the crack front. The fracture energy required to form a unit area of fracture surface can be expressed by a relationship of the form;[17]

$$\gamma = \gamma_0 + F(D)\,\frac{T}{d} \qquad (1.2)$$

where,

γ_0 = surface energy / unit area of fracture surface

T = critical line energy / unit length of the crack front

d = average distance between the particles

The crack front has a line energy which depends on the applied stress. The critical stress required to propagate the crack defines the critical value of line energy per unit length of the crack front. This value is constant for a given material, as it is given by the volume integral of the strain energy adjacent the crack front just before the atomic bonds are broken. An estimate for T in glass for example is given as 15 to 60 ergs/cm.[23]

F(D)[$0 \leq F(D) \leq 1$] is a dimensionless function dependent on the average particle size D, which reflects the increasing effectiveness of larger particles in pinning the crack front and increasing the fracture resistance. It is conceivable that for larger particles a greater amount of bowing should occur before the stress fields in front become large enough to cause the crack front to break through. Thus, the magnitude of F(D) increases with increasing particle size, contributing more resistance to crack propagation. More importantly, the above result suggests that the interparticle spacing is a more significant parameter than the volume fraction in fracture

toughness determination of a particulate composite. Supporting this phenomenon is the result of a three dimensional finite element analysis of spherical particle composites,[26] that shows the strong dependence of internal stress distribution of such materials on interparticle spacing.

In the original Griffith's theory of brittle fracture, the surface energy γ_0 is identified as the main energy sink term. Thus, an increase in total relative fracture surface area can also be expected to increase the fracture toughness. The presence of surface steps and surface roughness resulting from a particle dispersion increases the fracture surface area, and in turn, the value of γ_0 . It has been shown[17] that for the glass-Al_2O_3 system the magnitude of γ resulting from this mechanism is approximately 1.5 to 2.0 times the fracture energy of glass without a second-phase dispersion. Other mechanisms that might be responsible for the increased fracture toughness of this system have been excluded. These include the energy absorption by transparticle fracture of the dispersed phase and the contribution of the friction between parting fracture surfaces.

Similar conclusions have been made in the previously mentioned S-glass-Ni system. Fractographic observations have indicated a local resistance to crack motion that has changed the crack front configuration,

especially at low volume fractions. It has been suggested[21-22] that this impedance to crack motion was the major contribution to increased fracture toughness while a minor contribution could have resulted from surface roughness and surface step formation. However, as the nickel volume fraction increases a maximum in fracture energy is reached. It has been proposed that the local crack front interaction may not be effective in increasing the fracture toughness once this maximum is exceeded when the particles become too closely spaced within the matrix.

To date, published data on polymer composites show similar results and conclusions. Broutman and Sahu[27] have reported an increase in fracture energy with increasing volume fraction of glass particles in glass-sphere filled polymeric composites, up to a maximum at around 20% volume fraction of particles. These results are in parallel with measurements of work- to-break in uniaxial tensile tests reported by Lavengood et al[28] and Nicolais et al,[29-30] though in fracture toughness or notched impact tests a lesser enhancement of toughness by glass particles is expected. The results of a similar study on an epoxy-alumina trihydrate composite system by Lange & Radford[31] are also qualitatively consistent with this mechanism of crack interaction. As the volume fraction of the particle dispersion increases, a significant increase in fracture energy has been observed. When fracture energy values are plotted against the average interparticle spacing an

increase in fracture energy is observed with decreasing particle spacing. Prior to the occurrence of a maximum, the increase in fracture energy is found to be greater, the larger the particle size. The transition from a fracture surface containing many cleavage steps to a surface that appeared almost polycrystalline implies the continuous nature of crack propagation that may prevail at higher volume fractions, when crack pinning become unfeasible energetically.

In contrast to these observations, recent work carried out in this department by Godoy[32] on Al_2O_3 filled epoxy has shown that the fracture toughness (or the critical stress intensity factor) of these composites is independent of particle size. The results of three-point bend tests and wedge loading tests show that this is true irrespective of the specimen configuration employed. However, an increase in fracture toughness has been observed with increasing volume fraction of Al_2O_3 particles. Godoy maintains that this increase in fracture toughness is associated with increase in fracture surface area caused by surface roughness.

In contrast, a model of linear dependence of fracture energy on volume fraction has been suggested for fine grained ceramics by Wahi et al.[33] The fracture surfaces of fine grained Al_2O_3-TiC composite have not shown the characteristic wedge-shaped cleavage steps expected on

the basis of the crack pinning model. In fact, the assumptions that lead to the crack interaction model imply that the grain size of the matrix is small relative to the size of the pinning particles. In this composite the grain size of the Al_2O_3 matrix was comparable to the average particle size and little interaction of the crack front with the particles could be expected. Fractogrphic observations revealed that TiC particles mostly had a transparticle fracture. The average fracture energy γ of the composite can therefore be expected to lie between the fracture energies of the matrix and the particle, varying linearly with the fraction of the total fracture surface area occupied by the particles. The observed values of the fracture energy show a linearly increasing trend with increasing volume fraction. Experimentally measured elastic modulus E of this composite has also been found to vary linearly with the volume fraction of the particles. This, and the mathematical interdependence of K_{IC} , γ and E suggest that the magnitude of K_{IC}^2 is approximately represented by a linear function of the volume fraction. Again, the observed increase in K_{IC} has shown a very good agreement with this model of linear dependence of K_{IC}^2 on volume fraction.

This has also been the explanation for the fracture behaviour of a Si_3N_4-SiC system studied by Lange.[19] When the average particle size was close to the grain size, little, if any, interaction of the crack front

with the particles was observed. Fracture energy was found to vary linearly with the particle volume fraction except when the particles were large. Crack interaction was considered to be a plausible mechanism only when the average particle size is many times larger than the grain size of the matrix.

Studies are still being made to understand in detail the fracture processes in particulate composite systems and establish quantitative expressions for more realistic predictions of their behaviour. Attempts have been made to verify the influence of such variables as the particle shape,[34-35] the interfacial bond strength,[27 36] elastic and thermal expansion mismatch etc.[36-37] on the mechanical properties of these materials. Difficulty has been encountered in separating the effects of these variables. Besides, discrepancies between theoretical predictions and experimental data still continue to limit our understanding of these materials.

The particle filled composites discussed here and the physical processes which have been postulated to explain the fracture behaviour of these systems are briefly tabulated in Table II.

Table II Summary of Particle Filled composite fracture:-

Matrix material	Filler	Possible fracture controlling mechanisms	Variables which influence fracture	Ref No.
CERAMICS				
Glass	Al_2O_3	Crack front interaction plus surface roughness	increases with VF and D	17
Glass	Ni			21
Al_2O_3	TiC	Transparticle fracture for smaller particles	depends on VF	33
Si_3N_4	SiC	Crack front interaction for larger particles	increases with VF and D	34
POLYMERS				
Epoxy	Glass	Crack front interaction	increases with VF and D	27
Polyester	Glass			
Epoxy	Al_2O_3	Surface Roughness	increases with VF	32

Nomenclature:-

VF = Volume Fraction of Particles

D = Particle Size

1.2.2 Fibre Reinforced Composites:-

The characteristics of a fibrous composite depend very much upon the properties of the fibres and of the matrix, the nature of the interfacial bond between them and the content and arrangement of fibres within the matrix. The properties of a finished composite, in particular the strength and the modulus, are to a great extent dictated by the same properties of the fibres and found to be proportional to the fibre volume fraction.[38-39] Since a great majority of fibres are brittle, the strength values quoted for the fibres are generally the fracture strengths dependent on fracture energy, Young's modulus and the size of the largest flaw. The latter is particularly important as the average strength of a fibre is determined by the presence of flaws of variable size, shape and orientation as well as by their frequency of occurrence.

The interactions between fibres and matrix are very complex, and not fully understood. Attempts have been made to explain,[40-42] the mechanics of the reinforcement processes by which fibres contribute strength, stiffness and toughness to the matrices, in terms of several theories. These include the elastic stress transfer and slip mechanisms that can account for the composite strength and modulus, and several energy absorption processes for their toughness. These explanations are generally based on

simple models of aligned fibre composites and vary according to whether the matrix is polymeric or metallic, eg., plastic deformation in metal matrices and frictional sliding near the fibre ends in polymer and ceramic matrices, are considered to be very significant in composite strengthening.

In view of the foregoing remarks, a word of comment is thought to be appropriate here. Although the terms strength and toughness describe different properties, they are somewhat related. The term strength is often associated with the maximum load a given material can withstand before it fails by some means. Here, the mode of failure may range from a gross plastic deformation to a complete macroscopic separation, or fracture due to initiation, coalescence and growth of a defect in the material. The toughness, on the other hand, is related to the material's sensitivity to sharp cracks, and is defined empirically as the minimum amount of energy required to create a unit area of fracture surface. It enables the failure loads to be established for real engineering applications in service, when crack like defects exist in the material.

Many of the present day fibre composites are sensitive to sharp cracks and the resistance of these materials to brittle fracture through the propagation of sharp cracks is an important material property. Since the

present work is concerned with such composites and their fracture, the discussion here is mostly restricted to those events that are involved in this process.

Although much work has been done to provide analytical techniques, useful in achieving the desired strength and stiffness in composite design,[41] relatively little progress has been made in the area of composite fracture. This is partly due to the relative complexity of the failure process resulting from the very nature of composite materials, their heterogeneity and anisotropy. In addition, the flexibility in their design that has resulted in a wide variety of composite materials with a range of laminate geometries and lay-up angles, has demanded extensive studies be carried out. It is likely that no unified approach has yet evolved from fracture mechanics principles to treat the subject of fibre composite fracture in general terms. However, an accurate analytical treatment capable of characterizing their fracture behaviour is essential if these composites are to be designed for optimum toughness and used to their ultimate capabilities.

One useful parameter that can establish the materials resistance to fracture is the fracture surface energy, γ . Different methods of measuring γ yield conceptually different values of fracture energy, namely the Griffiths fracture surface energy γ_I and the work of fracture γ_F . γ_I is based on the Griffiths criterion for

unstable crack propagation and is determined by the small amount of initial crack propagation;

$$\gamma_I = -\frac{1}{2}\frac{\partial V_F}{\partial a} \tag{1.3}$$

where,

V_F = elastic energy stored in the material at the point of rapid crack propagation.

a = area of the initial crack plane.

The work of fracture, γ_F , on the otherhand is obtained by breaking a specimen in a controlled manner so that all the stored elastic energy in the specimen-machine system goes into the creation of fracture surface. This is given by

$$\gamma_F = \frac{U_T}{2A} \tag{1.4}$$

where,

U_T = integrated area under the load- deflection curve.

A = specimen cross-sectional area.

While γ_I is related to the initial rate of release of stored elastic energy, γ_F is determined by the total separation of the two fracture surfaces giving the absorbed energy, averaged over the whole of the fracture process. The relative magnitudes of γ_I and γ_F depend upon the actual physical processes that would take place during crack initiation and propagation stages. For many engineering materials, γ_I (or G_{IC} , where $G_{IC} = 2\gamma_{IC}$) is found to be more useful in that it may be used as a design parameter to predict the failure loads when fracture occurs by unstable crack propagation. For linear elastic isotropic homogeneous materials a connection between this and the critical stress intensity factor K_{IC}, has been shown to exist according to the equation,[4.3]

$$2\gamma_I = G_{IC} = \frac{K_{IC}^2}{E} \qquad \text{(plane stress)} \qquad (1.5)$$

$$2\gamma_I = G_{IC} = \frac{(1 - \nu^2)}{E} K_{IC}^2 \qquad \text{(plane strain)} \qquad (1.6)$$

where,

E = Young's modulus.

ν = Poisson's ratio

G_{IC} = Critical strain energy release rate.

For linear elastic homogeneous orthotropic materials this relationship can be written as;[44]

$$G_{IC} = K_{IC}^2 \sqrt{(a_{11}a_{22}/2)} \sqrt{[\sqrt{(a_{22}/a_{11})}+(2a_{12}+a_{66})/2a_{11}]} \qquad (1.7)$$

where a_{ij}'s are the coefficients of the elastic compliance matrix.

The critical stress intensity factor K_{IC}, known as the fracture toughness is found to be a more useful concept than fracture surface energy in engineering design. Westergaard's equations[45] for the stress distribution around a crack tip in a homogeneous material can be written in the form; $\sigma_{ij} = \psi_{ij}(r,\theta,K)$ $(i,j = 1,2,3)$ where, r and θ are the cylindrical co-ordinates and K is the stress field parameter, defined as the stress intensity factor. It has been shown that $K = f(\sigma,a)$ where σ and a are the stress and the crack length and the functionality depends on the configuration of the cracked component and the manner in which the loads are applied. The basic fracture mechanics requirment for the onset of unstable crack propagation in tensile opening mode is K reaching its critical value K_{IC}.

To extend the applicability of fracture mechanics principles to fibre reinforced composites, the inhomogeneity and anisotropy of these composites have to be taken into account. In composites several processes are

likely to occur and the actual sequence of microscopical fracture events which take place may also be important in determining the applicability of these concepts. However, fracture mechanics techniques developed for homogeneous, isotropic materials are usually applied to fibre reinforced composites, sometimes with empirical extensions of linear elastic fracture mechanics (LEFM) to cope with the anisotropic response of the material.

With some composites a considerable success has been achieved with the use of LEFM and a reasonable agreement observed between different measurements on similar materials for various reinforcement, test specimen and loading geometries. In many studies, values of fracture surface energy calculated using K_{IC} and Equations 1.5 and 1.6 have shown close agreements with absorbed energies deduced for various fracture mechanisms.[46-48]

On the other hand, the use of various stress intensity calibrations for different crack geometries in some composites has been justified by correcting the crack length to allow for crack tip damage.[49-50] H.Harel et al[51] has suggested using different K-calibration functions for every new reinforcement geometry to obtain valid stress intensity factors. The effect of reinforcement has been taken into account in the form $K = f(\sigma,a,g)$, where g is a parameter reflecting the nature and geometry of the reinforcement. Generalizations of these approaches to deal

with more complex situations are still under investigation. A typical model developed by Kanninen et al[52] treats the local heterogeneity in the vicinity of a crack tip of a unidirectional fibre composite, assuming a homogeneous anisotropic continuum for regions away from the crack tip.

Studies on composite fracture report several energy absorption processes responsible for the increased fracture toughness.[42-53] Among these the fibre pull-out, debonding, fibre stress-relaxation and matrix yielding are found to be very significant. When broken fibres pull-out of the matrix, energy is dissipated against the frictional forces at the interface. These frictional forces are generally brought about by matrix shrinkage on to the fibres. Debonding, or the separation of the fibres from the matrix before they fail may also occur as a result of the stress intensification at the crack tip. The creation of a debonding zone has been reported for many fibre reinforced composites and is analogous to the development of a plastic zone in homogeneous materials, with large amounts of energy being expended during the process. In addition the stored elastic strain energy in the debonded length of a fibre is also not recovered when it finally breaks. Even if the fibres are not debonded from the matrix, elastic energy is lost from the snapped fibre due to stress relaxation over the critical transfer length. With ductile matrices energy is also expended through plastic deformation.

Marston et al[54] have proposed that no single mechanism described above is responsible for the observed fracture toughness of composites, but rather a number of them taking place simultaneously. Analytical relations have been developed for each of these and are found to be functions of fibre volume fraction and critical length. Although many observations on fibre composite fracture suggest the pull-out and debonding mechanisms to be predominant, the actual events that take place seem to depend upon the bond strength between the fibres and the matrix, and the specific combination of fibres and the matrix.[55]

It has been shown by means of model composites that the fracture energy of a glass fibre /polyester combination is determined largely by the work done against friction between the fibres and the matrix after the debonding process has occured.[56] Specifically, the fracture measurements of a random glass fibre/polyester composite system[46] have indicated that different mechanisms control different stages of crack propagation and that γ_I is determined by a debonding mechanism while γ_F is the sum of a debonding mechanism plus a pull-out contribution. With a unidirectional glass fibre-epoxy composite,[57] γ_F agreed with the pull-out model while γ_I corresponded with the surface formation model proposed by Marston et al[54] indicating that the creation of new fibre, matrix and fibre-matrix surfaces controls the stage of fracture

initiation.

Many studies have also been directed towards the understanding of the effects of specimen and testing variables on the fracture of fibre reinforced composites. The measured values of fracture toughness of a given composite are found to be dependent on some or all of the following variables.

1. Fibre volume fraction
2. Specimen type
3. Specimen size
4. Crack length
5. Reinforcement geometry
6. Loading rate(or strain rate)

Fracture toughness measurements in glass reinforced plastics reported by a number of researchers have been compiled by Owen and Cann.[58] A modified tabulation of some of these measurements is given in Table III. The measurements clearly show that the fracture toughness of some fibre reinforced composites are influenced by the type of test specimen employed, its dimensions and the original crack size.

Fracture toughness tests carried out by the same authors[58] on polyester resin, reinforced with glass chopped strand mat using a centre notch specimen configuration have indicated an increase in K_{IC} with specimen width W at a constant a/w ratio, where a is half the crack length. Only

Table III Fracture Toughness Test Results of some glass reinforced plastics:-[58]

Composite system	Specimen geometry	t (mm)	a (mm)	w (mm)	K (MPa.m$^{0.5}$)
Balanced weave fabric in epoxy and polyester	CN	0.25	0.25	38.1	8.4
		0.25	0.64	38.1	11.2
		0.25	1.04	38.1	12.9
		0.25	1.27	38.1	14.8
		0.25	1.70	38.1	16.4
		0.25	2.29	38.1	15.8
		0.25	3.30	38.1	17.8
		0.25	4.98	38.1	18.2
		0.25	6.20	38.1	17.8
	DEN	0.25	1.04	38.1	18.4
		0.25	1.78	38.1	18.2
		0.25	2.52	38.1	18.2
		0.25	2.54	38.1	18.5
		0.25	3.56	38.1	16.0
		0.25	5.72	38.1	18.4
		0.25	6.35	38.1	19.3
		0.25	6.35	38.1	20.6
Random chopped fibres in polyester	DEN	1.5	1.25	25.0	6.93
		1.5	2.50	25.0	9.68
		1.5	3.75	25.0	10.27
		1.5	3.95	25.0	8.15
		1.5	4.38	25.0	5.99
		1.5	5.00	25.0	9.35
		3.5	1.25	25.0	4.39
		3.5	2.50	25.0	6.04
		3.5	3.75	25.0	6.58
		3.5	5.00	25.0	6.41
		3.5	6.25	25.0	5.59

Table III (Continued);

Composite system	Specimen geometry	t (mm)	a (mm)	w (mm)	K (MPa.m$^{0.5}$)
Random chopped fibres in polyester	BEND	1.5	0.30	10.0	7.9
		1.5	1.00	10.0	8.1
		1.5	1.05	10.0	10.1
		1.5	3.05	10.0	9.4
		1.5	4.80	10.0	10.0
		3.5	0.29	10.0	7.9
		3.5	1.30	10.0	9.9
		3.5	1.30	10.0	7.8
		3.5	2.90	10.0	9.9
		3.5	4.80	10.0	7.1
		3.5	4.85	10.0	9.4

Nomenclature:-

CN Centre notch specimens
DEN Double edge notch specimens
BEND 3 or 4-point bend specimens
t Specimen thickness
a Crack length (half crack length in CN specimens)
w Specimen width
K Critical stress intensity factor (MPa.m$^{0.5}$)

a negligible change in K_{IC} with specimen thickness has been observed, indicating that plane strain conditions are unlikely to occur even in many plied laminates. In a homogeneous material plane strain conditions are established when the less strained material adjacent to a

crack front prevents the contraction along the crack front of the highly strained crack tip material. In glass reinforced plastics the interfacial and interply strength is probably too low to support tensile forces along the crack front. It has also been noted that K_{IC} varies continuously with the crack length, with a maximum occurring at crack lengths close to half the specimen width.

Linear elastic fracture energy measurements of a random glass fibre composite, containing E- glass fibre in a polyester matrix have been reported by Beaumont and Phillips.[46] These measurements have been carried out on 3 point bending beams and double edge notched tensile plates of two different thicknesses, at a range of crack lengths. The results of tensile tests have indicated a clear variation of fracture energy (γ_I) with crack size and specimen thickness, but the results of bending tests have displayed no such variation. Although the mean values of γ_I are approximately the same for both specimen configurations, a maximum has occurred in the tensile test results for an intermediate value of crack length. Further, the γ_I obtained from the thick tensile plates was less than that obtained from the thinner plates. No strain rate dependence of has been observed for any of the two specimen configurations.

The results have been explained in terms of the

debonding model, with a stress state dependence of debonding zone size and the stress field interaction with free surfaces explaining the variability of the tensile test data. However, it has been found difficult to reconcile these ideas with the invariability of the bending beam results. In contrast to the strain rate independence of γ_I, the work of fracture (γ_F) measurements on bending beams show an increase with increasing strain rate, displaying no variation with crack size or specimen thickness. This has been explained in terms of a strain rate dependent finite interfacial shear stress, which resists the fibres when they pull-out of the matrix.

In summary, the mechanics of the reinforcement processes which account for the mechanical properties of fibre composites are based on simple models of aligned fibre composites. There is still much to be done, both theoretically and experimentally, to characterize and predict the behaviour of these heterogeneous anisotropic materials in service. In particuler, predictive techniques capable of coping with the complexity of the fracture processes have to be established. Studies on fibre composite fracture given in the literature generally fall into one of the following catagories. These are;

1. formulation of accurate analytical techniques for their failure analysis

2. development of various energy absorption mechanisms linking the microscopical fracture events with observed toughness and
3. the evaluation of the influence of specimen and testing variables on the actual toughness.

The present trend in developing analytical representations for failure analysis of fibre reinforced composites is to account for their anisotropic nature in a modified fracture mechanics formulation. The microscopical fracture events which take place are important in determining the applicability of these concepts. With such concepts, the effect of specimen and testing variables on fracture of these composites can be evaluated.

1.2.3 Fibre & Particle Reinforced Composites:-

Three phase composites containing both fibres and particles in a matrix material have received less attention than those which contain only fibres of another material as the third phase reinforcement.[11] Comparative studies of resin based composites[12] have shown that part of the increase in the stiffness of some three phase composite was due to the filler material. By extending theories of two phase composites Chang and Weng[13] have developed an

analytical method to determine the elastic modulus of a filled resin reinforced by randomly oriented chopped fibres and have shown that their results compare well with available experimental data. These results show that, when reinforced by the same amount of glass fibres, a filled resin is often stiffer than the unfilled resin, but with increasing fibre content the elastic modulus of the filled composite is increased only moderately as compared to an unfilled composite. For example, a 50% increase in the fibre content of a typical automotive type sheet moulding compound, filled with $CaCO_3$ results in only a 10% gain in elastic modulus of the composite, while a 30% increase is realized in case of an unfilled compound. In contrast to the beneficial effects of these filler materials on the final stiffness properties of composites, a reduction in strength and work to break has been observed by Ogorkiewicz et al.[14]

Cawthorne and Harris[15] have measured the fracture toughness of some model glass/resin/chalk composite systems and discussed[59] the sources of fracture energy in these materials. These model materials representing the commercial polyester dough moulding and sheet moulding compounds have been prepared by hand mixing the chopped glass fibres and chalk into the catalysed polyester resin. Single edge-notched fracture toughness testing in three-point bending have been carried out to determine the total fracture work, by integrating the load-deflection curve,

and an apparent critical stress intensity factor by means of the Srawley-Brown expression.[60] By comparing the results with other published work they have been able to suggest that the fracture energy and the apparent fracture toughness of a wide range of glass reinforced thermosets is a simple function of fibre content, provided the fibre distribution was roughly uniform, and that the filler particles have a relatively little effect on the toughness of these materials.

The major contribution to the energy absorption during fracture appeared to be directly attributable to the fibre debonding, the other mechanisms of fibre pull-out and interfacial friction providing much smaller contributions. The addition of up to about 30 wt% of short glass fibres increases both the total fracture energy and critical stress intensity in roughly linear fashion, irrespective of the addition of filler particles. On the other hand, they also observed that the addition of crushed, rather than precipitated, chalk fillers can lead to serious reductions in fracture toughness of these materials as a result of fibre damage by abrasion against the sharp filler particles occurring during composite preparation and fracturing.

1.3 PRESENT WORK:-

In view of the fact that very little progress has been made in the area of three phase resin based composites, it was considered appropriate to investigate the simple fabrication techniques of both binary and ternary composite systems incorporating randomly distributed chopped glass fibres and/or heavy metal powders in a polyester matrix, and examine their resistance to fracture. The effects of such variables as the specimen geometry, fibre and filler volume fractions, and particle size on the fracture of these composites have been evaluated.

1.3.1 Experimental Methods:-

Compact tension specimens of two phase powder composites were first prepared by a simple casting method. These specimens contained different volume fractions and particle sizes of iron and nickel powder. Attempts to incorporate glass fibres of very short length in to the resin by similar methods of hand mixing and casting were all unsuccessful due to the difficulty involved in wetting the fibres and removing the entrained air. Further, the maximum quantities of glass fibres that could be added to

the resin were also limited to about 2-3% of volume fraction. The glass fibres were about 2-4 mm in length and randomly oriented, as it was originally intended to make these castings with no strong directionality.

It was then proposed that to make these composites, a procedure, employing high pressure injection was necessary. An injection moulding unit was built and fibre composite specimens of bending beam configuration were made. But again, difficulties were encountered when the resin injected through the fibres was filled with metal powders. At high glass contents the penetration of metal powder was non-uniform and almost incomplete. Further, the frequent failure of the fittings and sealings in withstanding the high pressures involved and the less overall productivity, resulted in eventual abandonment of this method.

In view of the foregoing difficulties, associated with incorporating together the metal powders and three dimensionally random short glass fibres in a resin matrix, a compromise had to be made in the non-directionality of fibre orientation. Instead of short fibres, mats of randomly dispersed chopped glass fibres were used. A reasonably good penetration of metal powders at a high fibre content was achieved satisfactorily with a simple wet lay-up technique. Layers of glass mats, after wetting with filled or unfilled liquid resin, were laid on top of each

other and rolled down with a roller brush to make castings, from which the bending beam test specimens were cut. Although unsuitable as a means of producing nearly isotropic composites, it was the only way a greater control over the volume fractions of constituent fibres and particles was gained with little or no voids.

A series of bend specimens containing different volume fractions of metal powders and/or glass fibres were made and tested for their fracture toughness. The metal powders used were either coarse iron powder or fine nickel powder. Standard plane strain fracture mechanics techniques were used throughout the testing and evaluation and the results compared with those of an experimental compliance calibration procedure.

The experimental work summarized above is presented here in separate sections with the descriptions of equipment, specimen preparation, testing and analysis of any one of the specimen geometries or different fabrication techniques put together. However, a chronological presentation of the work done is not attempted; rather, the most comprehensive study on cast bending beams is presented at the beginning followed by the studies on injection moulded bending beams and cast double cantilever beams. The common materials used in this work are all described below.

1.3.2 Materials Used:-

Polyester Resin:-

The resin used for the matrix material of all the composites was the Vibrin P-35/15 general purpose polyester supplied by Fibreplast Products, Burnaby, B.C. This was used with MEK (methyl ethyl ketone) peroxide catalyst produced by Noury Chemical Corporation, Burlington.,NY, in the ratio of 3 drops (approximately 0.12 ml) of catalyst per ounce of pure resin. This is the normal proportion suggested by the supplier which provided sufficient gel time (20-30 min.) for mixing and moulding while preventing settling out of the solid constituents of the composite. The density of the cured resin was found to be 1.21 g/cm^3.

Iron Powder:-

Atomet 95 high purity, $\overline{=}$325 mesh iron powder supplied by the Quebec Metal Powders Ltd., Sorel, Quebec, was screened in the laboratory to obtain powders of less than 45 μm diameter. (-325 mesh size.) The density of the powder was determined by a simple immersion technique and found to be approximately 7.19 g/cm^3.

Nickel Powder:-

This was used in two different particle sizes.

Nickel Powder:-

This was used in two different particle sizes. The finer 1 μm diameter particles are the Nickel (Superfine) Sherritt grade NF-1M, supplied by the Sheritt Gordon Mines Ltd., Saskatchewan, Alberta. Experimentally determined density of this powder was 6.23 gm/cc. The coarser particles of particle size 40-45 μm were obtained by screening the Sheritt grade C nickel powders supplied by the same company. These particles had a density of 8.85 gm/cc.

Glass Fibres:-

A 50 in. wide roll of chopped strand E-glass mat supplied by Fibreplast Products in Burnaby, B.C., was used to cut rectangular pieces of mats required for random fibre composite laminates. This mat weighed approximately 450 gm/m^2 and cost $0.96 per pound. The roving of E-glass fibres used to make chopped short fibre segments for random fibre composites (including injection moulded specimens) was obtained from Fibreglass Canada Inc., Burnaby, B.C. The fibre diameter was approximately 10 μm. in both types and its density was taken as 2.55 gm/cc.

II. CAST BENDING BEAMS.

A bending beam specimen configuration was used to study the mechanical properties of composites containing the following particles and/or fibres over a range of volume fractions in a polyester matrix.

(I). Coarse iron powder

(II). Coarse nickel powder

(III). Fine nickel powder

(IV). Coarse iron & fine nickel powder

(V). Randomly oriented glass fibre mat

(VI). Randomly oriented glass fibre mat & coarse iron powder

(VII). Randomly oriented glass fibre mat & fine nickel powder

Castings containing each of these in a polyester matrix were made for the volume fractions of interest using a mould. Test pieces were then cut from these castings.

2.1 PREPARATION OF COMPOSITES:-

A wooden mould enclosed in a rectangular wooden box was made in two parts as shown in Fig.1. The inside of the bottom half of the mould contained the mould cavity lined with a layer of silicone rubber, approximately 1/2 in.thick, to give a smooth inner surface. Two drain channels were made close to the two ends of a lengthwise edge, to allow for flow of resin into and away from the mould. The inside of the top half of the mould was also lined with silicone rubber to give a smooth flat surface. Two metal clamps that could slide around the assembled mould held the assembly together. The mould was used both as a closed vertical mould with drain holes running vertically up through the top surface and as an open mould in a horizontal position with the holes running horizontally through one of the sidewalls.

Composites that contained only the powders were made by mixing a weighed quantity of powder, predetermined for the intended approximate volume fraction as explained in Appendix B., with a weighed quantity of liquid resin catalysed just before the addition of powders. The resulting mixture was stirred manually for 5 to 10 minutes to provide a uniform slurry which was then cast into the mould, the mould being kept closed in its vertical position. Care was taken throughout the process to avoid introducing air bubbles into the mixture. The mould surfaces were coated with a mould release agent to

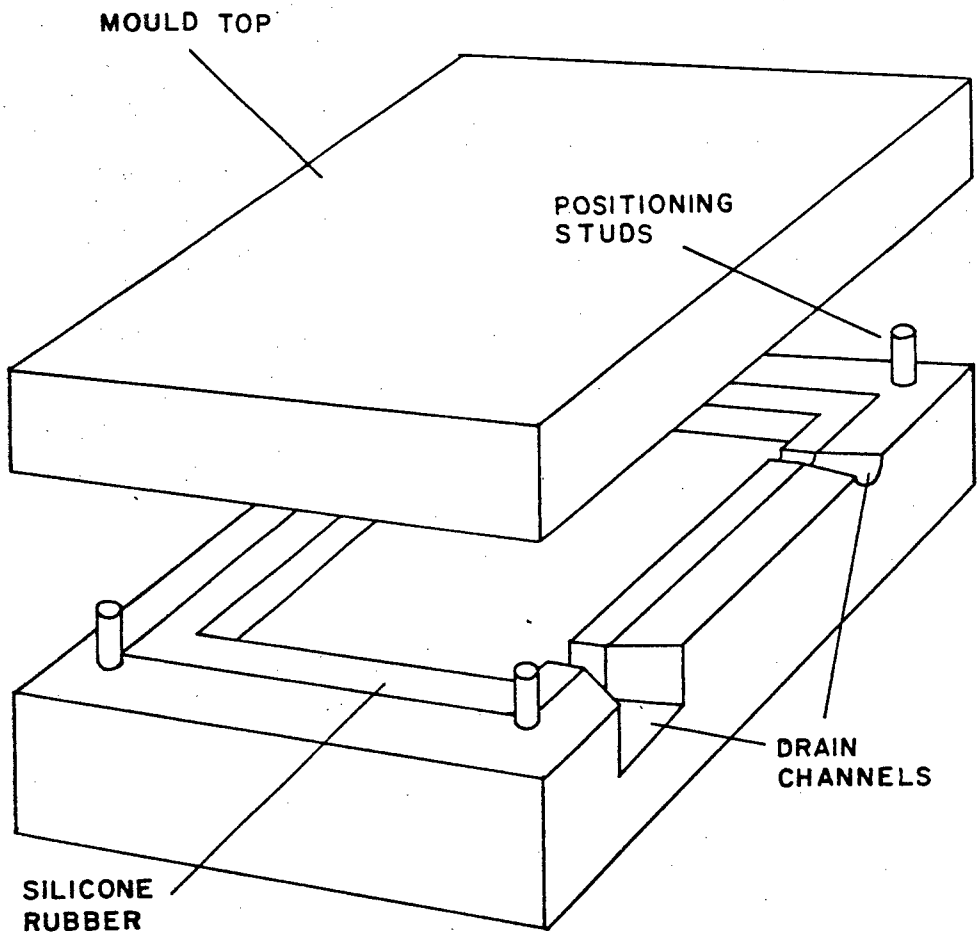

WOODEN MOULD

FIG. 1. The mould used for the fabrication of cast specimens.

facilitate the removal of the cast composite plate after 24 hours of curing at room temperature. Further ageing at room temperature for at least one week was allowed before making test specimens from the casting.

Composites that contained glass fibres were made in an open mould. Rectangular pieces of glass mat, with planar dimensions slightly less than the dimensions of the mould cavity, were cut from the randomly oriented glass fibre mat. The liquid mixture was prepared as explained before with or without the metal powder. After 5 to 10 minutes of stirring to give a uniform mixture, it was placed in a wide plate lined with a thin aluminium foil. The layers of glass fibre mats were then dipped in this bath allowing the liquid mixture to wet the fibres well. The wetted mats were laid on top of each other inside the open mould, taking precautions to prevent air bubbles from creeping into the layup. The layup was rolled down with a roller brush after every 3 or 4 layers of mat, placing a thin sheet of polythene on top to prevent contact of liquid resin mixture with the surface of the brush. The polythene sheet was then peeled off carefully and the process continued. When the layup was complete the mould was closed and the clamps were slipped into position and tightened. As the clamps were tightened the excess resin mixture squeezed out through the drain holes. The casting was then allowed to cure for at least 24 hours at room temperature, before removing from the mould. Test specimens were prepared from these castings after at least one week of curing at room temperature.

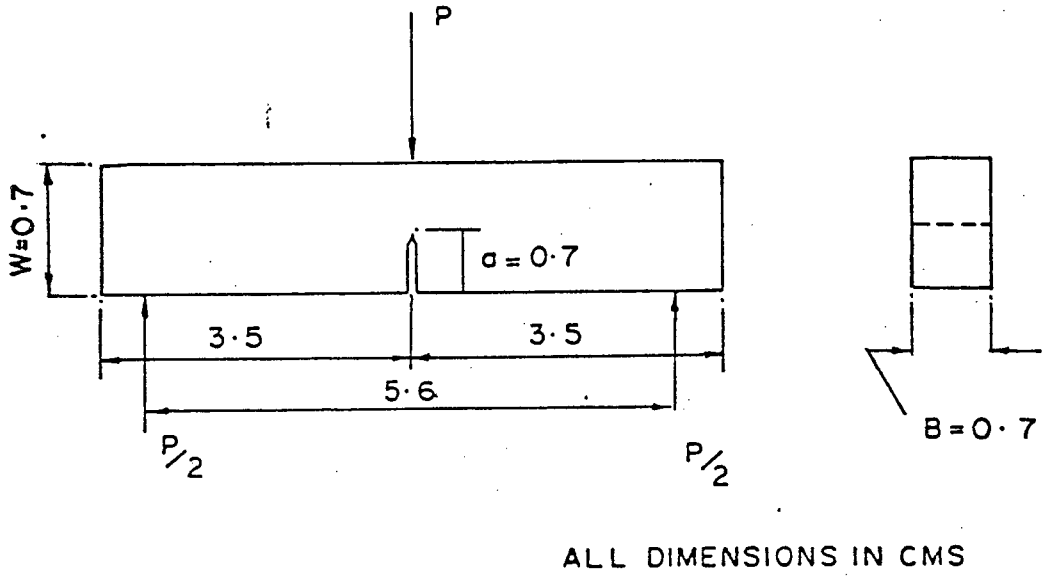

BENDING BEAM GEOMETRY

FIG. 2. The dimensions of the bending beam fracture toughness test specimens used.

2.2 FRACTURE TOUGHNESS TESTING:-

2.2.1 Specimen Preparation:-

Test specimens were cut from the cast plates with a diamond wheel, and the surfaces were ground with Grit 320 silicone carbide paper. This was done in order to achieve the dimensions of a standard three point bending beam as set by Sec.7.2 of ASTM E399-78a. As shown in Fig.2, the nominal dimensions of the specimens for the purpose of this work were selected to be 7.0x1.4x0.7 cm. and the surfaces were ground carefully to be within ±0.020 cm. in its cross-sectional dimensions. A centre notch of 0.7 cm. nominal depth was made using a Norton Diamond Wheel of 0.3 mm. thick. The tip of the notch was sharpened by pressing a single edge blade against the tip of the notch. A small hand press was used for this purpose.

2.2.2 Testing & Measurements:-

A minimum of 4 specimens were made for each volume fraction, except in the case of coarse iron powder polyester specimens. The width and thickness of each specimen were measured using a Vernier caliper, to the

nearest 0.025 mm. The thickness, t was measured at three positions between the crack tip and the unnotched edge of the beam and the average of these measurements was taken as the actual thickness. The width W, was measured at three positions near the centre notch and the average of these measurements was taken as the actual width.

The test specimens were loaded in three point bending on a servo-hydraulic testing machine (hereafter referred to as MTS) using a span of 5.6 cm. between the centres of the support rolls. The two support rolls were mounted on a jig that was attached to the movable, lower arm of the MTS. The central loading roll which was attached to the fixed upper arm of the MTS was positioned exactly midway between the two support rolls.

The specimen was positioned with the crack tip midway between the two support rolls and loaded under a constant loading rate of 44.5 N/sec. This produced at the tip of the crack a stress intensity increase rate,slightly higher than the minimum rate (0.55 MPa.$m^{0.5}$/sec.) specified in Sec.8.3 of ASTM E399-78a. The specimen was loaded until it failed and the load- displacement curves were obtained on a Honeywell recorder and an X-Y plotter. The crack length was measured to the nearest 0.025 mm. using a caliper after the specimen was fractured. The average of three measurements made along the crack front (one at the centre and the others midway between the centre and the end

of the crack front on each side) was taken as the actual crack length.

For composites containing only powders, the initial estimates of their volume fractions were assumed to be true volume fractions. A detailed explanation for this is given in Appendix B. But in composites containing fibres no such prior estimate of the fibre content could be made and the incorporation of these fibres significantly altered the initial estimates of powder volume fractions. Hence, as explained in Appendix B., an alternative method of burning a small sample of composite was used to determine both the fibre and filler volume fractions of all fibre composites.

2.2.3 Calculation & Discussion of Results:-

Pure polyester and all composites which contained only powders, exhibited a linear load- displacement behaviour upto the point of fracture, as shown in Fig.3. The load at fracture was taken for the calculation of critical stress intensity factor, K_{IC}.

The composites which contained glass fibres always exhibited a slight deviation from initial linearity of load- displacement record before reaching the final fracture point. A typical load-deflection curve is shown in

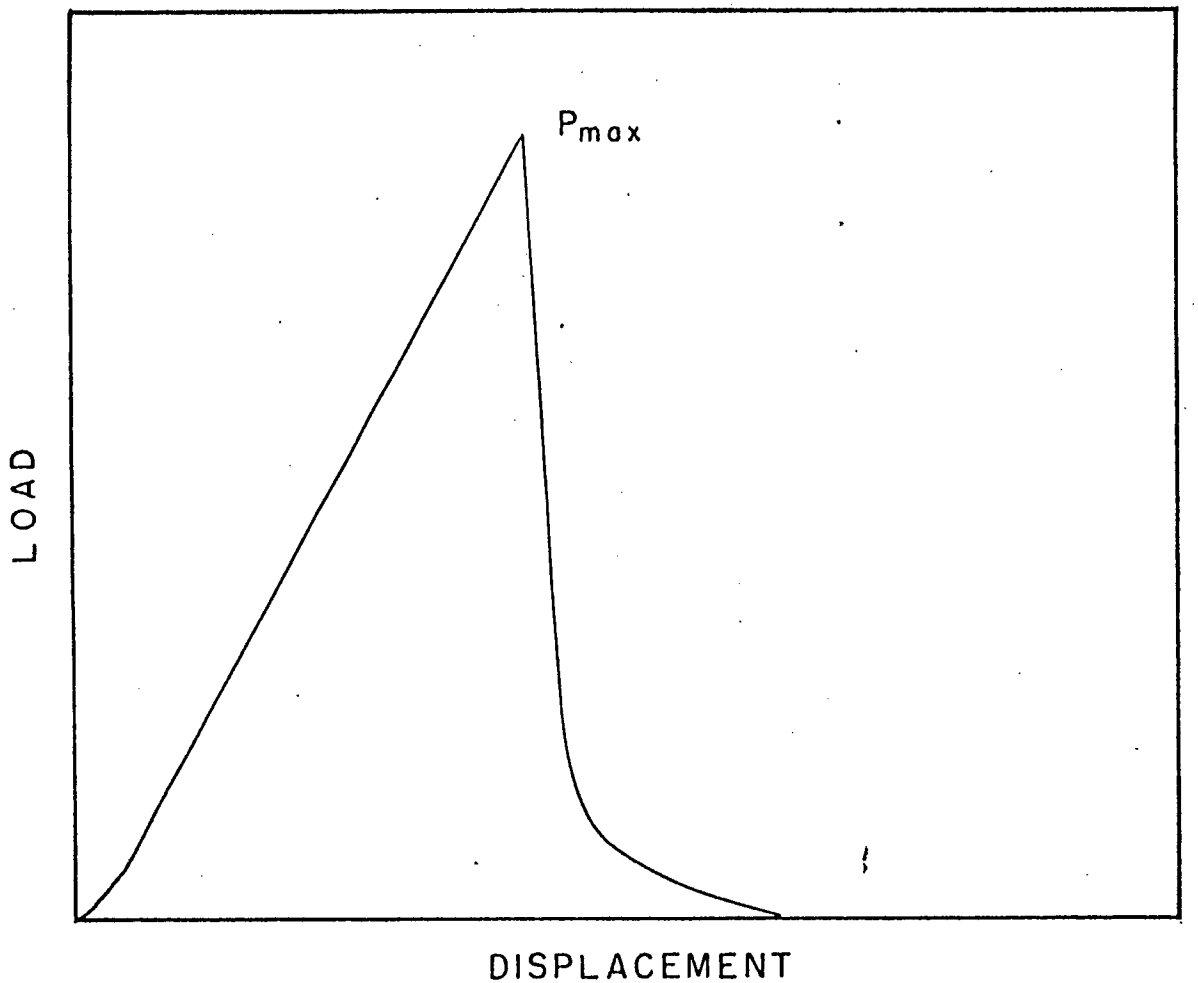

FIG. 3. A typical load-displacement curve of type 1.

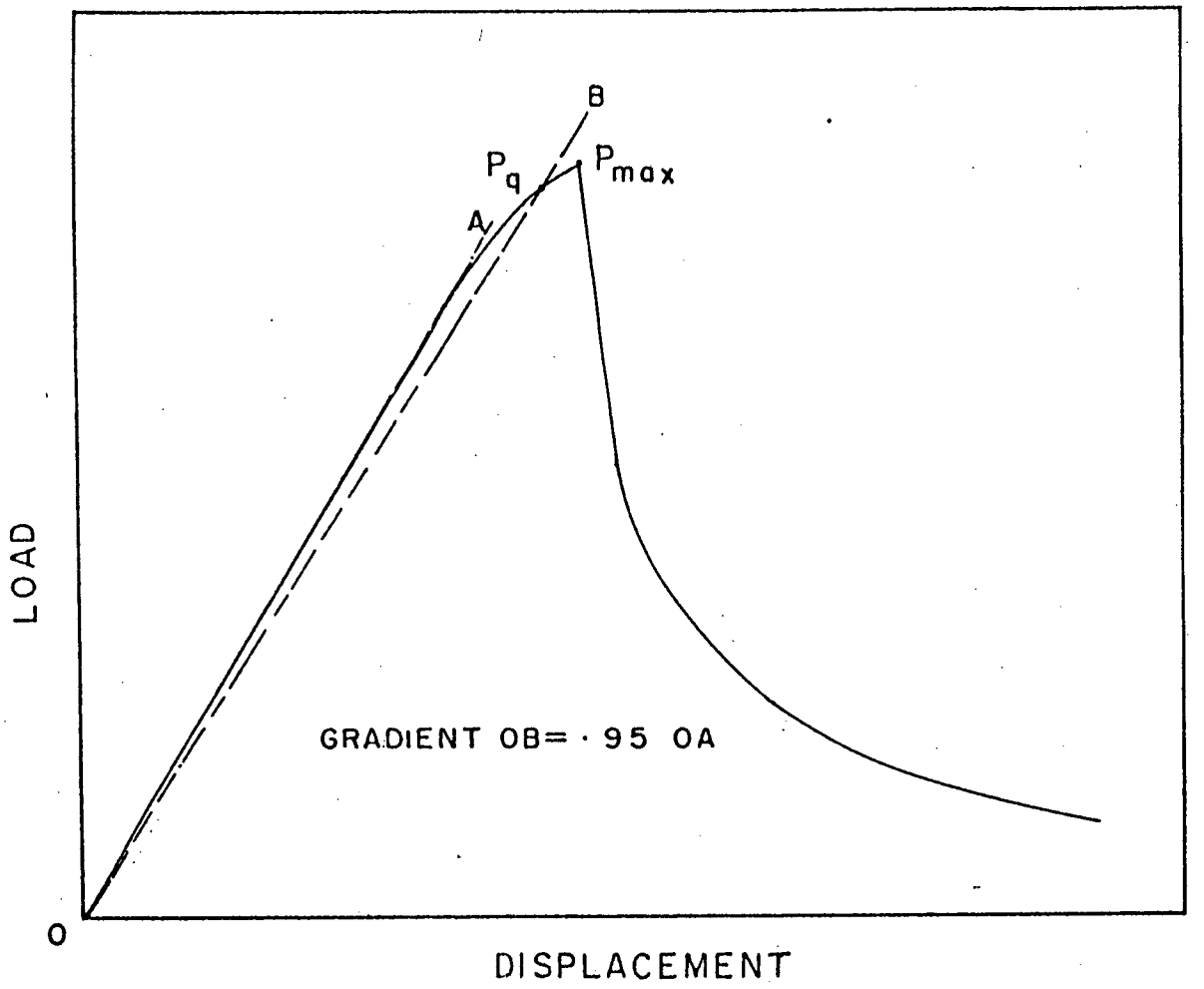

FIG. 4. A typical load-displacement curve of type 2.

Fig.4. For these composites both the maximum load at fracture and the 5% offset value, were used for the calculation of critical stress intensity factor, K_{IC}. This resulted in two different values of K_{IC}, and are referred to as Kmax & Kq respectively in this work. In determining the 5% offset value the procedures described in Sec.9.1.1 of ASTM E399-78a were followed.

For the calculation of critical stress intensity factor in units of $MPa.m^{0.5}$ the following equation given in Sec.9.1.3 of ASTM E399-78a was used.

$$K_{IC} = \frac{PS}{BW^{3/2}} \cdot f(a/W) \qquad (2.1)$$

where,

$$f(a/W) = \frac{3\sqrt{(a/W)}\,[1.99-(a/W)(1-a/W)(2.15-3.93a/W+2.7a^2/W^2)]}{2(1+2a/W)(1-a/W)^{3/2}}$$

where,

B = Specimen thickness (cm)

a = Crack length (cm)

S = Span (cm)

W = Width of the specimen (cm)

P = Load in kN determined as explained above.

Appendix C. lists some of the results obtained. The calculated values of critical stress intensity factor

for all these composites have been plotted against the approximate volume fractions of constituent components and are shown in Figs.5-12. The curves drawn were plotted using a computer routine (see Appendix D.) that employs a parabolic curve fit through the averages of stress intensity factors derived at each volume fraction.

For particle filled composites the use of Equation 2.1 to calculate the values of K_{IC} was justified by the observed homogeneity and isotropy of these composites and the values calculated are considered to be representative of their fracture toughness. But with composites containing fibres no such observation could be made, and the accuracy of the Equation 2.1 in calculating critical stress intensity factor had to be verified by a compliance method. The methods involved and the results observed are described in Section 2.2.4. It has been shown that the Kq values calculated using the 5% offset load values are in close agreement with the values obtained using the compliance method. Hence the values of Kq are considered to be representative of the fracture toughness of composites, containing randomly oriented glass fibres.

As can be seen from Fig.5 the critical stress intensity factor of the pure resin is increased progressively by about 100-150% by the addition of 20-25% volume fraction of coarse powder. Specifically, the addition of 25% volume fraction of iron powder has

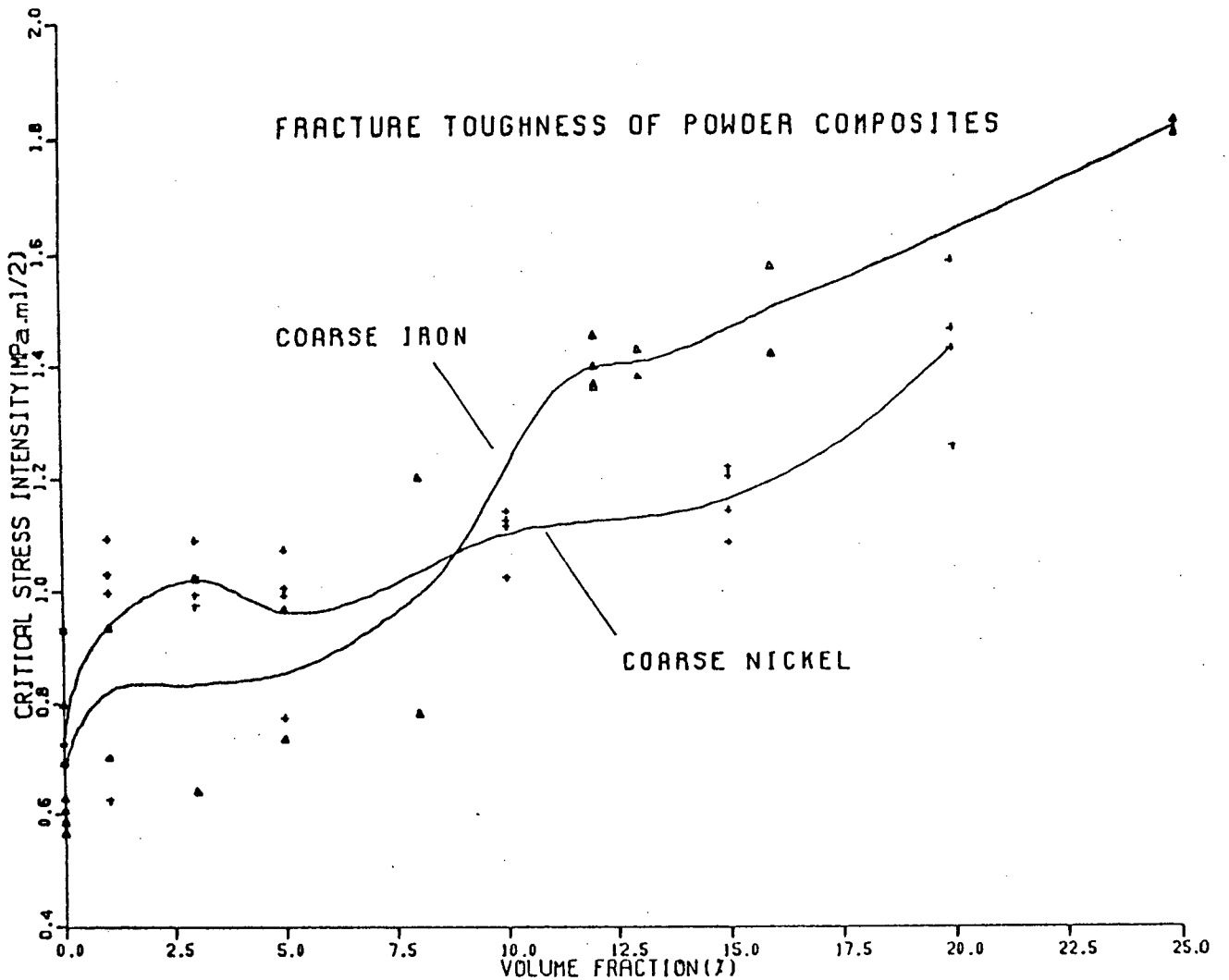

FIG. 5. Bending beam fracture toughness of coarse iron and coarse nickel composites.

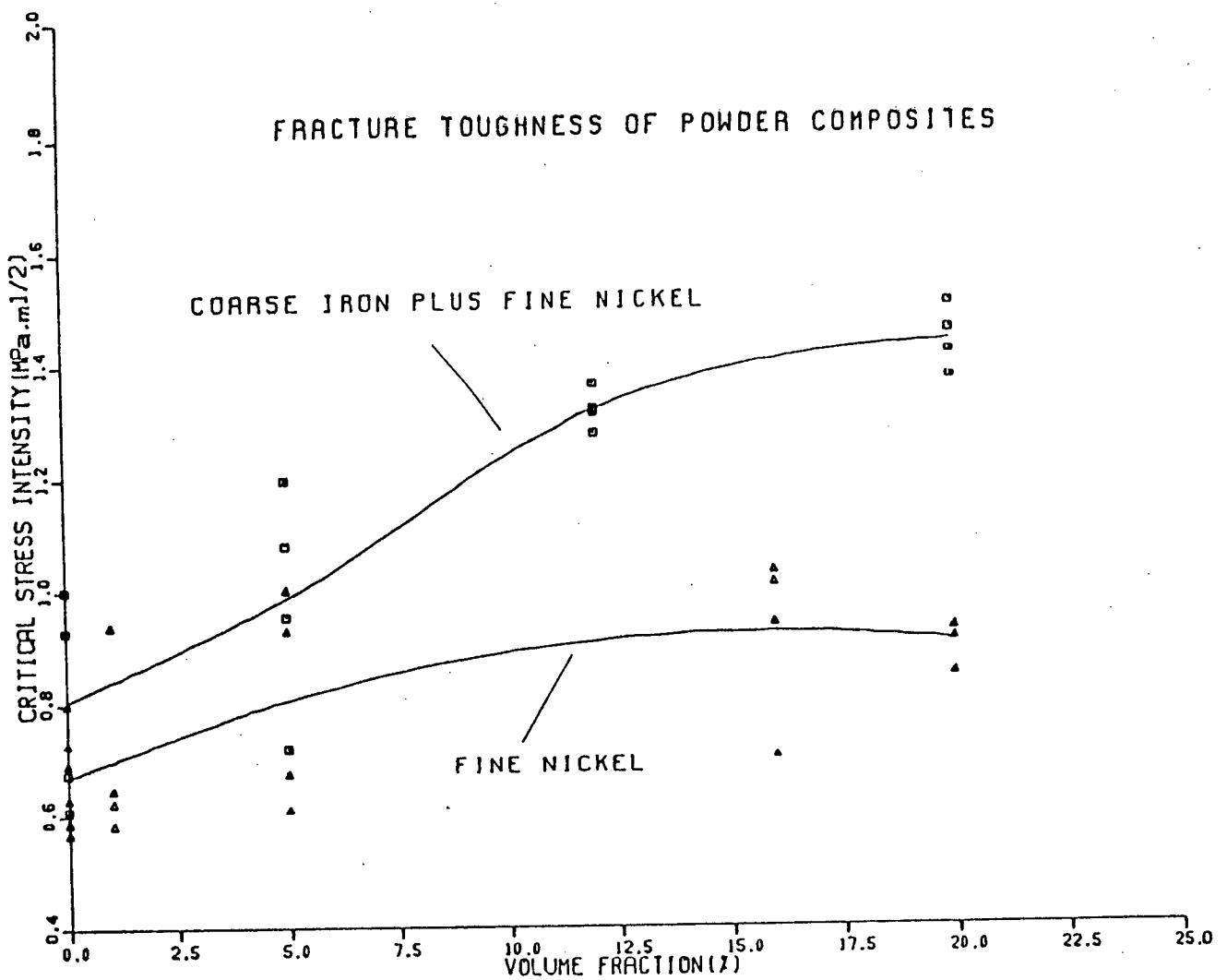

FIG. 6. Bending beam fracture toughness of fine nickel and coarse iron plus fine nickel composites.

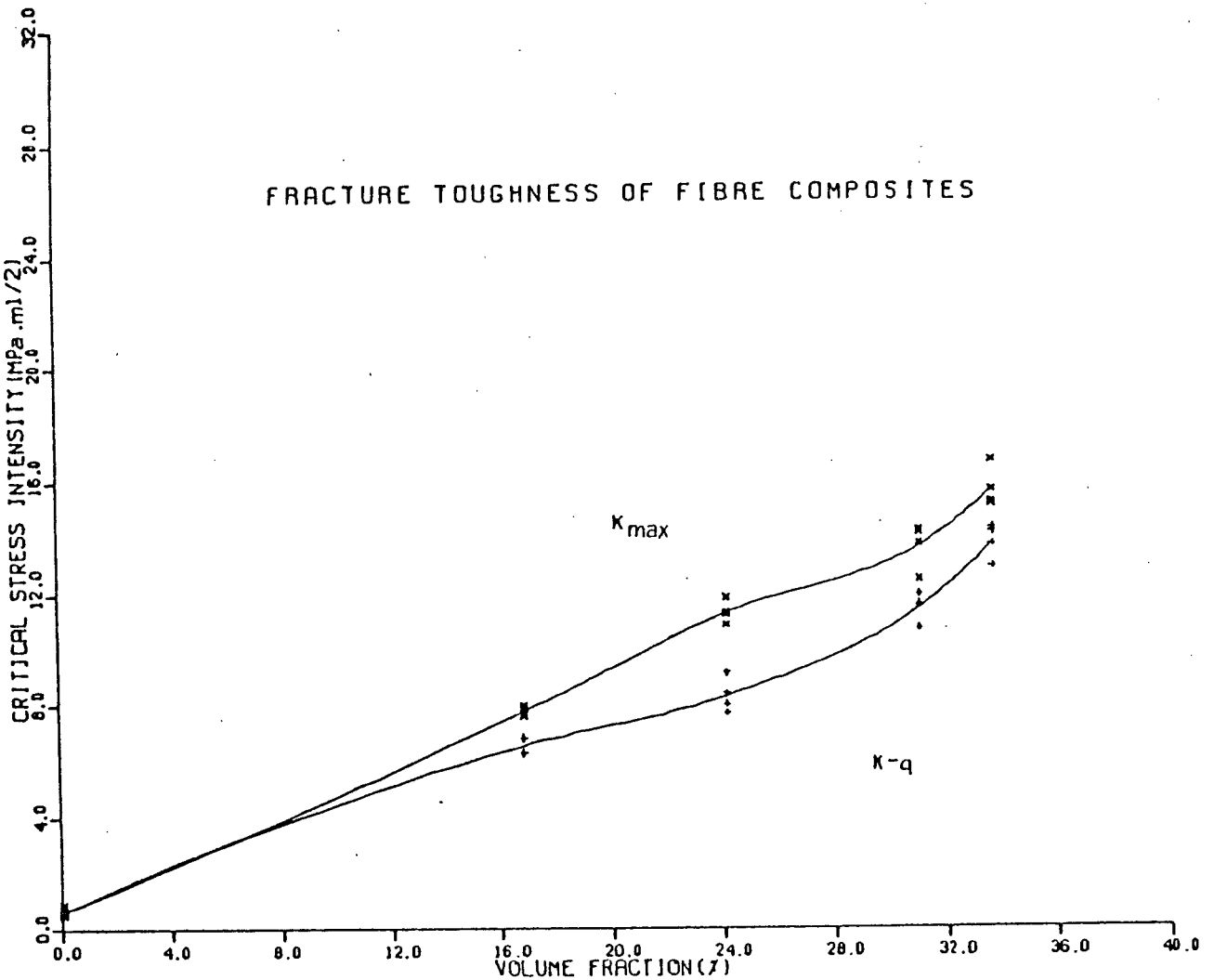

FIG. 7. Bending beam fracture toughness of glass reinforced composites.

increased the fracture toughness from 0.7 $MPa.m^{0.5}$ to 1.8 $MPa.m^{0.5}$ whereas 20% of nickel powder has raised this value to approximately 1.4 $MPa.m^{0.5}$. Fig.6 on the otherhand indicates that fine Ni powder has a less pronounced effect on fracture toughness, yielding an average value of 0.9 $MPa.m^{0.5}$ for K_{IC} at 20% volume fraction. The value of K_{IC} is increased continuously over the initial 12% after which there seems to be no effect of powder addition on the toughness of this system.

When both coarse iron and fine nickel are present in the resin the toughness increases but tends to level off near 20% volume fraction of coarse iron powder. The total volume content of fine nickel powder in these composites is kept constant at 5% irrespective of the amount of iron powder added. Here the value of critical stress intensity factor at 20% volume fraction of iron powder is little over 1.4 $MPa.m^{0.5}$, a value less than that of a system containing 20% of iron powder alone in resin.

As shown in Fig.7, the apparent fracture toughness of glass reinforced composites is greatly influenced by the amount of fibres present. Over 100% increase in toughness is obtained simply by doubling the volume fraction of fibres. At nearly 16.8% volume fraction of fibres a value of 6.5 $MPa.m^{0.5}$ was recorded for Kq while at 33.7% it was nearly 13.8 $MPa.m^{0.5}$ A continuous approximately linear variation of Kq was observed within

this range of volume fractions.

However, it is evident from Fig.8 that the addition of fine nickel powder does not significantly affect the toughness of these composites. The critical stress intensity factor of the resulting three phase composite remains almost unaltered within a wide range of powder volume fractions. At higher fibre contents however, a slight decrease was observed with increasing amounts of powder additions.

The effect of powder additions on the toughness of three phase composites just discussed, seems to be somewhat different in the case of coarse powders. The results of the fracture toughness tests of a series of three phase composites containing up to 16% volume fraction of iron powder are depicted in Figs.9-11. For clarity Kq values are shown separately in Fig.12. It is significant to note that, unlike the fine nickel powder, the coarse iron powder tends to increase the fracture toughness at lower concentrations of glass fibre. The critical stress intensity factor of a composite containing 16.8% volume fraction of fibres increases with increasing amounts of iron powder up to about 6% powder volume fraction. But, as the fibre content is increased, the effect of powder additions on the toughness of these composites seems to be somewhat detrimental. At 33.7% volume fraction of glass fibres, the fracture toughness of the resulting composite

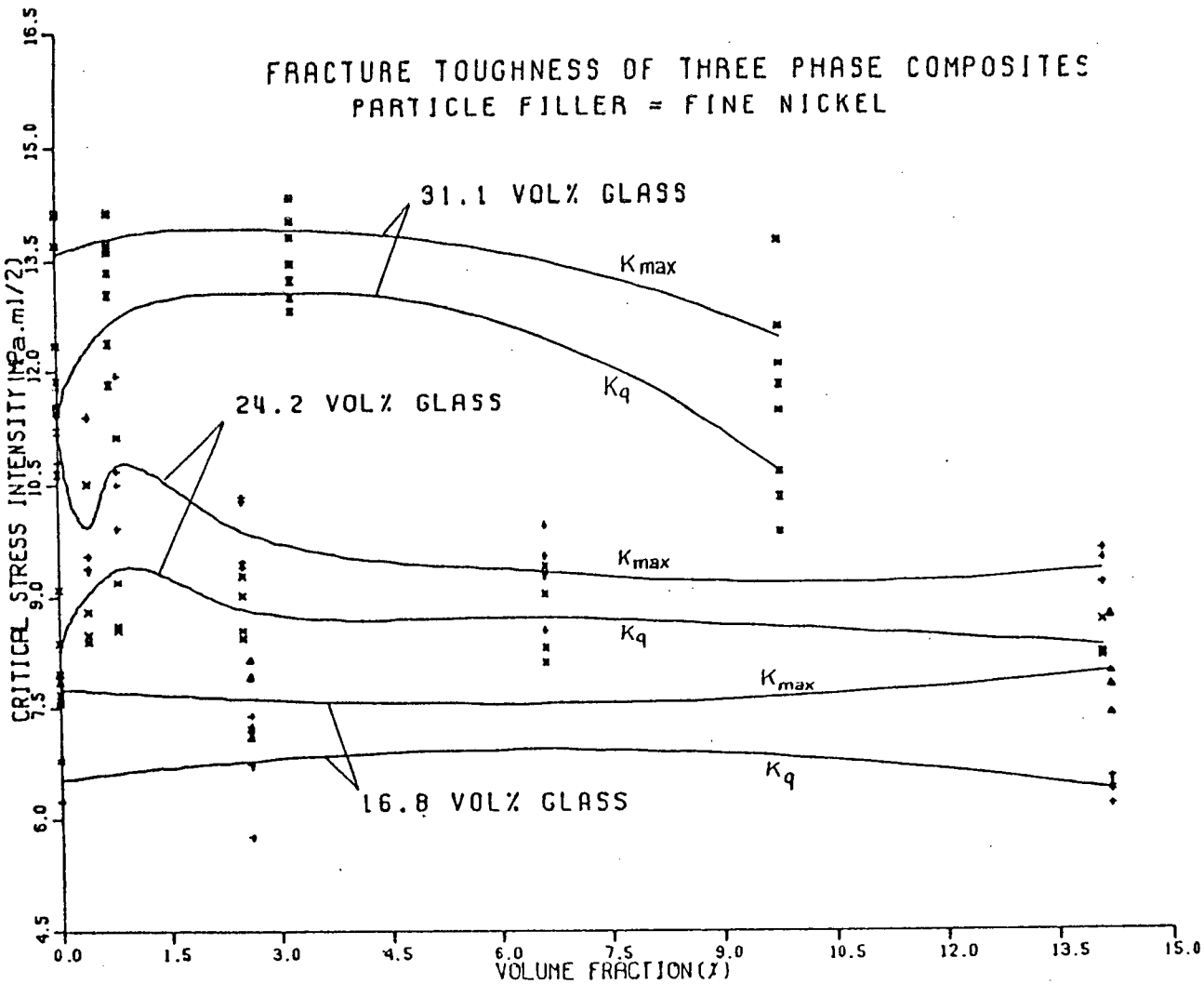

FIG. 8. Bending beam fracture toughness of glass reinforced nickel filled composites.

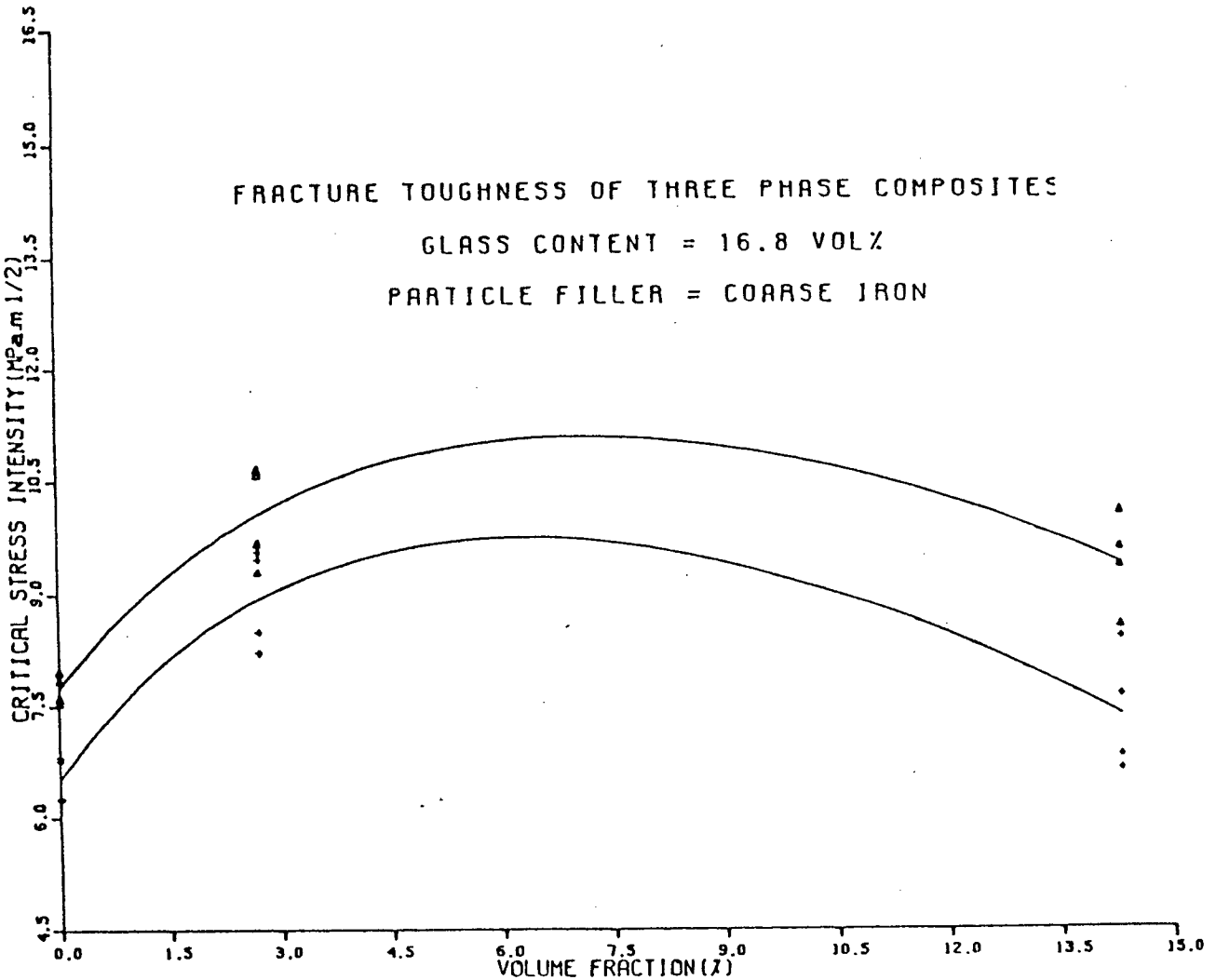

FIG. 9. Bending beam fracture toughness of glass reinforced iron filled composite. Glass volume fraction is 16.8%.

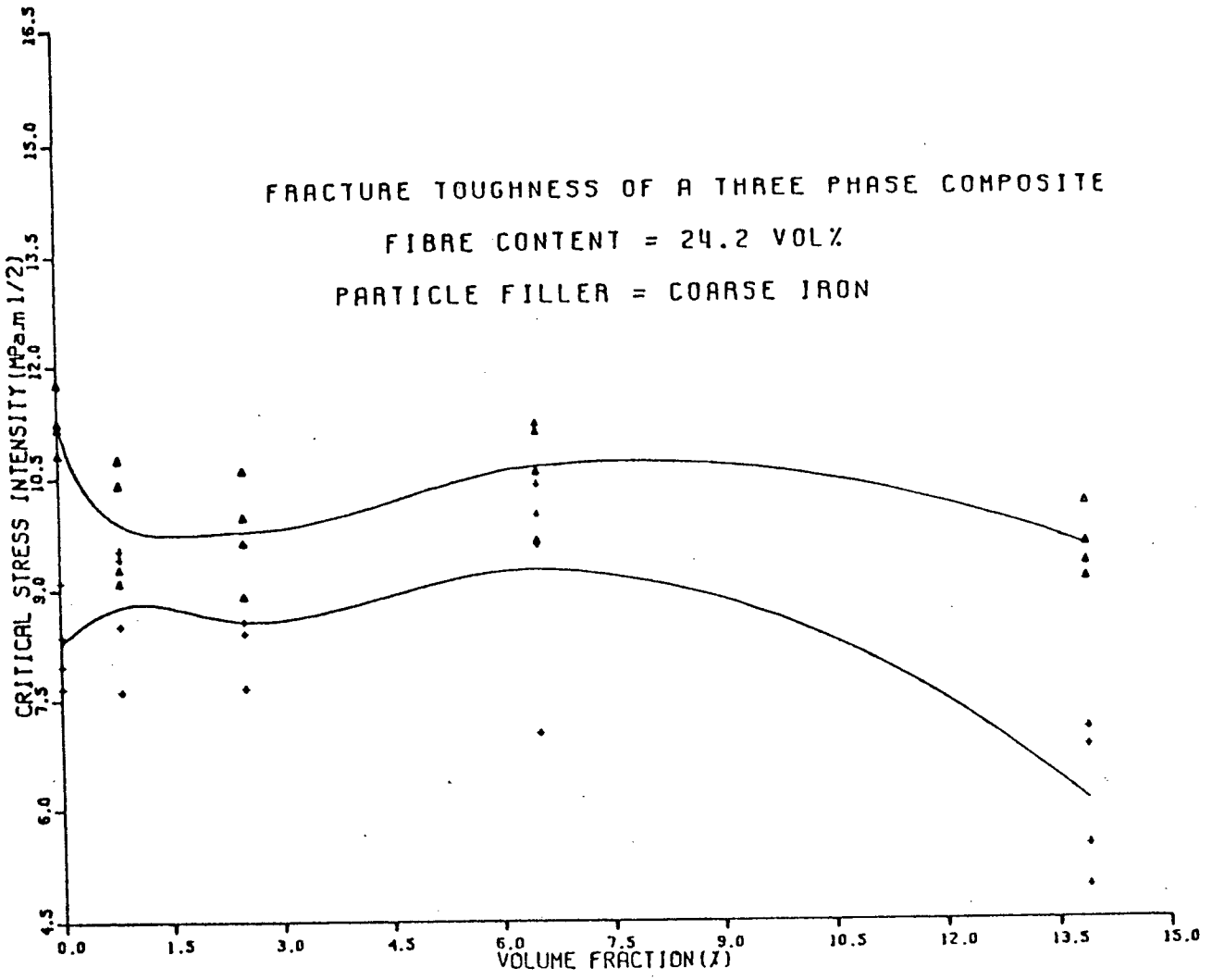

FIG. 10. Bending beam fracture toughness of glass reinforced iron filled composite. Glass volume fraction is 24.2%.

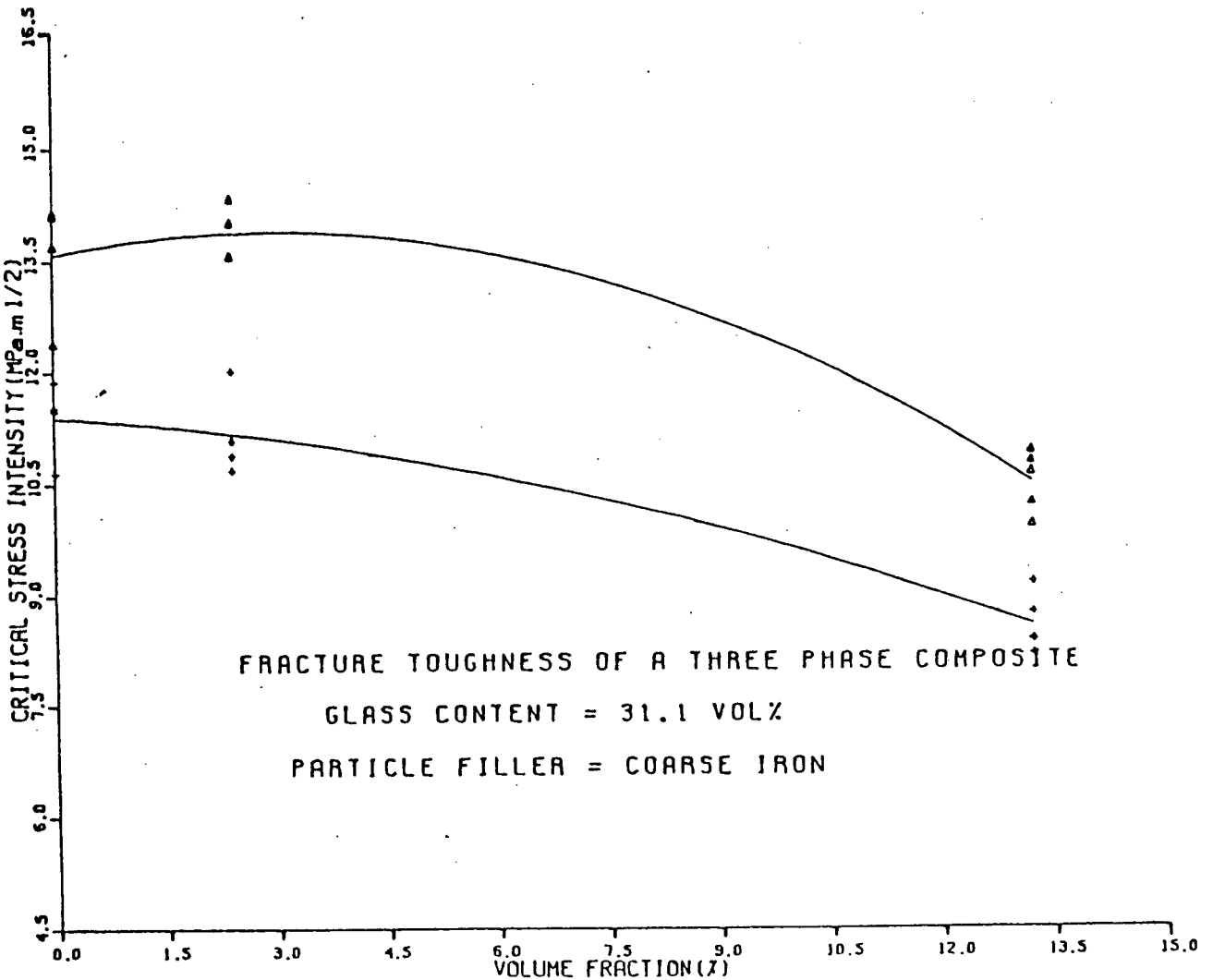

FIG. 11. Bending beam fracture toughness of glass reinforced iron filled composite. Glass volume fraction is 31.1%.

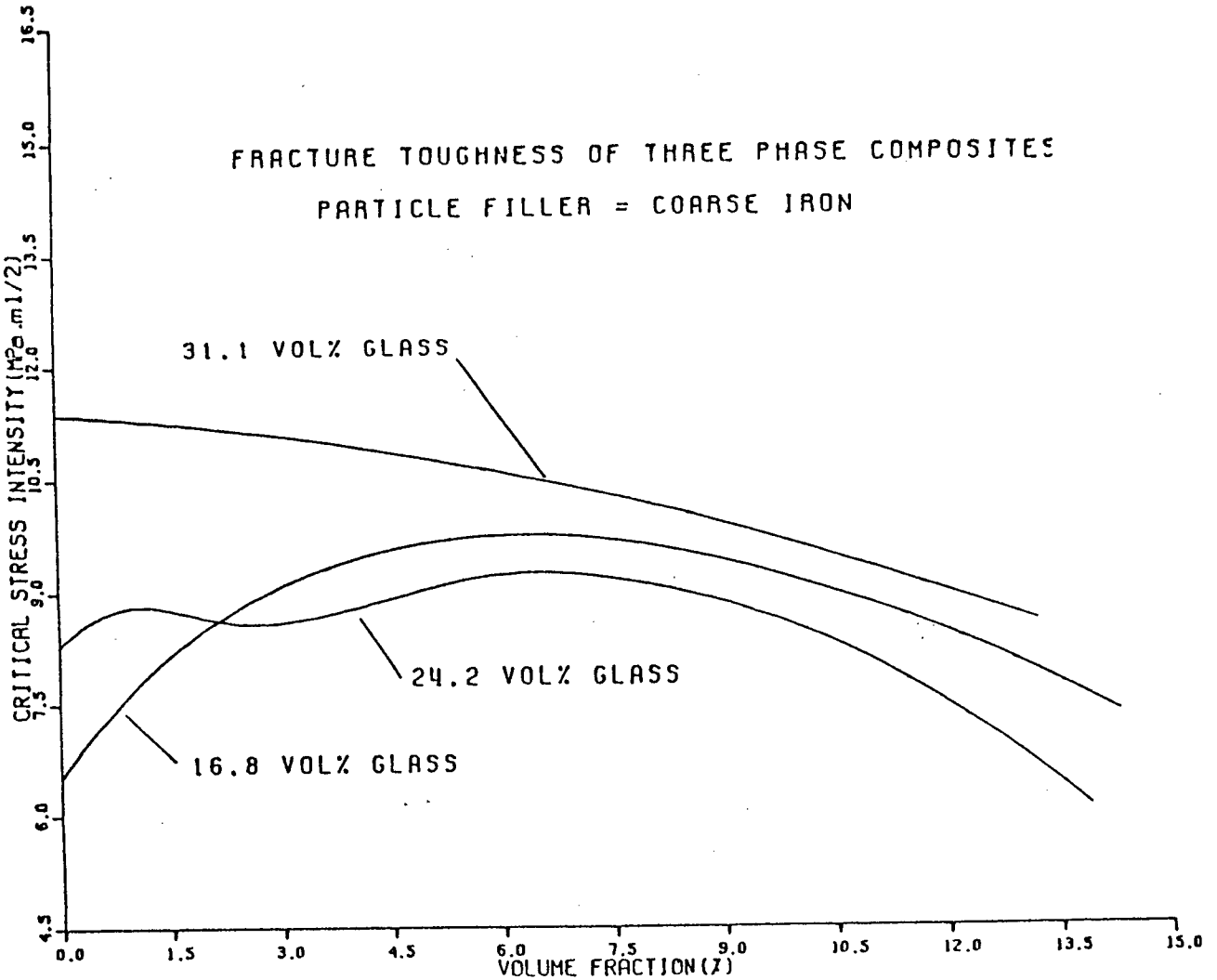

FIG. 12. Comparison of K_q values of glass reinforced iron filled composites.

is reduced by approximately 25%, when the volume content of iron powder is increased from 0 to 16%.

2.2.4 Microscopic Observations:-

Micrographic observations of all the composites mentioned before were made on polished interior surfaces. The micrographs shown in Figs.13-14 indicate the nature of particle distribution observed in powder filled composites. In coarse powder composites a uniform distribution of particles was observed. In contrast, aggregates of particles were observed within the matrix of fine nickel filled composites. These aggregates or clumps of fine nickel were also observed in composites containing both iron and nickel together.

Micrographs of three phase composites show the distribution of particles, as well as fibres, within the resin matrix. Here again, clumping was observed in composites incorporating fine nickel powder. Regions of different distribution densities were observed on polished surfaces of these composites.

Fractographic observations were made using a scanning electron microscope. Matrix cracking and fracture along the paths of particle-matrix interfaces were

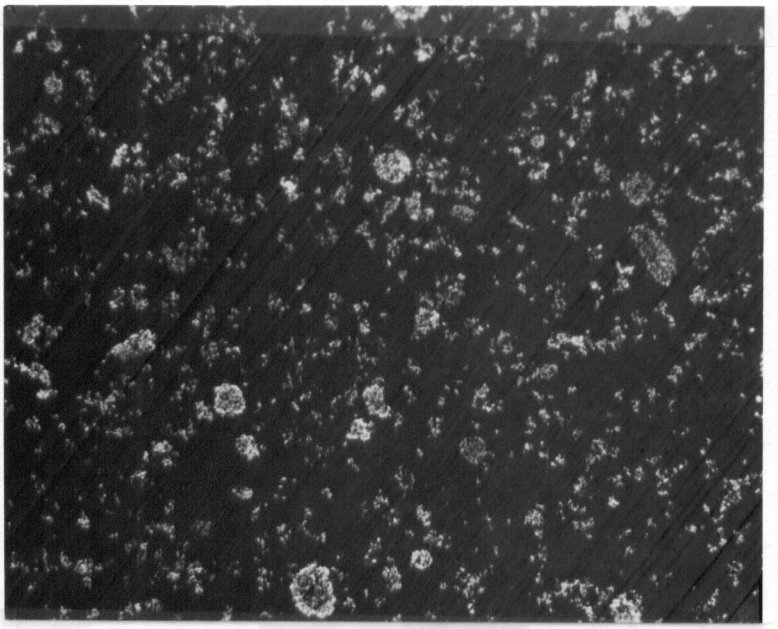

(a). 5.0 volume % fine Nickel (X 200)

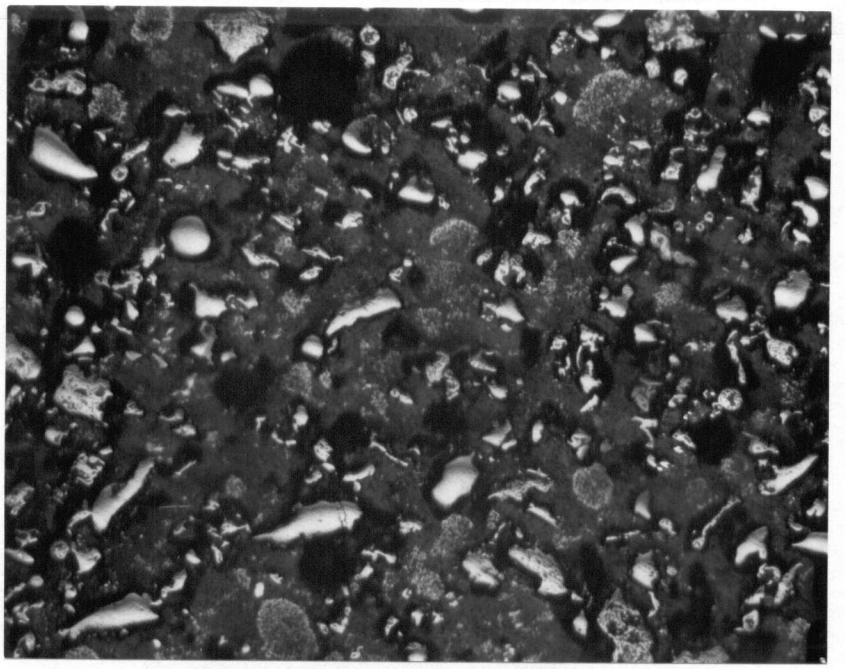

(b). 5.0 volume % fine Nickel
plus 20.0 volume % Iron (X 200)

FIG. 13. Micrographs showing the nature of particle distribution in powder composites.

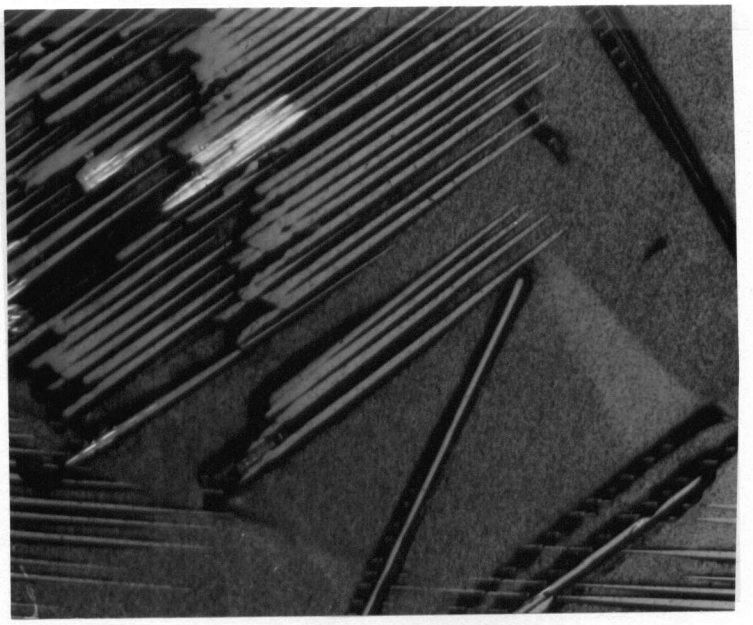

(a). 24.2 volume % Glass (X 200)

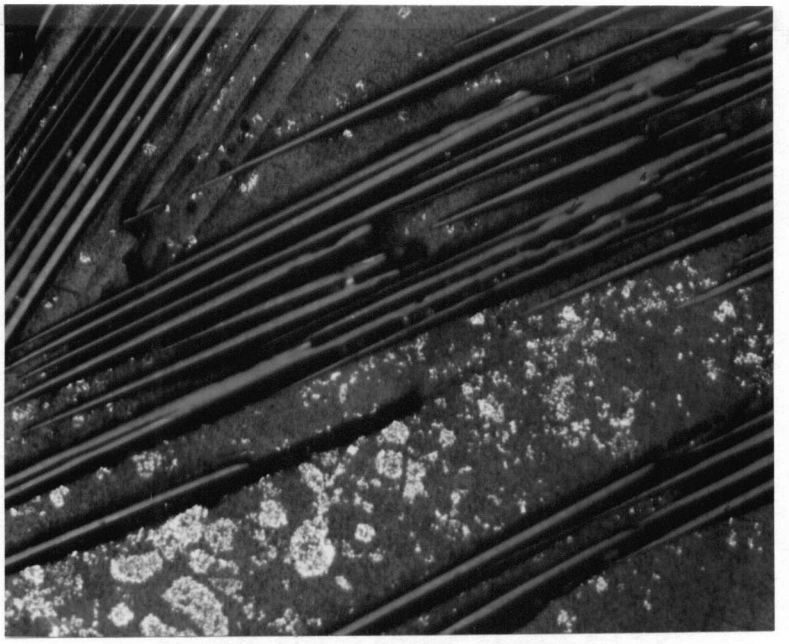

(b). 24.2 volume % Glass
plus 25.0 volume % fine Nickel(X 200)

FIG. 14. Micrographs showing the nature of fibre distribution and particle distribution in fibre reinforced composites.

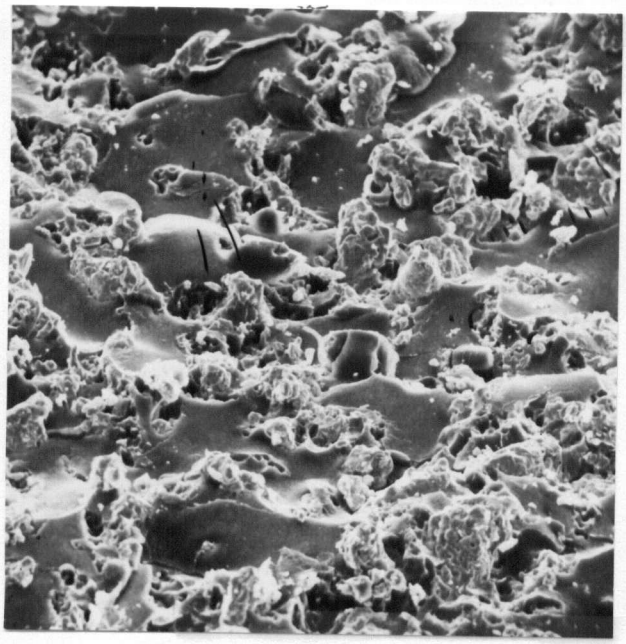

(a). 25.0 vol% coarse iron
magnification = 200

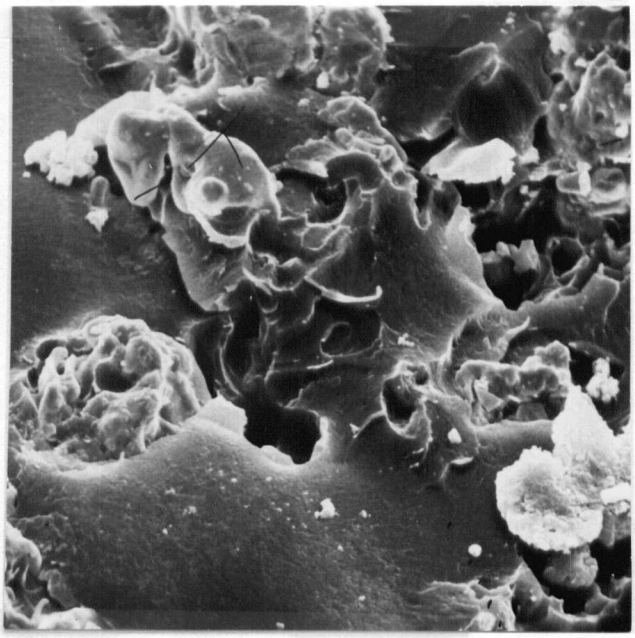

(b). 25.0 vol% coarse iron
magnification = 800

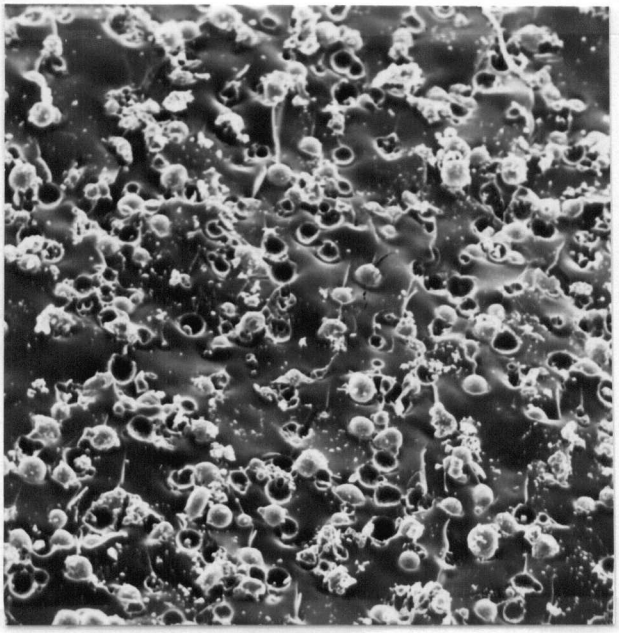

(c). 20.0 vol% coarse nickel
magnification = 80

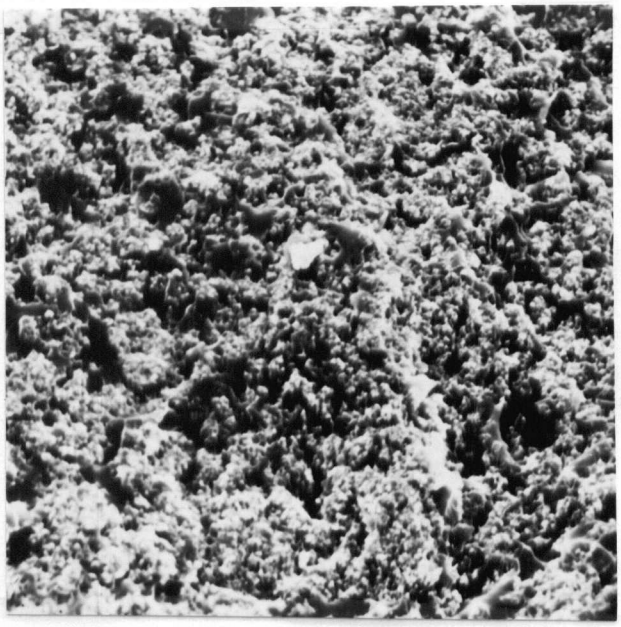

(d). 20.0 vol% fine nickel
magnification = 800

FIG. 15. Fractured surfaces of powder composites.

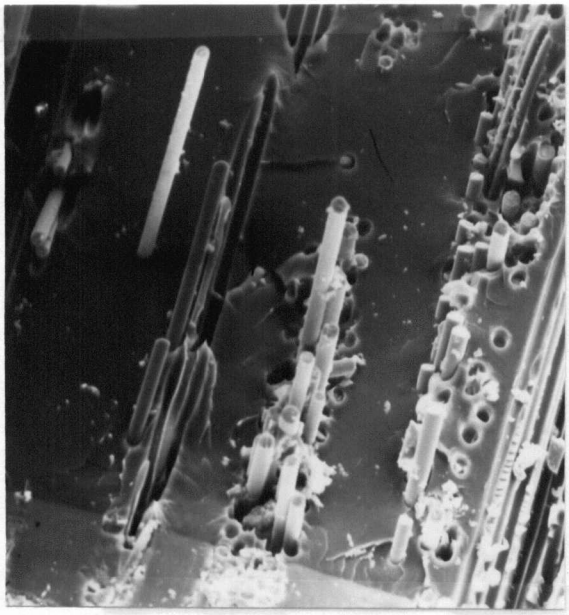

(a). 24.2 vol% Glass
magnification = 200

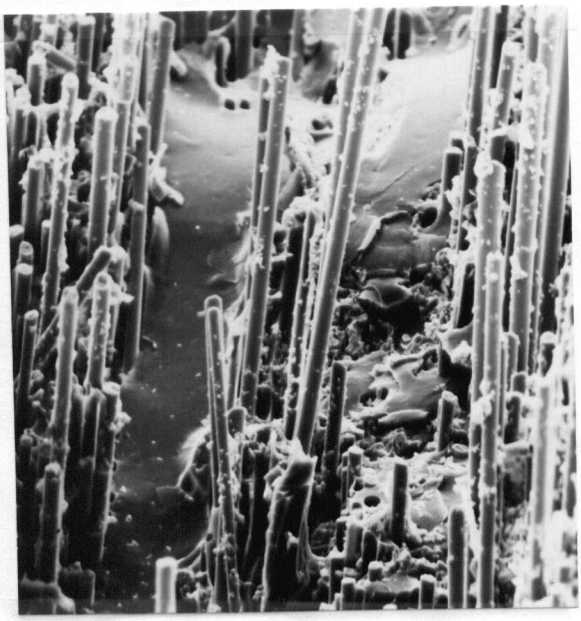

(b). 2.5 vol% iron plus
24.2 vol% Glass
magnification = 200

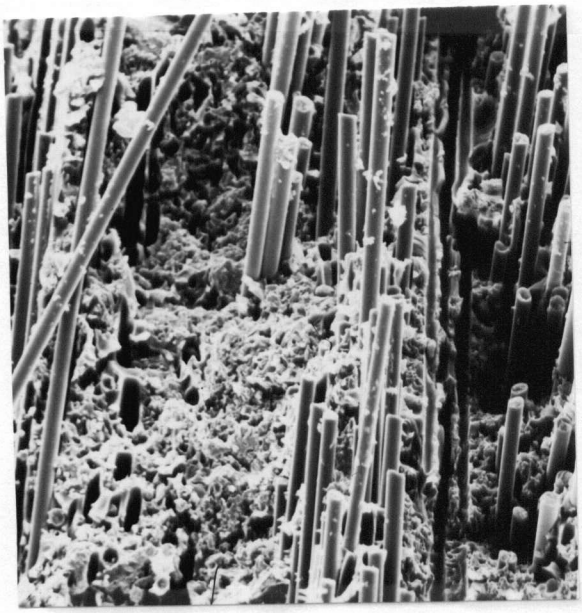

(c). 13.9 vol% iron plus
24.2 vol% Glass
magnification = 200

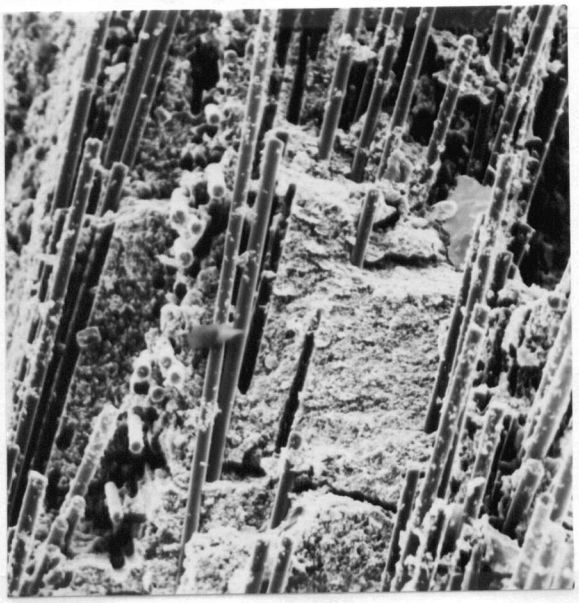

(d). 14.1 vol% fine nickel
plus 24.2 vol% Glass
magnification = 200

FIG. 16. Fractured surfaces of fibre reinforced composites.

prominent in two phase powder composites. Fracture steps were seen on the surfaces of coarse nickel composites. These steps, associated with some of the particles, were present on the side opposite to that which faced the moving crack front.

In fibre composites fibre pull-out was usually observed. The pull-out length varied extensively. Fibres sticking out at different angles from fracture surfaces were always observed on these composites. In three phase composites loose particles were observed on the surfaces of pulled out fibres. The failure of the matrix surrounding the fibres exhibited features similar to that observed in two phase powder composites.

2.2.5 Compliance Method of Fracture Toughness Determination:-

As mentioned previously in Section 2.2.3, a compliance calibration of stress intensity was done in order to check the accuracy of Equation 2.1, in calculating the critical stress intensity of presumably anisotropic composites of glass fibre. The calibration was done for the entire range of volume fractions of composites containing only glass fibres and for composites containing glass fibres and nickel powder, up to a volume fraction of 3% in

the latter.

Specimens for calibration were cut from the same original castings used to make fracture toughness test specimens of the above compositions and volume fractions. These were prepared in exactly the same way as described in Section 2.2.1 maintaining the same dimensional accuracy of ±0.020 cm. in cross-sectional dimensions. The initial centre notch made was much less deep than that mentioned in Section 2.2.1 and was around 0.400 cm. The crack length was measured from the notched edge of the specimen to the crack front on each side, using a travelling microscope and the average of these values was recorded.

The specimens were loaded on the MTS using the same fixture mentioned in Section 2.2.2 and a span of 5.6 cm. Loading was continued up to about 40 lbf. and a load-displacement record was obtained on a Honeywell recorder. The specimen was removed and the centre notch was extended using the Diamond wheel. After measuring the new crack length it was loaded again as before, and another record of load- displacement was obtained. This was repeated several times extending the crack by at least 0.1 cm. each time, except near the regions of nominal crack length used for actual fracture toughness testing, when steps of approximately 0.05 cm. were used. The records thus obtained for load- displacement were used to calculate the compliance, by measuring the slope of the linear portion of

the plot, neglecting the initial non-linearity. For each crack length a compliance value was computed, and a similar set of values generated for all composites mentioned earlier.

In order to verify whether the displacements recorded on the Honeywell plots had reflected the true specimen displacements, the recorded displacements were compared with an accurate, independent measurement of the specimen deflections. A travelling microscope was used to measure the vertical deflections of the mid-point along the centre line of an unnotched specimen during loading. The machine was stopped several times during loading and a quick measurement of the deflection was obtained on the microscope. At the same time the corresponding displacement on the Honeywell plot was also recorded. After repeating this several times up to a total specimen deflection of about 0.3 mm. the two sets of values were compared. A close agreement was found to exist between the two methods of specimen displacement measurements. Accordingly, the displacements recorded on the Honeywell plots which were used to compute the compliance were considered to reflect the actual specimen displacements.

The compliance plots shown in Figs.17-18 were obtained by fitting in each, a polynomial function through the set of experimental values of the compliance and the crack length, using a least squares technique. The choice

of a least squares technique is appropriate when the random errors in the dependent variable have a normal distribution. First derivatives of these polynomial functions were then computed for measured crack lengths of specimens used for actual fracture toughness testing, mentioned in Section 2.2.2, and substituted in the following equation to obtain the critical strain energy release rate, G_{IC}. A derivation of this formula is given in Appendix E.

$$G_{IC} = \frac{P_B^2}{2B^2} \cdot B^* \left(dC_B^*/da \right) \qquad (2.2)$$

where,

B^* = Thickness of the specimen used for compliance calibration.

B = Thickness of the specimen used for actual fracture toughness testing.

P_B = Fracture load.

C_B^* = Compliance of a specimen of thickness B^*.

The values of Young's modulus determined experimentally, as described in Section 2.3 were used in conjunction with critical strain energy release rates to compute the critical stress intensity factors, according to the formula,

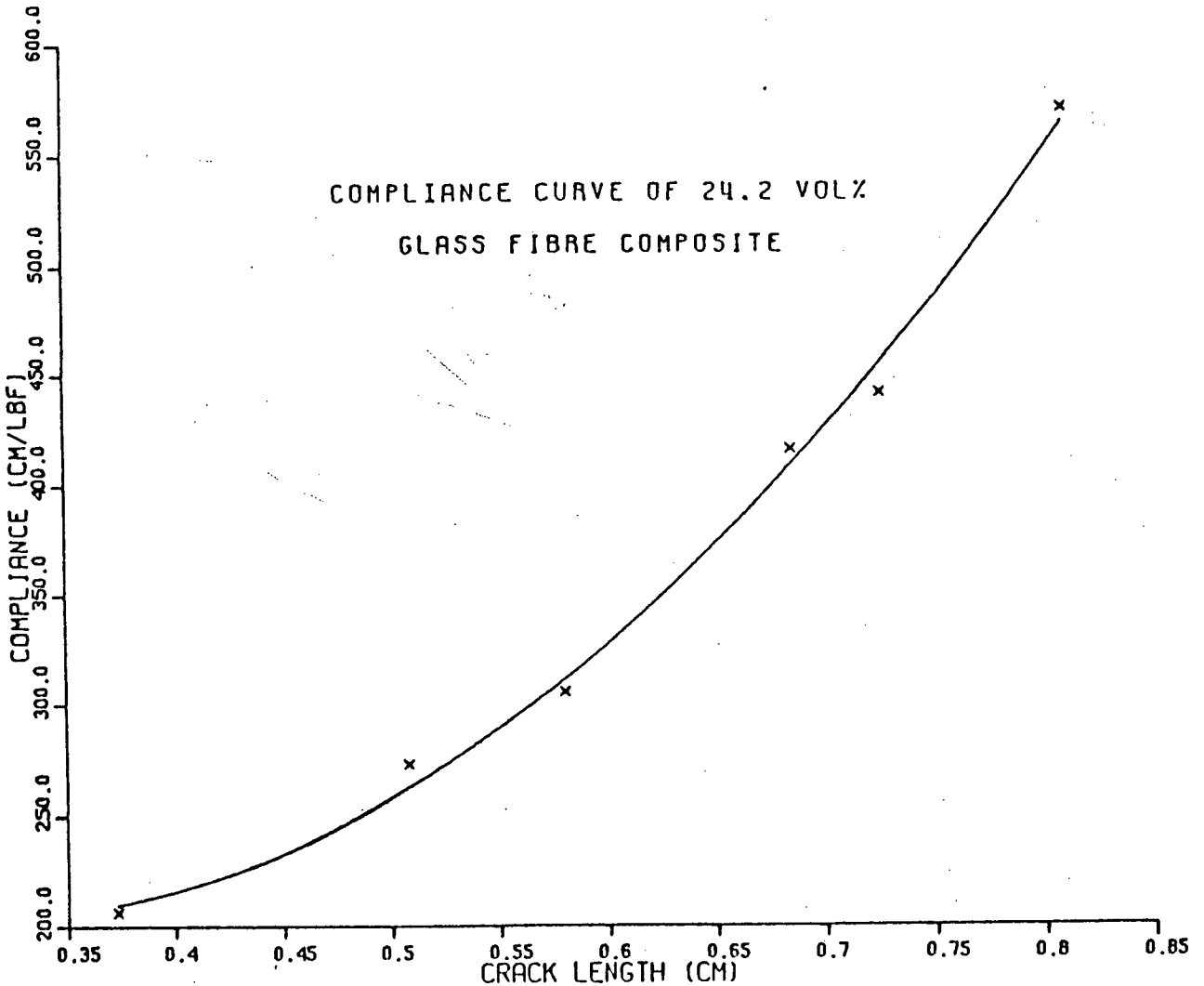

FIG. 17. A typical experimental compliance plot for a glass reinforced composite.

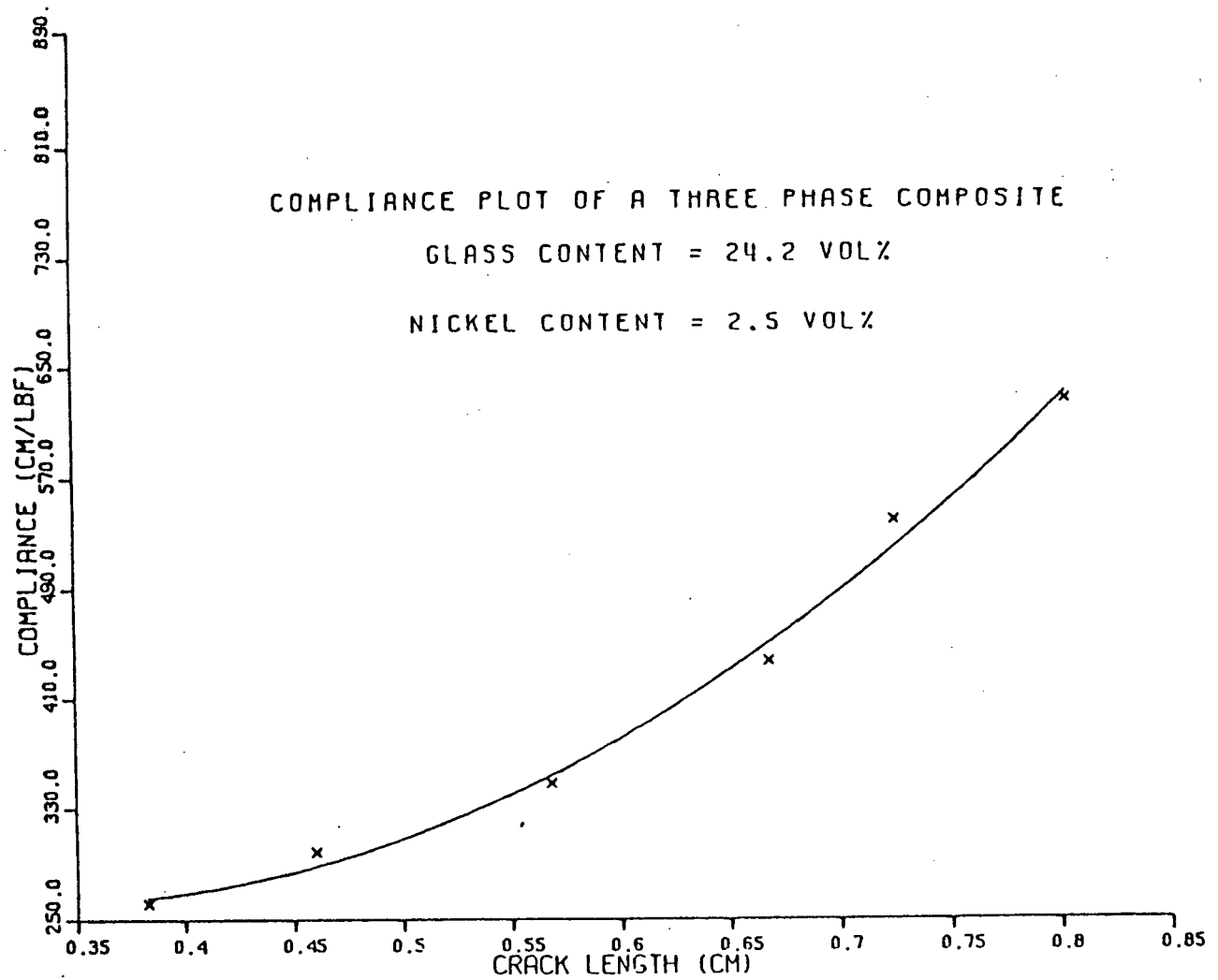

FIG. 18. A typical experimental compliance plot for a glass reinforced nickel filled composite.

$$K_{IC} = \sqrt{(EG_{IC})} / \sqrt{(1-\nu^2)} \qquad (2.3)$$

A value of 0.3 was assumed for the Poisson's ratio v. The values of K_{IC} calculated accordingly, for composites containing only glass fibres and composites of glass and nickel, have been plotted against the volume fractions of glass and nickel respectively, in Figs.19-20. The corresponding values of Kmax and Kq have also been included in these diagrams for comparison. The curves drawn pass through the averages of these values and show the best parabolic fit for regions in between the experimental values. It is evident from these diagrams that in composites for which this calibration was done, a good correlation exists between the calculated values of Kq and the values of stress intensity obtained by the compliance method. For example, at 24% volume fraction of glass fibres the compliance values were within ±18% of Kq of these specimens containing upto 3% of nickel powder. They seem to agree in terms of their order of magnitudes. Assuming that it holds true for all composites containing both glass and metal powders, the values of Kq can be considered to reflect the actual resistance of these materials to crack propagation.

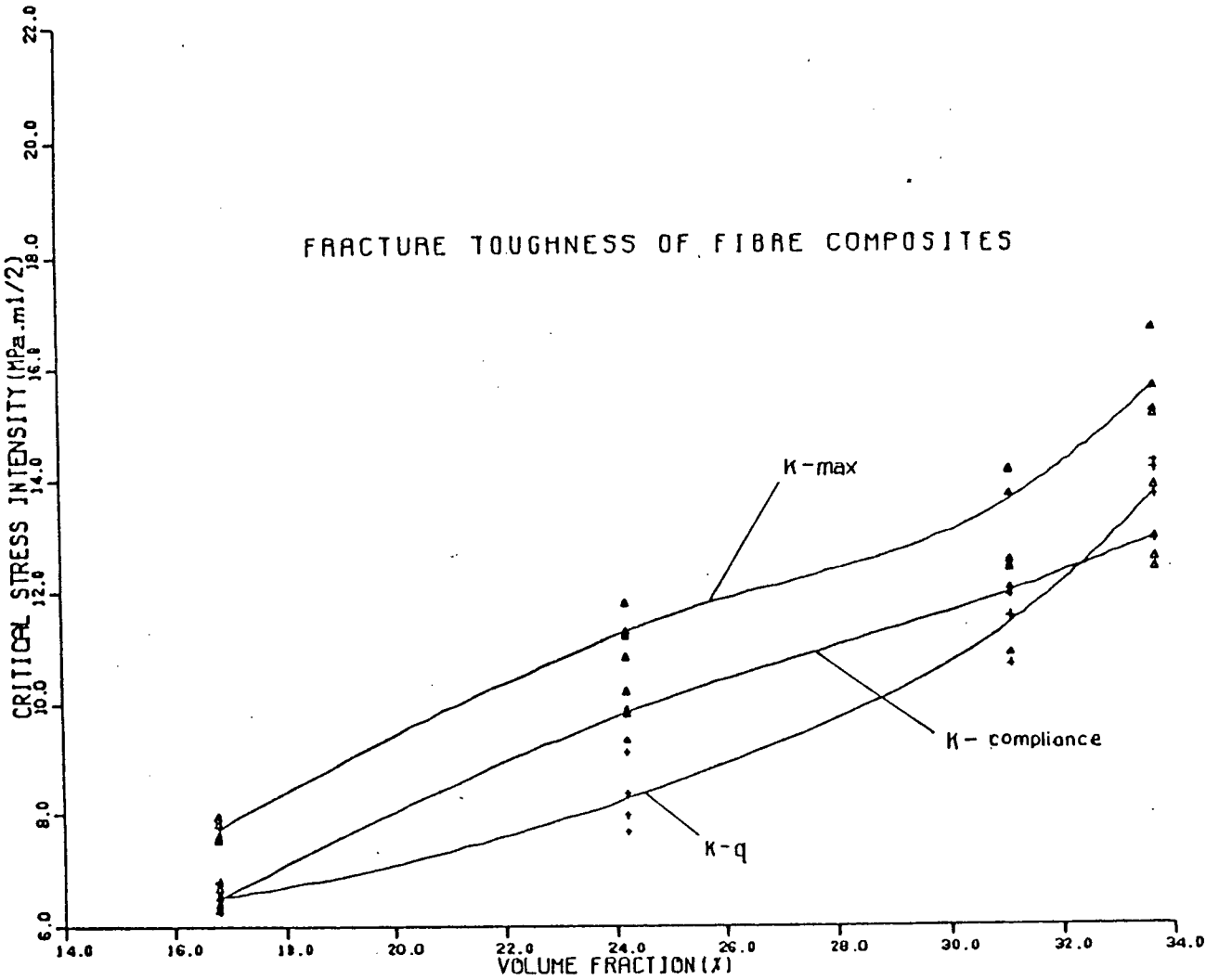

FIG. 19. Comparison of experimental values of fracture toughness of glass fibre composites with the corresponding compliance values.

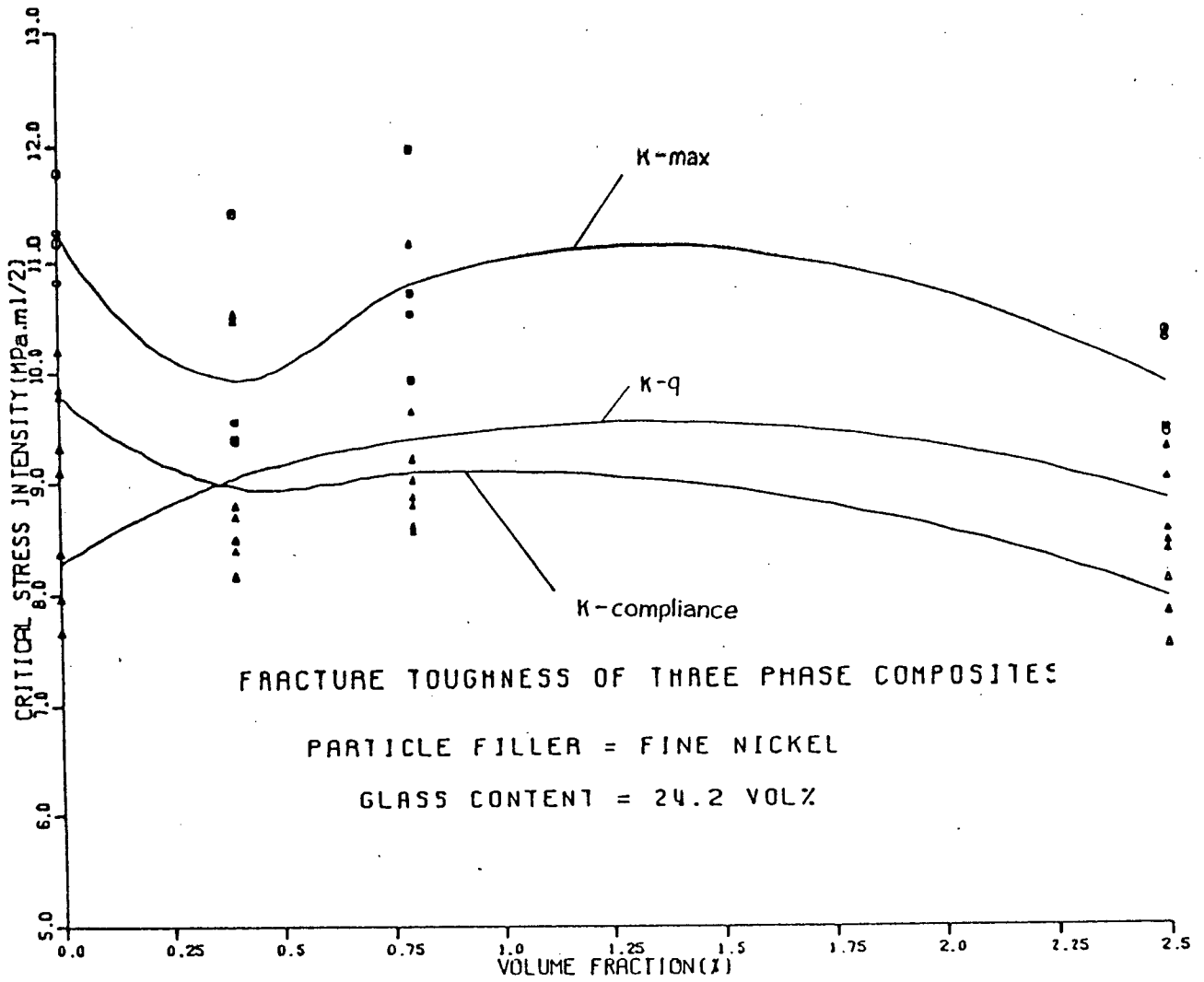

FIG. 20. Comparison of experimental values of fracture toughness of glass reinforced nickel filled composites with the corresponding compliance values.

2.3. DETERMINATION OF YOUNG'S MODULUS:-

The elastic moduli of some fibre composites were determined experimentally, in order to calculate the critical stress intensity factors using the compliance calibration procedures described in Section 2.2.4. This was done for the entire range of volume fractions of composites containing only glass fibres and for composites containing glass fibres and nickel powder, up to a volume fraction of 3% in the latter.

Test specimens were cut from the original castings used to make bending beam specimens for fracture toughness testing. These were prepared in exactly the same way as described in Section 2.2.1 maintaining the same dimensional accuracy of ±0.020 cm. in cross-sectional dimensions. The cross sectional dimensions of each specimen were measured accurately using a Vernier caliper, to the nearest 0.025 mm.

The specimens were loaded on the MTS using the same fixture mentioned in Section 2.2.2 and a span of 5.6 cm. The specimen was loaded at a constant loading rate and a load-displacement record was obtained on a Honeywell recorder. A travelling microscope was also used to measure the vertical deflections of the mid-point along the centre line of the unnotched specimen. The machine was stopped several times during loading and a quick measurement of the deflection was obtained on the microscope. At the same time the corresponding

load recorded on the Honeywell plot was also noted. This was repeated several times up to a maximum load of about 150 lbf.

These values were then used to make a plot of load on specimen against the deflection and the slope of the straight line which passes through these points was used to calculate the young's modulus E, according to the formula,

$$E = \text{SLOPE}. \frac{l^3}{4\ B\ W^3} \tag{2.4}$$

where,

l = Span

W = Width of the specimen

B = Specimen thickness

The elastic moduli of the composites used for the compliance calibration are listed in table IV.

Table IV. Elastic Moduli of some Fibre Composites:-

Fibre Composite	Elastic Modulus (GPa)
16.8 Vol% Glass	4.60
24.2 Vol% Glass	5.87
31.1 Vol% Glass	7.35
33.7 Vol% Glass	8.89
24.2 Vol% Glass + 0.4 Vol% Ni	6.32
24.2 Vol% Glass + 0.8 Vol% Ni	6.28
24.2 Vol% Glass + 2.5 Vol% Ni	4.77

III. INJECTION MOULDED BENDING BEAMS

A bending beam specimen configuration was used to study the fracture toughness of injection moulded composites containing randomly oriented chopped glass fibres of 3 mm. average length in a polyester matrix. A high pressure injection moulding technique had to be employed to achieve high volume fractions in chopped fibres. A number of attempts were made to fabricate these composites by means of a simple moulding process, but none of them was successful in producing a satisfactory casting that contained a high volume fraction of glass fibres with little or no voids. Incomplete wetting of fibres too was a problem that could not be avoided on many occasions. Hence a high pressure injection moulding technique was proposed and an equipment was built to fabricate composite specimens of a bending beam geometry. This proved to be a satisfactory way of making these chopped fibre resin composites. Specimens were made containing fibres of volume fractions ranging from about 10% to 30% and tested in the as cast condition.

3.1 PREPARATION OF COMPOSITES:-

3.1.1 Description of Equipment:-

An injection moulding unit was built and used to make rectangular beam specimens of 6.0x1.4x0.7 cm. dimensions. Fig.21 shows the whole assembly put together and identifies various parts. The main parts of this set up are;

a. A cylindrical hopper that holds the catalysed liquid resin mixture and delivers it to the system.

b. A pressure gauge connected to the inlet of the injecting cylinder.

c. An injector consisting of a piston and a cylinder.

d. The mould consisting of a main specimen chamber and a top chamber to accumulate the excess resin, plus a slider-clamp arrangement to ram the fibres in.

For a detailed description of the parts and its assembly procedures the interested reader should refer the Appendix F.

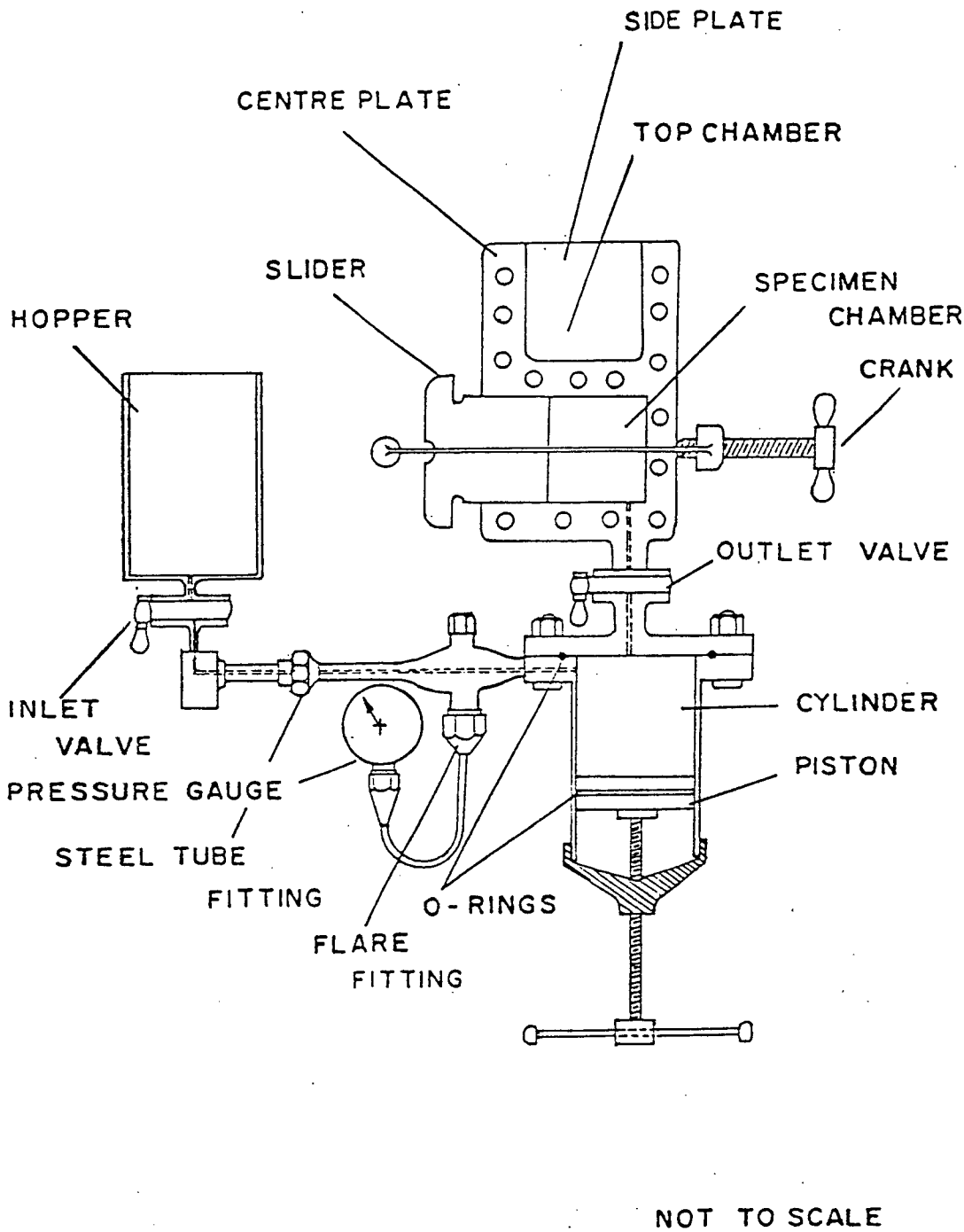

INJECTION MOULDING UNIT

FIG. 21. A detailed view of the injection moulding unit.

3.1.2 Specimen Preparation:-

Fibres for the specimen were prepared by chopping a roving of continuous glass fibre strands into short segments of 2-4 mm. in length, each strand being about 10μm in diameter. These were kept in a closed container and a blast of compressed air was sent in through an opening near the bottom. The turbulance so created caused these fibres to swirl around and orient themselves in a random manner. The container was covered on top with a sieve of mesh size -325 in order to prevent the fibres from escaping.

A weighed quantity of these chopped glass fibres, which yield the intended volume fraction, was then packed inside the specimen chamber of the moulding unit. The slider was pushed into position & clamped and the unit was mounted inside a fume hood. The parts of the mould were sprayed with a mould release agent, before being assembled, in order to faciliate the disassembly and removal of the casting. The cylinder was attached to the base of the mould and the pressure gauge and the hopper were connected to its inlet. The valves were left open and the piston was brought near the top closing the inlet port.

A sufficient quantity of catalysed resin was poured into the hopper and the piston was cranked down, after closing the outlet valve of the cylinder. This caused

the resin to be sucked into the cylinder. The piston was cranked down to its lowest position, making certain that the hopper was not left empty. The inlet valve was closed and the outlet valve was opened. The piston was then cranked up quickly until the pressure built up to at least 350 lbf/in^2. During the subsequent injection the pressure was maintained between 300 and 600 lbf/in^2 by means of intermittent cranking. This was continued until the excess resin filled the top chamber completely. The outlet valve was closed and the inlet was opened to release the pressure inside the injector. The hopper, pressure gauge and the injector were removed and cleaned with acetone. The mould was left undetached inside the fume hood for over 24 hours, allowing the specimen to cure at room temperature. When it was complete the mould was taken apart and the specimen was removed. Fracture toughness tests were carried out on these specimens after at least one week of further curing at room temperature.

3.2 FRACTURE TOUGHNESS TESTING

Since the specimens were tested as cast no machining except the cutting of a centre notch was required. A centre notch of 0.7 cm. nominal depth was made using a diamond wheel of approximately 0.3 mm. thick. The notch was sharpened by

pressing a single edge blade against the tip of the notch, using a small hand press.

3.2.1 Testing & Measurements:-

A minimum of 2 specimens were made for each volume fraction selected. The width and the thickness were measured to the nearest 0.025 mm. using a vernier caliper. The actual width was taken as the average of three measurements made near the centre notch. The thickness was measured at three positions between the crack tip and the unnotched edge of the beam and the average of these measurements was taken as the actual thickness.

The specimens were loaded in three point bending on an MTS, using a span of 5.6 cm. between the centres of the support rolls. The procedure was exactly the same as that adopted for bending beams described in Section 2.2.2 of the previous chapter. Again a constant loading rate of 44.5 N/sec., which produced, at the crack tip, a stress intensity increase rate higher than the minimum rate specified in Sec. 8.3 of ASTM E399-78a, was used. The specimen was loaded to fracture and the load- displacement curves were obtained on a Honeywell recorder and an X-Y plotter. The crack length was measured to the nearest 0.025 mm. using a caliper and the average of three measurements

made along the crack front, one at the centre and the others midway between the centre and the end of the crack front on each side, was taken as the actual crack length.

3.2.2 Calculation & Discussion of Results:-

All specimens exhibited a slight deviation from initial linearity of load- displacement record before reaching the final fracture point, as shown in Fig.4 for one such specimen. Hence, both the maximum load at fracture and the 5% offset value were used for the calculation of critical stress intensity factor, K_{IC}. This resulted in two different values of K_{IC} referred to as Kmax and Kq respectively. The 5% offset value was determined according to the procedures described in Sec. 9.1.3 of ASTM E399-78a and the Equation 2.1 in Section 2.2.3 of the previous chapter was used to calculate the critical stress intensity factor in units of $Mpa.m^{0.5}$.

The calculated values of critical stress intensity factor have been plotted against the volume fraction of glass fibres and are shown in Fig 22. The curves were drawn using a computer routine that employs a parabolic curve fit through the averages of the critical stress intensity factors derived at each volume fraction. Although a large scatter of values is apparent from this

figure the Kmax values show a slight increase with increasing volume fraction of glass fibres. While Kq remain relatively unchanged at or near 3 $Mpa.m^{0.5}$ within the range of volume fractions from 10-30% nearly a four-fold increase over the toughness of pure polyester has been observed. However, the toughening of the polyester by these fibres appears to be much lower than that due to random glass mats discussed in the previous chapter.

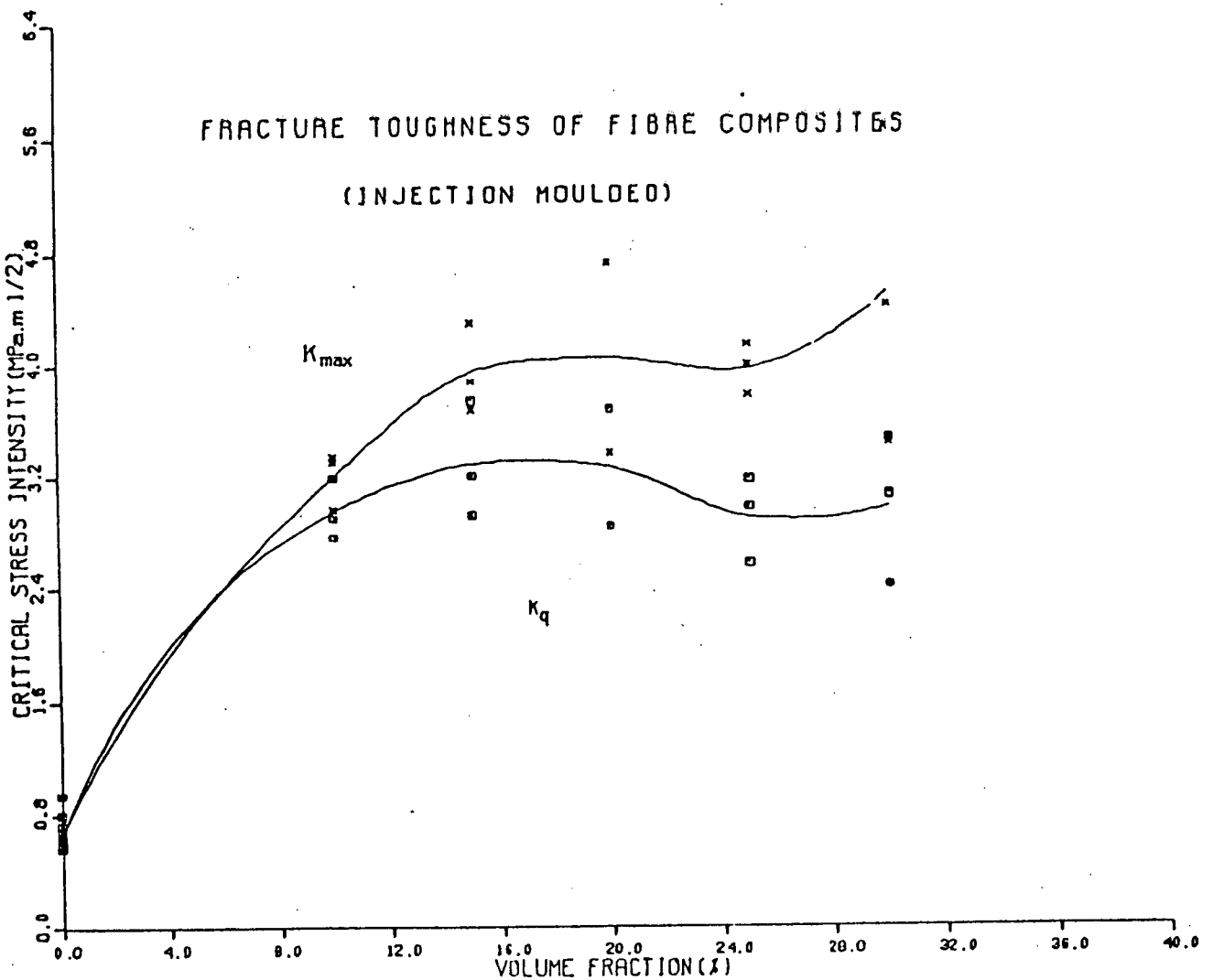

FIG. 22. Fracture toughness of injection moulded bend beam specimens.

IV. CAST COMPACT TENSION SPECIMENS

A compact tension specimen configuration was used to study the fracture toughness of composites containing following particle's over a range of volume fractions in a polyester matrix.

(I). Coarse iron powder.

(II). Coarse nickel powder.

(III). Fine nickel powder.

(IV). Coarse iron & fine nickel powder.

Castings containing each of these in a polyester matrix were made for the volume fractions of interest using a mould and the test pieces were cut from these castings.

The same specimen configuration was used to study the effect of ageing on the toughness properties of pure polyester. Castings of pure polyester, cured for different lengths of time, were used to cut the test specimens.

4.1 PREPARATION OF COMPOSITES:-

The same mould which was used to make the castings described in Section 2.1 was used again. The mould was kept closed in its vertical position. A weighed quantity of powder, predetermined for the intended approximate volume fraction, was mixed with a weighed quantity of liquid resin catalysed just before the addition of powder. The mixture was stirred manually for 5 to 10 minutes to give a uniform mixture and cast into the mould while taking precautions to prevent air bubbles from creeping into the mixture. The mould surfaces were coated with a mould release agent to facilitate the removal of cast composite plate after 24 hours of curing at room temperature. Test specimens were prepared from these castings after at least one week of curing at room temperature.

The castings of pure polyester, which were used to make the test specimens for the ageing test, were made by casting a sufficient quantity of catalysed liquid resin into the mould. These were again removed from the mould after 24 hours and allowed to cure at room temperature for different time intervals.

4.2 FRACTURE TOUGHNESS TESTING:-

4.2.1 Specimen Preparation:-

Compact tension specimens of 7.5x7.5 cm. planar dimensions were cut from the cast plates with a diamond wheel. Fig.23 shows the geometry of these specimens with the nominal dimensions of the notch and the loading holes. The notch was made using a diamond wheel and sharpened by pressing a single edge blade against the tip of the notch. The holes were drilled through the plate, at the positions shown, using a 1/2 in. diameter drill.

4.2.2 Testing & Measurements:-

A minimum of 3 specimens were made for each volume fraction of the powder composites and each curing time of the aged polyester. The thickness B of the specimen was measured to the nearest 0.025 mm. using a vernier caliper, at three positions between the crack tip and the unnotched edge of the specimen, and the average value was recorded. The width, W, from the plane of the centerline of the loading holes to the far edge was measured to the nearest 0.025 mm., at three positions near the notch

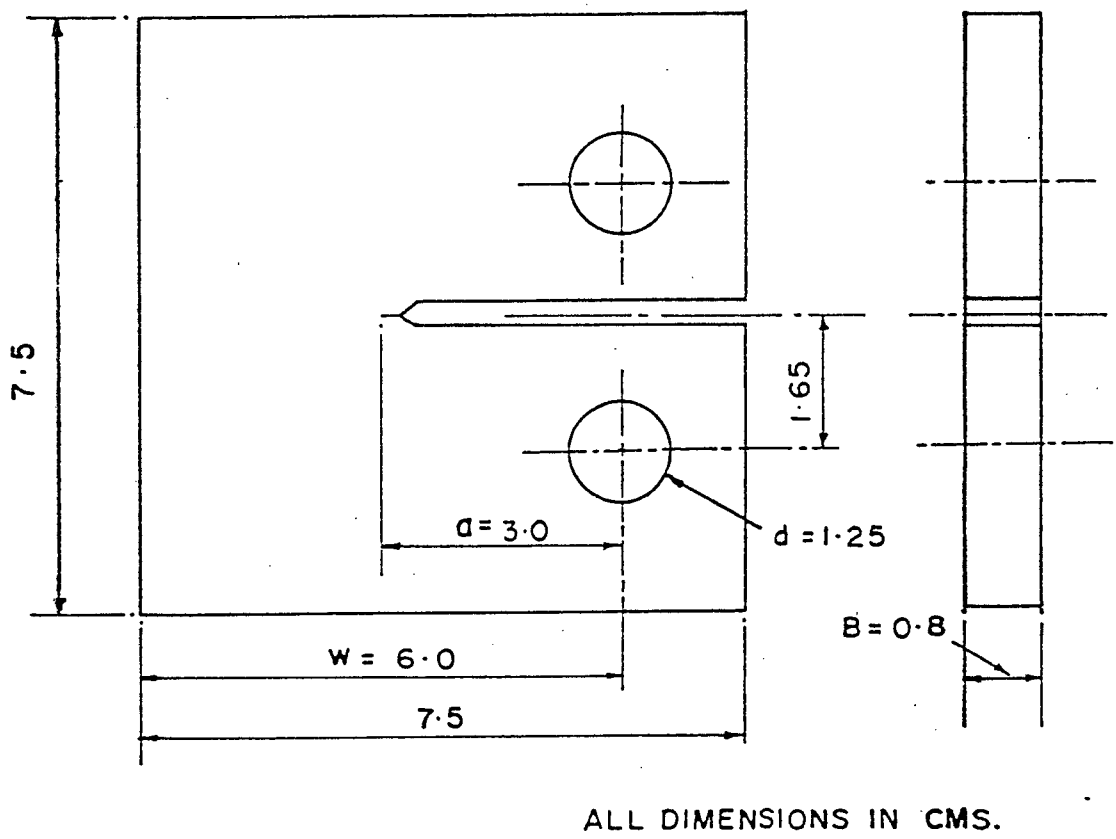

COMPACT TENSION SPECIMEN

FIG. 23. The dimensions of the compact tension specimen used.

location, and the average of these measurements was taken as the actual width.

The specimens were loaded on an MTS and were gripped by a clevis and pin arrangement, at both the top and bottom of the specimen, which allowed rotation as the specimen was loaded. Eccentricity of loading that could result from the incorrect positioning of the specimen was eliminated by centering the specimen with respect to the clevis opening.

The specimen was loaded under a constant loading rate of 44.5 N/sec. until failure and a load displacement curve was obtained on the Honeywell recorder. After the specimen was fractured the crack length was measured to the nearest 0.025 mm. at three positions; one at the centre and the others midway between the centre and the end of the crack front on each side, and the average of these measurements was recorded.

4.2.3 Calculation & Discussion of Results:-

All specimens exhibited a linear elastic behaviour up to the point of fracture. A typical load-deflection curve is similar to that shown in Fig.3. The load at fracture was taken for the calculation of critical

stress intensity factor, in units of $Mpa.m^{0.5}$, using the following equation given in Sec. 9.1.4 of ASTM E399-78a.

$$K_{IC} = \frac{P}{BW^{1/2}} \cdot f(a/W) \tag{4.1}$$

where,

$$f(a/W) = \frac{(2+a/W)(0.886+4.64a/W-13.3a^2/W^2+14.7a^3/W^3-5.6a^4/W^4)}{(1-a/W)^{3/2}}$$

where,

B = Specimen thickness (cm)

a = Crack length (cm)

W = Width of the specimen

P = Maximum load at fracture (kN)

The Figures 24-26 show the values of critical stress intensity factor against the volume fractions of particle fillers. The Fig.27 shows the effect of curing time on the fracture toughness of pure polyester. A smooth curve that passes through the averages of stress intensity factors has been drawn in each, using a parabolic curve fit routine.

It is clear from Fig.24 that with the addition of a very small amount of coarse powder the critical stress intensity factor of the resulting composite drops sharply

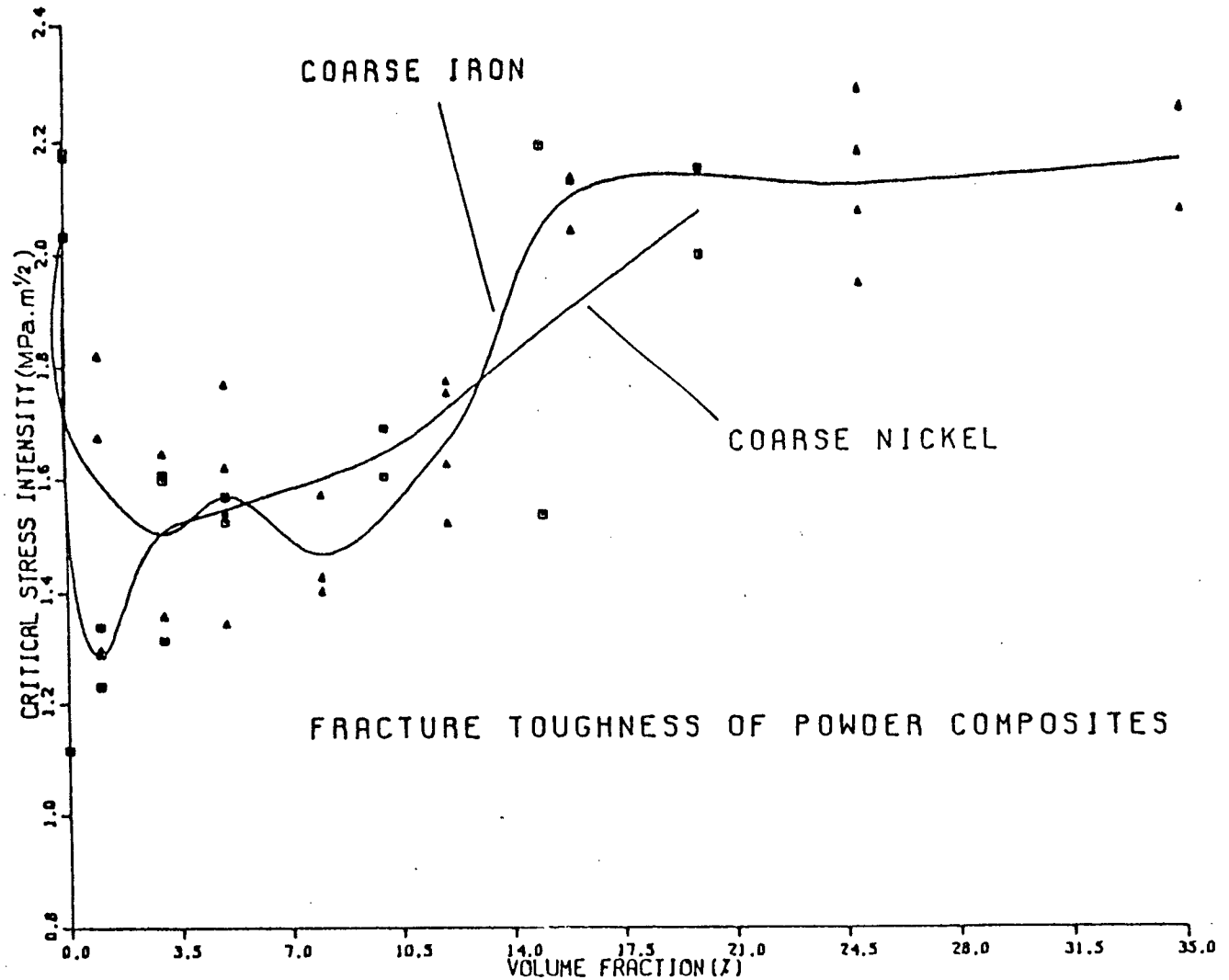

FIG. 24. Compact tension fracture toughness of coarse iron and coarse nickel composites.

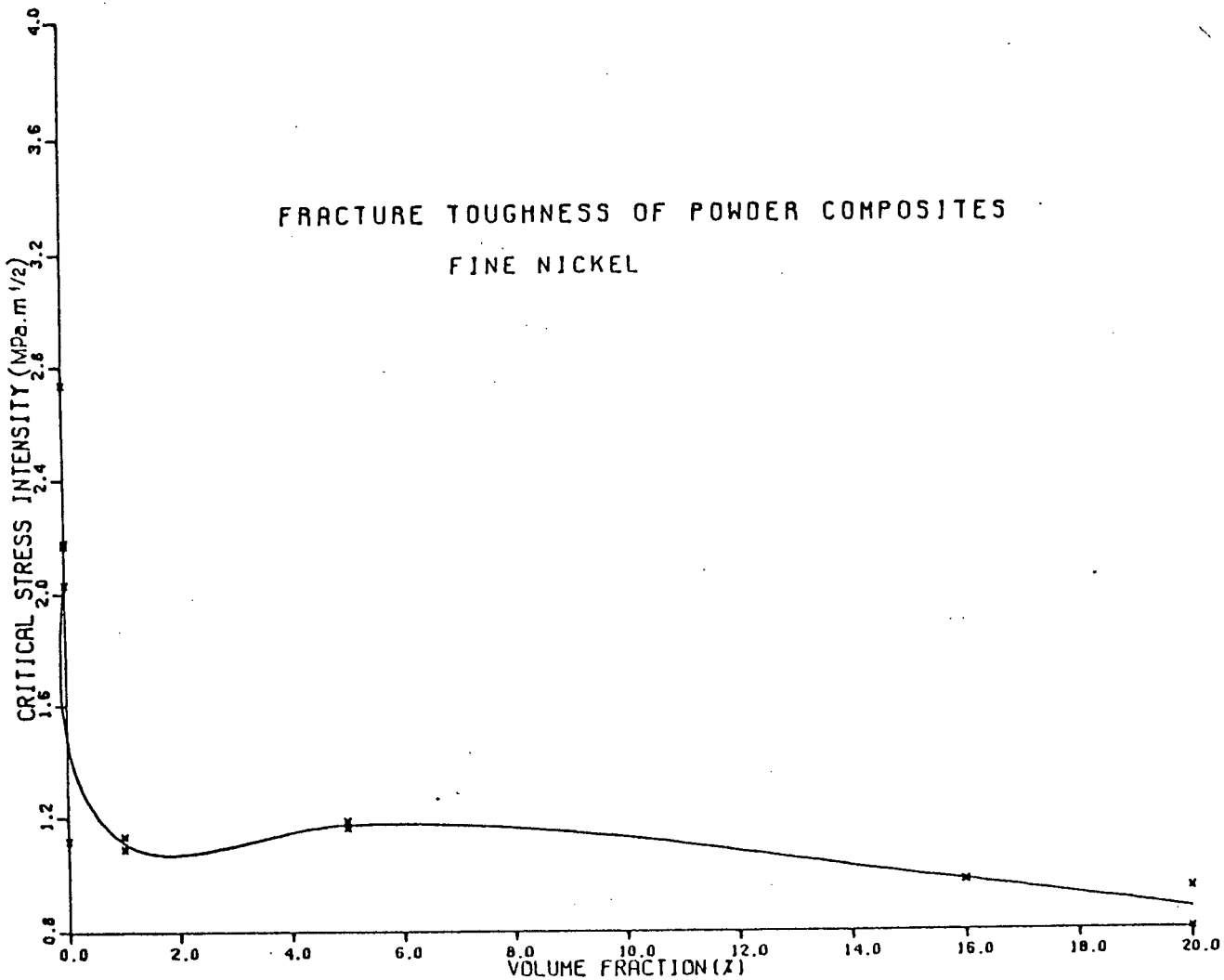

FIG. 25. Compact tension fracture toughness of fine nickel composites.

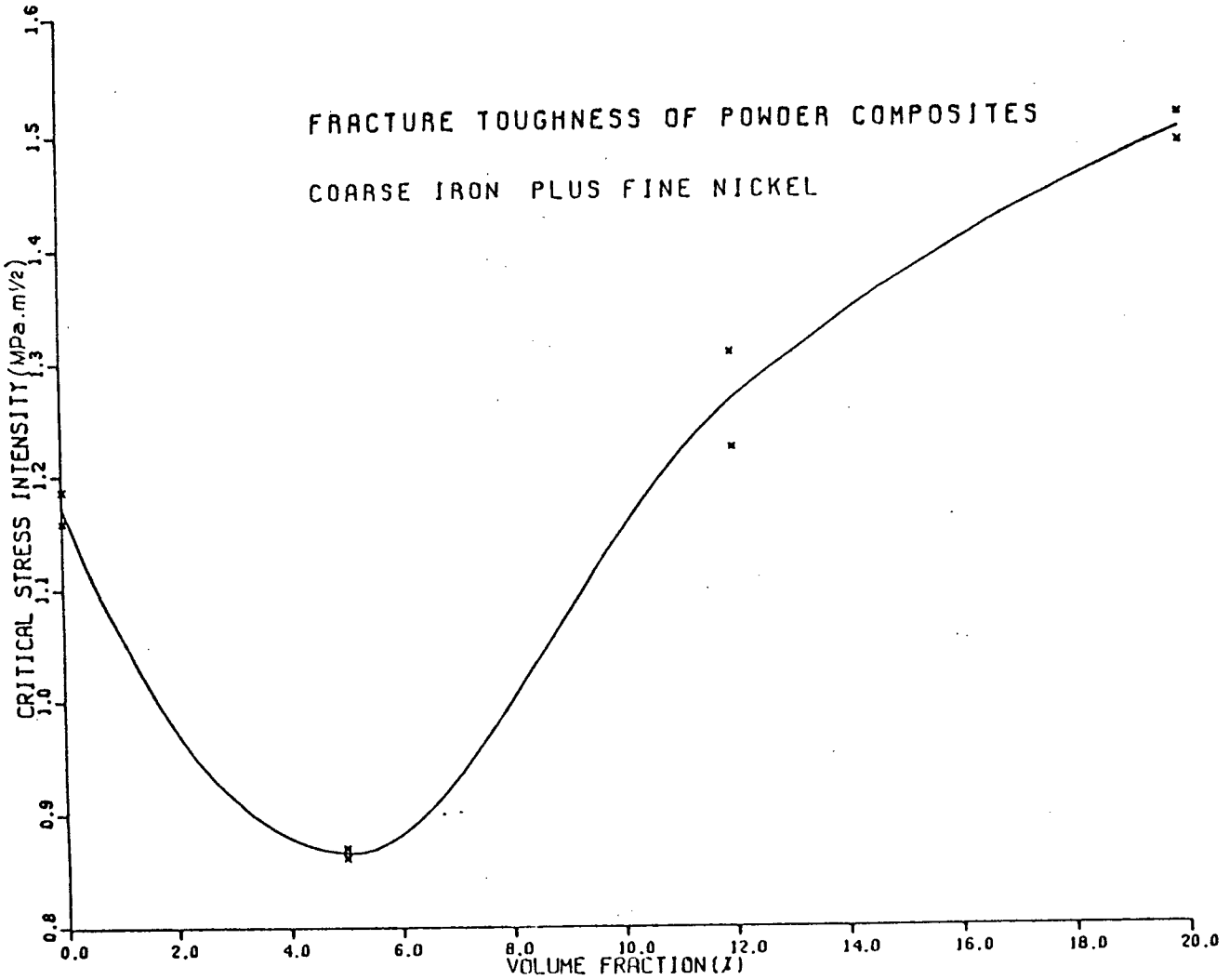

FIG. 26. Compact tension fracture toughness of coarse iron plus fine nickel composites.

from that of the unfilled polyester matrix. This initial reduction is quite distinct and observed in both composites of coarse iron and coarse nickel powder. With further additions the average critical stress intensity factor goes through a period of minimum before increasing again. This increase is about 40% over an average minimum when the filler content is increased to 20% volume fraction. In contrast, a continuous decrease in fracture toughness is observed for those composites which contain only fine nickel powder. Here the decrease is over 50% for 20% increase in volume fraction.

When both types of particles (coarse iron and fine nickel) are present together the overall toughness appears to be lower than that of coarse powder composites, but increased in roughly the same fashion by the addition of the iron powder. In these the volume content of fine nickel powder has been kept constant at 5%. After the initial distinct reduction in fracture toughness approximately 60-70% increase over an average value of 0.8 $MPa.m^{0.5}$ is observed when the volume fraction of iron powder increases from 5% to 20%.

Comparing these results with the bending beam toughness values of Chapter II, it can be inferred that a distinct increase in toughness is observed in all these composites when using a compact tension specimen configuration. At first, there is a marked difference in

fracture toughness observed for the unfilled resin matrix. With compact tension configuration nearly a three-fold increase in fracture toughness over that of the bending beam geometry has been observed. Unlike the bending beam toughness values, the results of the compact tension tests show a decrease in toughness with increasing volume fraction of metal powder. This decrease is more or less continuous in the case of fine nickel powder while an initial reduction plus a subsequent gain is observed in the case of coarse powder composites. The latter is true of all composites containing either coarse iron, or coarse nickel, or coarse iron plus fine nickel. However, the calculated values of critical stress intensity factor in any of these composites, do not in general fall below that of the bending test even at high volume fractions of filler material.

Fig.27 which shows the effect of curing time on the fracture toughness of pure polyester indicates that the curing of the resin would take at least 6-7 days before it leads to stable toughness properties. Therefore it can safely be assumed that the curing process is complete for the purpose of toughness measurements on composites based on polyester resin after at least one week of post-curing.

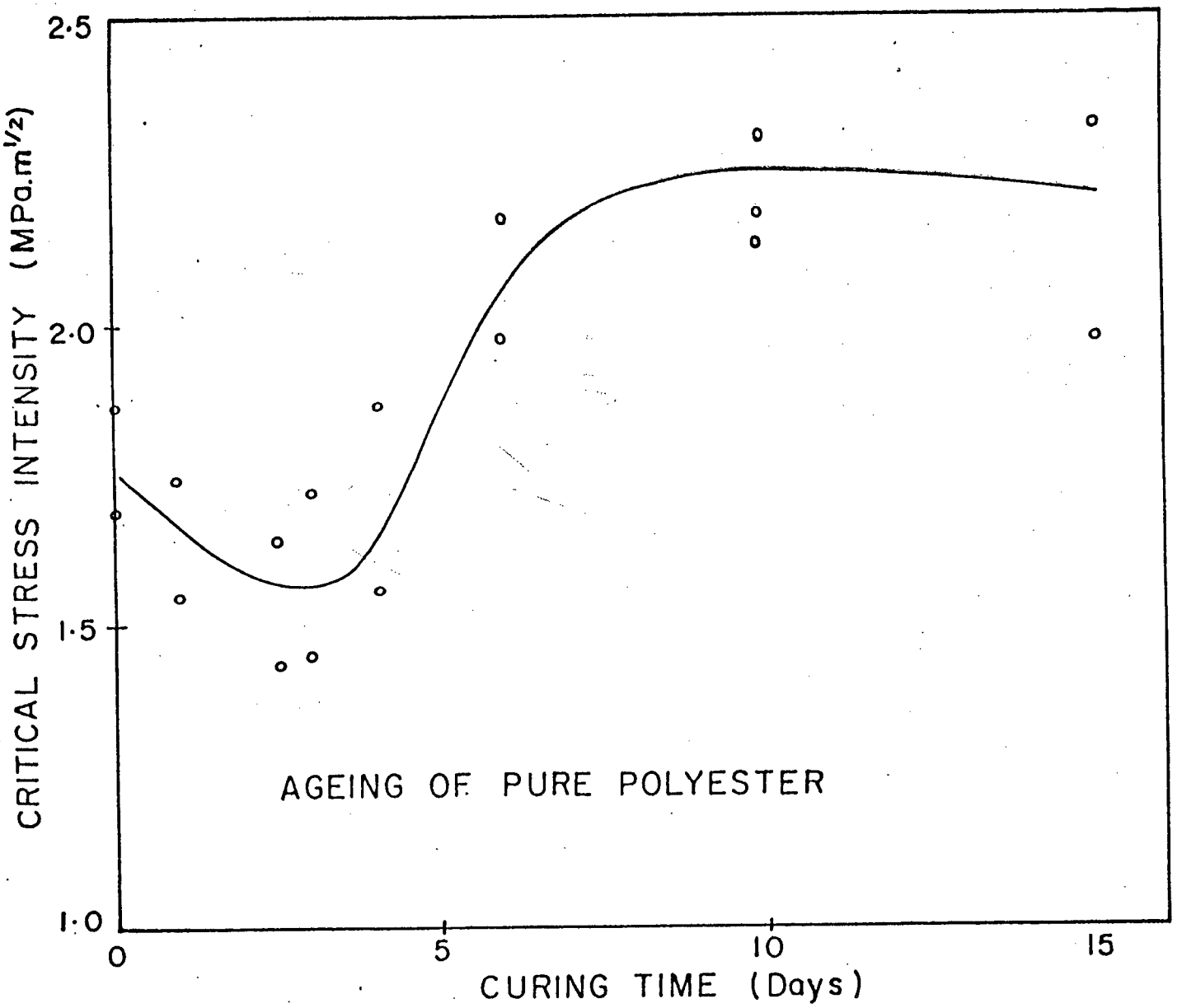

FIG. 27. The effect of curing time on fracture toughness of pure polyester.

4.2.4 Microscopic Observations:-

After the specimens were fractured the fracture surfaces were observed with a scanning electron microscope. The fracture surface topography observed for these composites was essentially same as that observed for bending beam specimens. The discussion of microscopical features of bend specimens, given in Section 2.2.4, applies to these specimens as well.

4.3 CHARPY IMPACT TESTING:-

4.3.1 Specimen Preparation:-

Test specimens of the dimensions shown in Fig.28 were cut from the CTS specimens that have been fractured. The surfaces were ground with Grit 320 silicone carbide paper, in order to achieve the dimensions of a standard subsize charpy impact test specimen within the permissible variations set by ASTM E23. A centre notch of the dimensions shown in Fig.28 was made on those specimens that were to be used for the notched impact test.

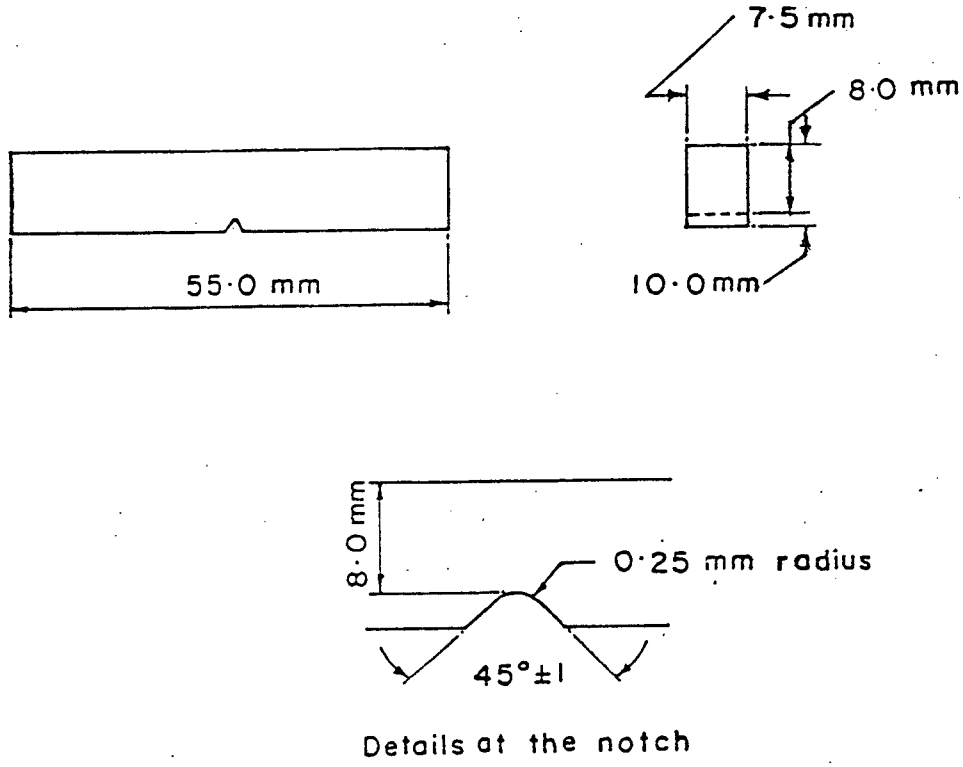

CHARPY IMPACT TEST SPECIMEN

FIG. 28. The dimensions of the charpy impact test specimens.

4.3.2 Testing & Measurements:-

A minimum of 4 specimens were prepared for each volume fraction of powder composites, out of which 2 were notched. The specimens were centered in the anvil with the notched surface or the specimen width lying vertical and the blow was struck on the opposite face fracturing the specimen. The angle of swing of the hammer was measured to the nearest $1/2^{o}$ degree.

4.3.3 Calculation & Discussion of Results:-

The energy absorbed by test specimens during fracture was calculated using the angle measured in above. An allowance was made for the frictional loss which was assumed to be independent of the swing angle. This was estimated by measuring the angle made in a free swing and converting that into energy terms.

The impact energies absorbed per unit area of fracture surface of both notched and unnotched charpy specimens have been plotted against the volume fraction of iron powder in Fig.29. For notched specimens these values are calculated on the basis of remaining cross sectional area at the notch.

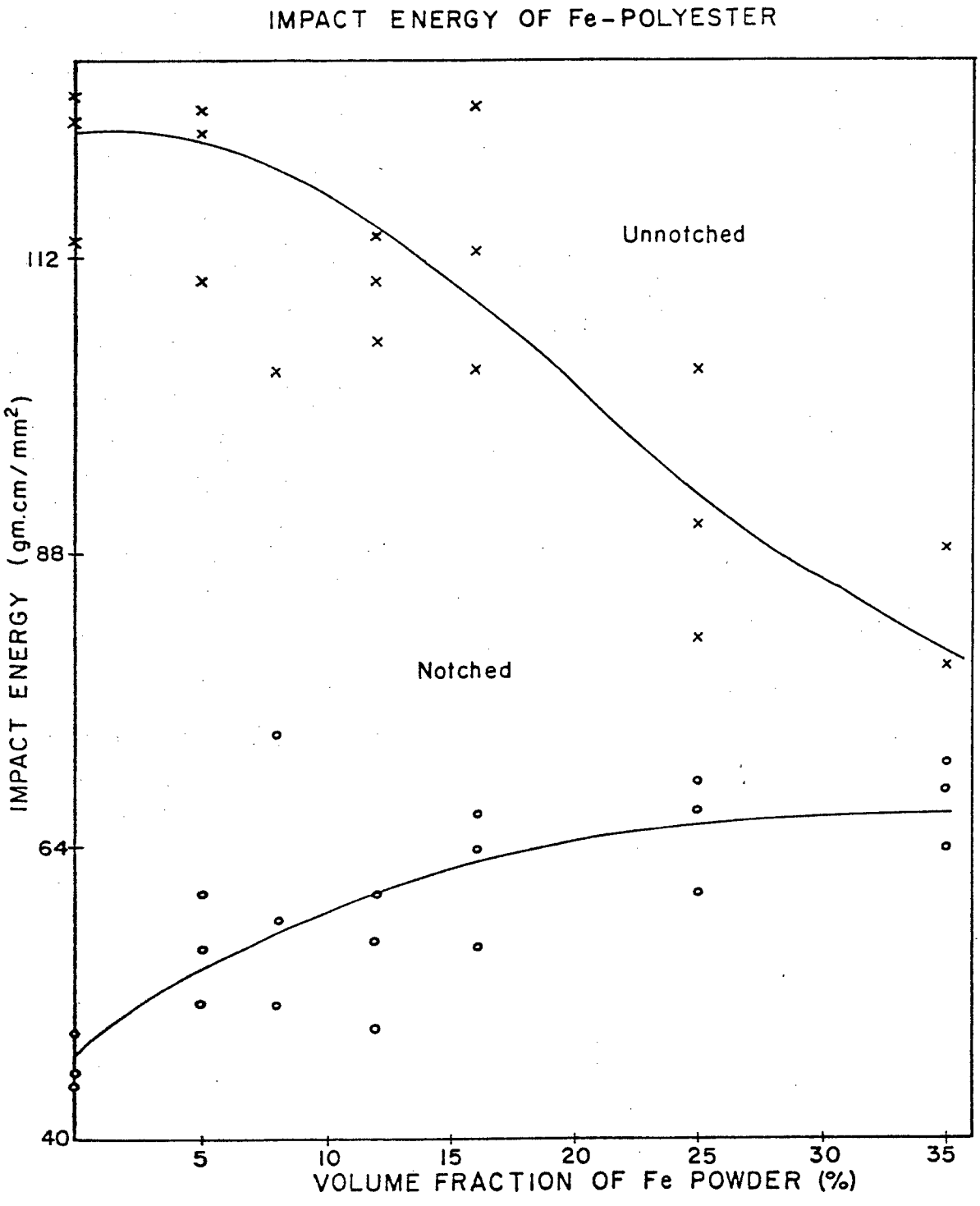

FIG. 29. The impact energy of iron powder composites.

Despite the large scatter of values, a significant difference in notched and unnotched energies has been observed at lower volume fractions of iron powder. This difference is smaller at higher volume fractions, as with the addition of powder the notched values are increased with a corresponding reduction in unnotched energy.

However, it is important to note that all these values are much higher than the fracture surface energies calculated on the basis of experimentally determined K_{IC} values or those reported in the literature. For example, a fracture surface energy of 220 J/m^2 is reported for polyester resin based on work of fracture measurements,[61] which involves fracturing a specimen in a controlled manner and integrating the area under the load-deflection curve. If the tensile modulus of polyester is taken as 1.32 GPa, an average value of 0.7 $MPa.m^{0.5}$ estimated for K_{IC} (from bending results of Chapter II) will yield a fracture surface energy of 185 J/m^2. These values are much smaller than that of the corresponding notch impact test result, which is nearly 2200 J/m^2.

V. DISCUSSION

Injection moulded bend specimens have been prepared only with short glass fibres and the results indicate a relatively unaffected fracture toughness over the entire range of fibre volume fractions. Although the fracture toughness of these specimens is 4-6 times that of the pure resin it was only a fraction (1/6 to 1/3) of that obtained for multi-layer composites of glass fibre mats. This was thought to be due to the smaller load carrying capacity of individual fibres resulting from their smaller aspect ratios. (fibre length to radius ratio) The bundling or the clustering of fibres during fabrication may also result in a lower toughness. Increasing amounts of fibres incorporated in these composites do not seem to contribute to the fracture toughness.

In the following sections the fracture toughness test results of the cast compact tension and bending beam specimens are discussed. In view of the variety of mechanisms that may be operative in different material systems, the particle filled composites are discussed first. Then follows the discussion of results obtained for fibre reinforced composites and three phase composites incorporating both particles and fibres.

5.1 Fracture Toughness of Particle Filled Polyester:-

There are various mechanisms which might be responsible for the observed fracture behaviour of particulate composites;[21-34]

(1) An increase in relative fracture surface area due to surface roughness may increase the surface energy and in turn the fracture toughness.

(2) Energy absorption by transparticle fracture may lead to increased fracture toughness.

(3) Crack front interaction with the second phase dispersion may increase the fracture energy and the resulting fracture toughness.

(4) The formation of a microcrack zone in the vicinity of the crack tip may also increase the total relative fracture surface area and hence the fracture toughness of a particulate composite.

Surface roughness:-

It has been shown by Lange,[17] that the fractional surface area increase per unit of apparent area of a particulate composite depends only on the volume fraction of the dispersed particles. This has been found by means of a

plane surface model analysis using cubic protrusions to represent the particles. One significant result of this analysis was that only a small increase in fracture surface area can be obtained by increasing the volume content of the particles. This may range from 0.1 to 1.5 for 10% to 50% volume fractions of the second phase dispersion regardless of particle size. This and the observation that the elastic modulus of powder composites is independent of particle size[32] suggest a size independent contribution from surface roughness to the fracture toughness of these composites.

But the toughness of the composites investigated in the present work was found to be dependent on particle size. This was observed for both compact tension and bending beam specimen geometries. In addition, a decrease in toughness with increasing volume fraction is also observed for some composites when using the compact tension specimen configuration.

Transparticle fracture:-

On the basis of transparticle fracture the average fracture energy of a particle filled composite is expected to lie between the fracture energies of the matrix and the particle,[33-34] varying linearly with the fraction of the total fracture surface area occupied by the particles. It has been shown[33] that if the elastic modulus also varies linearly with the volume fraction of the particles the magnitude of $K_{IC}{}^2$ can approximately be represented by a linear function of the volume

fraction. The results obtained here are not in agreement with this type of functional behaviour. Also, the fracture surfaces of powder composite specimens do not show clear evidence for transparticle fracture.

Crack front interactions:-

It has been found that the fracture behaviour of many particulate composite systems can be explained in terms of a concept of crack front interaction with the second phase dispersion.[17 23 31] When a crack front meets an array of particles present on the crack plane, it bows out between each pair of particles increasing its total length. This leads to an increase in fracture energy(see Section 1.2.1) as well as fracture toughness of a particle reinforced composite.

Combining Equation 1.1 and 1.2 in Section 1.2.1 and neglecting the higher order terms of volume fraction (ϕ), it can be shown that for a given particle size the fracture energy of a particulate composite should be approximately a linear function of the particle volume fraction. If the elastic modulus E of this composite were also to be a linear function of the volume fraction[32] the expression for $K_{IC}{}^2$ from Equation 1.5 could be written as follows;

$$K_{IC}^2 = 2(\Delta E.\phi + E_1)(\Delta\gamma.\phi + \gamma_I)$$

$$K_{IC}^2 = 2[(\Delta E.\gamma_1 + \Delta\gamma\ E_1)\phi + E_1\gamma_1 + \Delta E.\Delta\gamma\phi^2]$$

Neglecting the term $\Delta E\Delta\gamma\ \phi^2$, which is small compared to other terms the expression for $K_{IC}{}^2$ can be written as a linear function of the volume fraction

$$K_{IC}^2 = 2[\ (\Delta E.\gamma_1 + \Delta\gamma.E_1)\phi + E_1\gamma_1\ ] \tag{5.1}$$

E_1 and γ_1 are the elastic modulus and fracture energy of the matrix material and ΔE and $\Delta\gamma$ are the differences between these values of filler and the matrix.

The squares of the average critical stress intensity factor values obtained in the present work were plotted as a function of particle volume fractions. None of the composites however resulted in a linear plot with all the points lying on a straight line. Fig.30 for example illustrates this for the coarse iron-polyester system. The behaviour of these composites over the entire range of volume fractions can not thus be explained by a single model based on the interaction of a crack front with dispersed particles. Also, this mechanism can not be responsible for the difference in fracture toughness observed for the two specimen geometries. Nevertheless, the concept of crack front interaction can not totally be excluded for these composites, especially in view of the characteristic cleavage

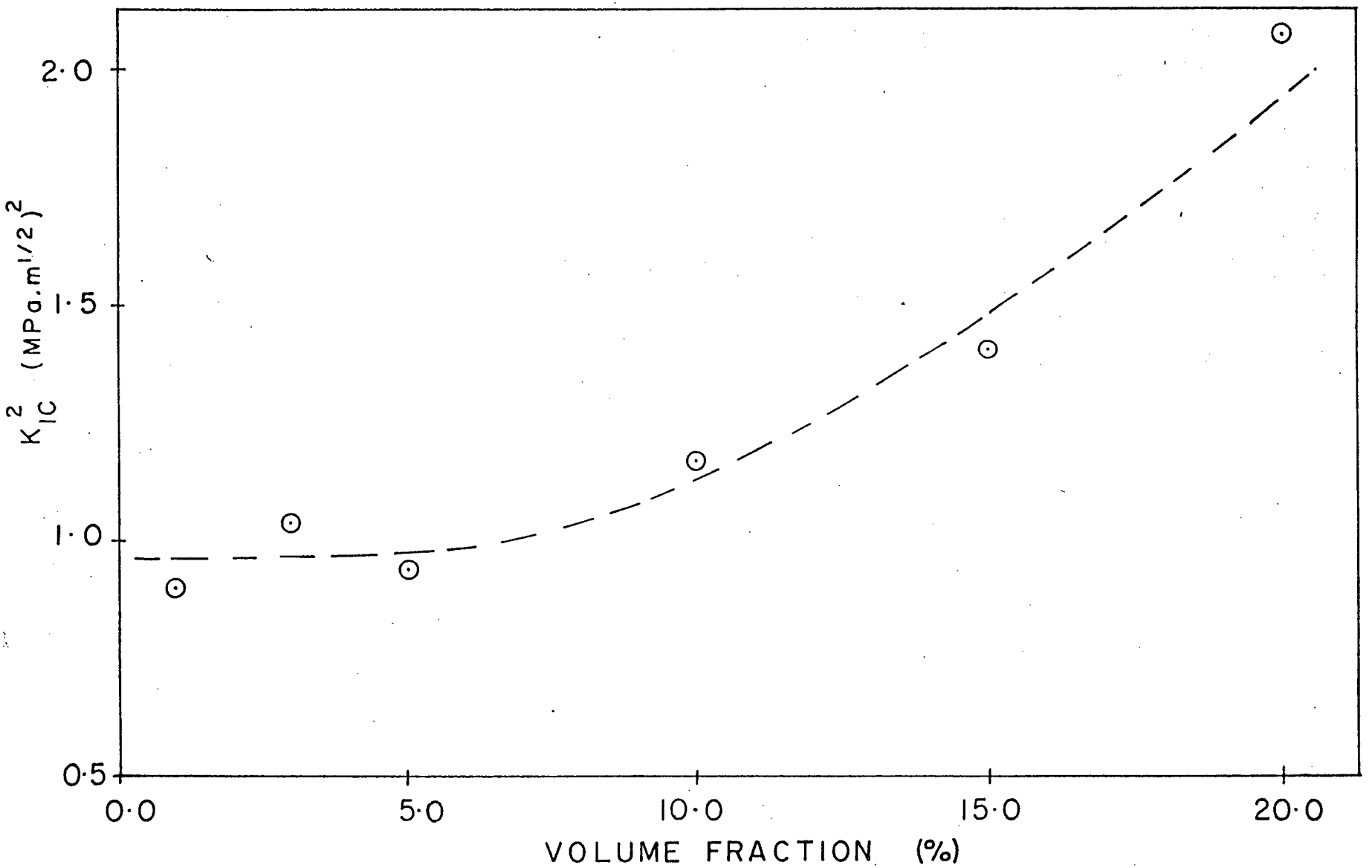

FIG. 30. A plot of the square of the average K_{IC} of coarse iron composites against particle volume fraction.

steps observed on the fracture surfaces of coarse nickel composites. There is evidence of such steps in other particulate systems[17 31] formed as a consequence of the bowing of crack front between the particles and eventual reunion of its segments.

Shrinkage stresses:-

To resolve this and forward an adequate explanation for the observed fracture behaviour, other mechanisms which might contribute to the toughness of these composites have been considered.

When thermosets are used as the matrix material, a significant shrinkage of the matrix occurs during the manufacture of the composite. With polyester the linear cure shrinkage could be as high as 4%[41] although considerable deviations from this value may be observed in practice. As a result, a large difference between the elastic moduli of the dispersed phase and the matrix may give rise to high residual stresses around the particles. The magnitude and distribution of these stresses are unknown, but a rough evaluation can be made by assuming a rigid cylindrical inclusion embedded in an infinitely large continuum. From the elastic stress solutions for cylindrical objects,[62] the values of the principal stresses σ_r, σ_θ and σ_z at a point outside the inclusion along the radial, circumferential and axial directions (see Fig.31) respectively can be written as;

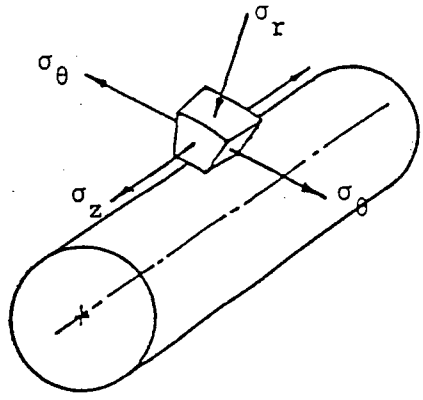

FIG. 31. Principal shrinkage stresses around a rigid cylindrical inclusion.

$$\sigma_r = A + B/r^2$$

$$\sigma_\theta = A - B/r^2$$

$$\sigma_z = \nu(\sigma_r + \sigma_\theta) \qquad (5.2)$$

where A and B are constants determined by the boundary conditions and r is the radial distance to a point within the matrix. It is seen that for a continuum with a stress free boundary the value of A is zero. The constant B can be evaluated by considering the hoop strain induced in the matrix just outside the interface, which would be numerically equal to the linear shrinkage of the matrix. If e is the linear shrinkage, E the Young's modulus and v the poisson's ratio of the matrix material, it can be shown that

$$E\,e = \sigma_\theta - \nu\,(\sigma_r + \sigma_z) \tag{5.3}$$

Substituting (5.2) in (5.3),

$$B = \frac{-E\,e\,r_0^2}{1+\nu}$$

where r_0 is the radius of the cylindrical inclusion. This value of B yields the following expression for radial and circumferential stresses;

$$\sigma_r = -\sigma_\theta = \frac{-E\,e}{1+\nu} \cdot (r_0/r)^2 \tag{5.4}$$

The principal stresses would vary as the inverse square of the distance from the centre of the inclusion. Polyester with 4% linear cure shrinkage and a Poisson's ratio of 0.34 may give rise to stresses as high as E/33 at the interfacial boundary. According to this expression, the tensile hoop stress is equal in magnitude to the compressive radial stress at any point around the inclusion. It is also evident that the magnitude of these stresses at the interfacial boundary is independent of the inclusion size.

Although the situation is somewhat different when these inclusions are spherical, a stress distribution which will closely resemble the above can be expected. The symmetry of the spherical inclusions however implies that the two

tangential stresses, which are both orthogonal to the principal radial stress, should be tensile and equal in magnitude reaching a maximum near the interface. The radial stresses around the inclusion would still be compressive and also reach their maximum at the inner boundary.

In view of the assumptions and approximations involved and the exact nature of the particle distribution, their shape and rigidity, the actual values of stresses that are realized in practice may not be so high. However, they may be large enough to influence the crack tip stress distribution or produce microcracks around the particles in the presence of an external stress field. The latter is particularly important as it will increase the fracture toughness of a composite through an increase in total fracture surface area. The microcracks are often formed by decohesion of weakly bonded internal boundaries or failure of the matrix along planes which are radial and subject to maximum normal tensile stresses. The formation of such zones has been reported for concrete and other materials.[63-64]

Increase in fracture toughness through the formation of microcrack zones:-

It is then conceivable that in particulate composites the formation of microcrack zones may contribute significantly to their fracture toughness, and that an increase in this value can be expected with increasing volume fraction of particles.

In the presence of a given stress field, the total fracture surface area associated with microcracks will statistically be proportional to the total volume of material, subject to residual tensile stresses of magnitude higher than a critical value. Using the model of cylindrical inclusion, it can be shown that this volume of material is proportional to the total volume fraction of particles present in the matrix, and that for a given volume fraction, it is independent of the particle size.

The results of bending beam fracture toughness tests illustrated in Figs.5-12 are consistent with the concept of microcrack formation around the second phase inclusions. As expected, an increase in fracture toughness has been observed with increasing volume fractions of metal powders. The lower toughness of fine nickel composites, as opposed to coarse powder composites, appears to be a direct consequence of the clustering of fine nickel particles. When this happens, the residual stresses around the particles would overlap with each other, the tangential tensile stresses being counterbalanced by the overlapping compressive radial stresses. The overall result of this would be a reduction in the total amount of microcracks produced and thus in the material's resistance to fracture. A similar effect is observed again at higher volume fractions, when interactions of the residual stress fields with each other may occur. This could mean a slower rate of increase in fracture toughness, with increasing amounts of particles at high volume fractions. The results of both the fine nickel and

fine nickel plus coarse iron composite series show this very clearly.

In explaining the above results the mechanism of crack interaction with dispersed particles can not be completely excluded. Even in terms of previously discussed concept of matrix shrinkage, it can be expected that the residual compressive stresses around the particles may tend to hinder the progression of a crack front by inhibiting interfacial separation. The characteristic fracture steps identified on fracture surfaces of coarse powder composites confirms the prevalence of such interactions. The particle size dependence of fracture toughness can also partly be attributed to this mechanism. Although the observed dependence of fracture toughness on volume fraction and particle size is in agreement with the above hypothesis, its actual contribution to fracture of these composites is unknown.

Interactions of residual stresses with the crack tip stress field:-

As mentioned earlier, the residual stresses that are developed during matrix shrinkage may also severely affect the crack tip stress field along the ligament of a loaded specimen. The tangential stresses around the particles would intensify the principal tensile stresses in regions near the crack tip, even causing premature failure of a specimen. This effect may be very pronounced in specimens of compact tension geometry,

where the crack tip tensile stresses extend deep into the specimen. A lowering of the apparent fracture toughness of compact tension specimens can therefore be expected. In bend specimens however, the absolute length of the ligament is much smaller than that of the compact tension specimen, limiting the extent of such stress magnification. The particular loading geometry associated with bending beams which develops compressive stresses on the unnotched side of the beam will also restrict this effect. Thus, the mechanism of stress intensification may not be as significant in bend specimens as in compact tension specimens.

The discrepancy between the results of compact tension and bending beam geometries can now be explained. The curves drawn in Figs.32-34 compare the experimental results obtained for these two specimen geometries. At first, the higher apparent fracture toughness of pure polyester -compact tension specimens can be associated with the existence of a larger microcrack zone at the crack tip. This is analogous to the difference in toughness observed with plate thickness in metals, which arise due to the differences in plastic zone size depending on whether plane stress (thin plate) or plane strain (thick plate) conditions exist.

As metal powders are added to polyester a decrease in critical stress intensity factor for compact tension tests is observed initially. It is possible that the effects of residual stress field interactions with the crack tip stress field might

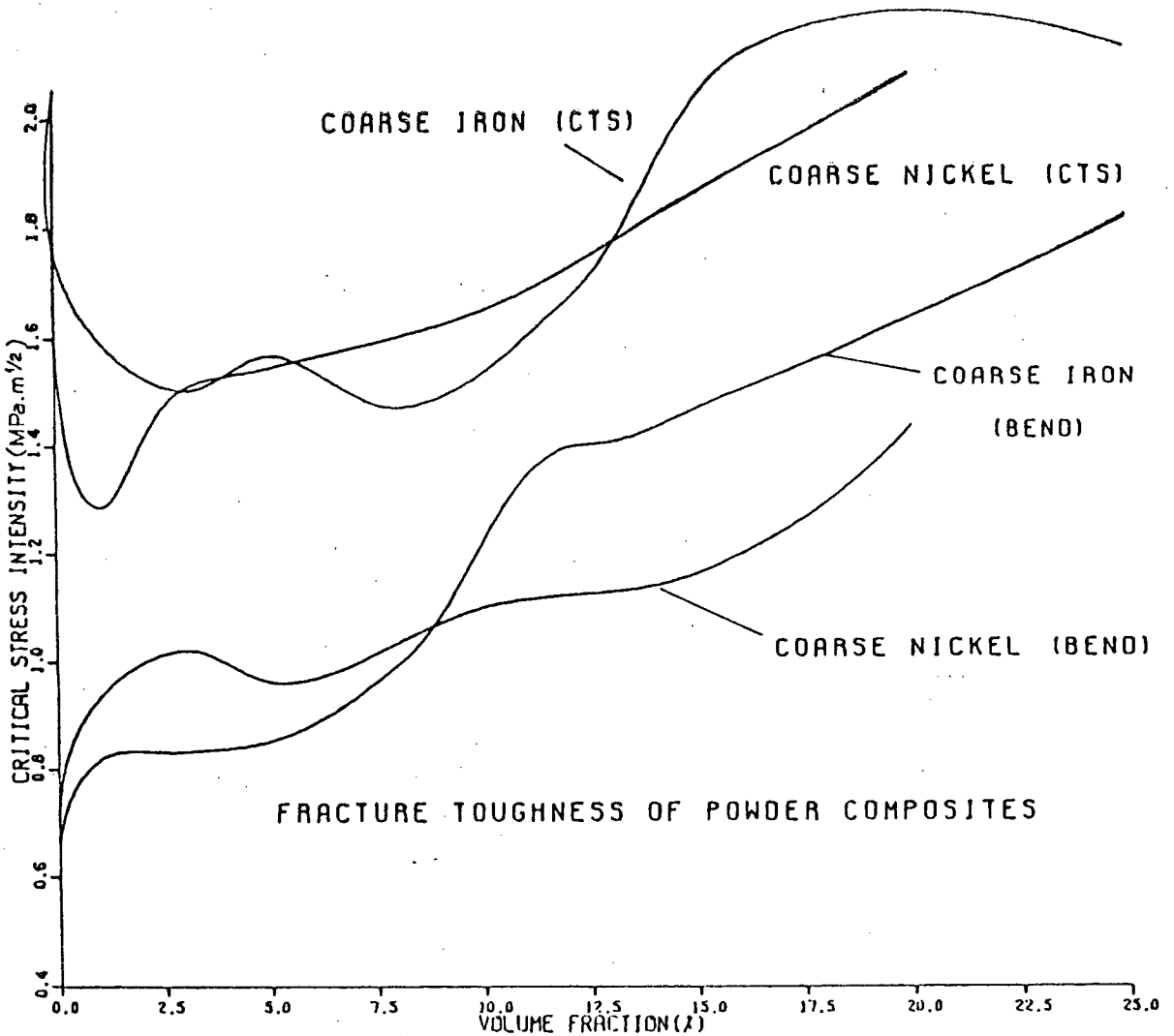

FIG. 32. A comparison of the fracture toughness test results of coarse iron and coarse nickel composites obtained for the two specimen geometries.

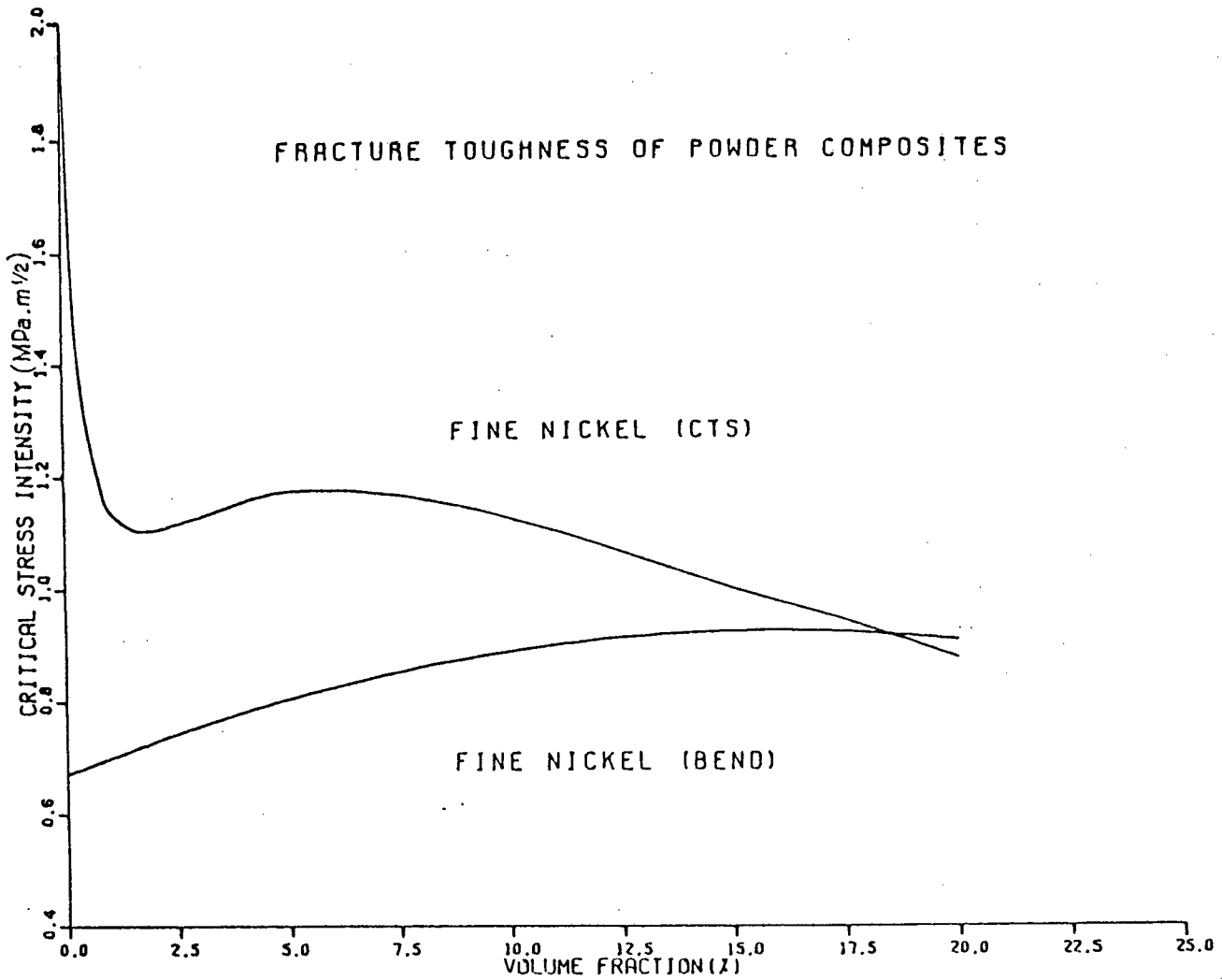

FIG. 33. A comparison of the fracture toughness test results of fine nickel composites obtained for the two specimen geometries.

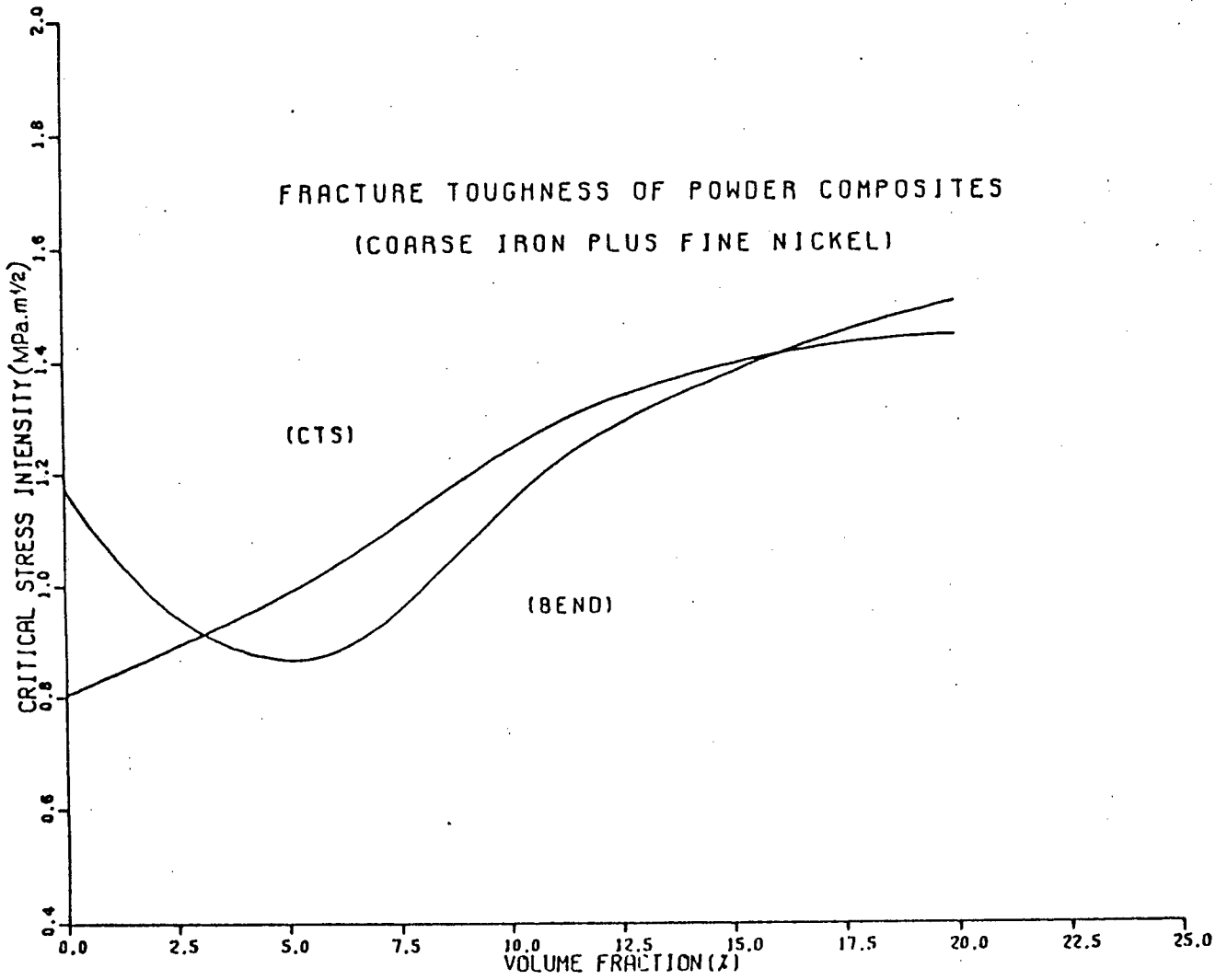

FIG. 34. A comparison of the fracture toughness test results of coarse iron plus fine nickel composites obtained for the two specimen geometries.

be responsible for this observation. The contribution of microcrack formation around the particles (at low volume fractions) is probably not sufficient to compensate for this reduction in toughness. However as the volume fraction of particles is increased, the latter may predominate over the specimen's response to fracture and consequently a gain in apparent fracture toughness is observed. The results of compact tension tests illustrated in Figs.24-26 are all consistent with this concept of stress magnification coupled with microcrack formation. Composites containing either coarse iron or coarse nickel powder exhibit a sharp drop in the critical stress intensity factor at very low volume fractions. This then, goes through a minimum and increases again with further additions of powder, until it reaches a value close to the original fracture toughness of pure polyester. In contrast to this behaviour, the composites which contained fine nickel powder have shown a continuous reduction in fracture toughness, subsequent to a sharp initial drop. This is perhaps due to a reduction in microcrack formation at high volume fractions resulting from clumping of fine nickel particles. In any event, the overall toughness resulting from compact tension tests can be higher than the bending beam toughness values of each material, at any volume fraction, due to the continued presence of a larger microcrack zone at the crack tip. This is evident from a comparison of fracture toughness test results of both compact tension and bending beam specimen geometries.

The fracture of composites which contained both iron

and nickel powder exhibited the cumulative effect of the addition of these powders. This material can be regarded as a nickel based matrix filled with varying amounts of iron powder. The fracture toughness of these composites have shown similar variations with volume fraction as in iron powder composites except for the corresponding contributions of nickel powder.

In explaining the results of compact tension fracture toughness tests, the applicability of the mechanism of crack front interaction is found to be inadequate. Neither the reduction in fracture toughness at low volume fractions nor the difference in toughness observed for the two specimen geometries could be accounted for. Although it can not alone be responsible for the fracture behaviour of these composites, the possibility of a fractional contribution of this mechanism can not be excluded.

In summary, the fracture behaviour of particle filled composites investigated in the present work is consistent with a concept based on microcrack formation and residual shrinkage stresses. Of the other mechanisms, crack front interaction with dispersed particles is also partly in accordance with the observed behaviour. These explanations are based on the following points;

(1) The difference in apparent fracture toughness of the unfilled polyester obtained for different specimen configurations can only be explained in terms of a varying

microcrack zone size associated with each geometry.

(2) The results obtained for filled composites using a compact tension specimen configuration are in general higher than those of the bending beam configuration. This can also be explained in terms of a larger microcrack zone size associated with each geometry.

(3) Within each of the composite series, the variation of fracture toughness with constituent particle volume fraction is consistent with the concepts of microcrack formation and stress field interactions.

(4) The apparent particle size dependence of fracture toughness can be attributed to varying degree of clumping effects associated with different particles.

5.2 Fracture Toughness of Fibre Reinforced Polyester:-

As discussed previously in Section 1.2.2 the theoretical models of fracture which have been postulated to account for the fracture toughness of fibre reinforced composites are generally based on mechanisms of fibre pull-out, debonding, fibre stress relaxation, matrix yielding and the creation of new fracture surfaces. Analytical formulae developed for energy absorption[53 54 65] through these

mechanisms are given in Table V. These formulae express the fracture energy in terms of volume fraction (V_f) and critical transfer length (l_c) of the reinforcing fibre. An analytical relationship for matrix plastic deformation is not included here as it was considered to be of no relevance in the present context.

In fundamental mechanics of fibre reinforcement[41] the critical transfer length of a fibre for stress transfer by slip, is defined as that length of the fibre which corresponds to the critical aspect ratio. The critical aspect ratio is the minimum fibre length to radius ratio required to be able to stress the fibre to its breaking-point. Thus, the critical transfer length is given by;

$$l_c = \sigma_f \, r \, / \, \tau_i \tag{5.5}$$

where,

σ_f = tensile strength of the fibre

r = radius of the fibre

τ_i is the interfacial shear stress brought about by frictional slip. ie;

$$\tau_i = \mu \, \sigma_r \tag{5.6}$$

Table V. Models of Energy Absorption:-

Mechanism of energy absorption	Analytical expression
Pull-out	
Debonding	
Stress-relaxation	
Surface formation	

Nomenclature:-

Fibre diameter

Volume fraction of fibres

Tensile strength of fibre

Elastic modulus of fibre

Critical transfer length of fibre

Debonded length of fibre

Fracture energy of the matrix

where, μ is the coefficient of friction and σ_r is the normal stress at the fibre matrix interface, which results mainly from matrix cure shrinkage. Since the latter can be in the neighbourhood of 20-30 MPa, and μ can be taken as 0.2,[41] the interfacial shear stress τ_i is around 5 MPa.

Using this value of τ_i in Equation 5.5 and a value of 2000 MPa for the strength of the fibres an approximate critical transfer length was estimated for the composites. This was 2.0 mm. for 10 μm. diameter fibres incorporated in the present composite. In order to compare the experimental observations with the proposed theoretical models of energy absorption, this value of l_c= 2.0 mm. was substituted in the formulae of Table V. In doing so, the tensile strength and modulus of the fibre were taken as 2000 MPa and 70 GPa, respectively. In the calculation of γ_s a value of 0.185 kJ/m^2 was used for the fracture energy of polyester. This was derived from the average fracture toughness of pure polyester obtained for bending beam configuration. (refer Section 4.3.3) The debonded length l_d which appears in the expression for debonding was taken as $l_c/2$ (=1.0 mm.). A rationale for this is given by Gershon & Marom.[57]

The critical stress intensity factors derived for the series of glass fibre composites have been converted to fracture energies using Equation 1.6 and compared with the theoretical models predicting fracture in Fig.35. The average values of fracture energy calculated for the set of composites exhibit a linearly increasing trend with volume fraction. A

between these values and the theoretical models reveals that the surface formation model provides the best explanation for the observed fracture behaviour. The values predicted by the pull-out mechanism are too high to account for the experimental results. The models of stress relaxation and debonding on the other hand, do not provide sufficiently high values.

This result is in agreement with the results of a unidirectional glass fibre-epoxy composite investigated by Gershon & Marom.[57] The general agreement of the surface formation model with the experimental values proposes that the creation of new fibre, matrix and fibre matrix interfaces is the main contribution to the fracture toughness of these composites. According Marston et al[54] the creation of new surfaces includes the process of energy absorption through debonding, indicating that γ_d is implicit in the expression for γ_s. It is expected that an even better agreement would prevail if

(1) an allowance was made for the random distribution of fibre alignment

(2) an accurate estimate was made for the critical transfer length of the fibres.

The first is justifiable because in a random fibre composite, not all the fibres will contribute to toughness in a given direction. The expressions given in Table 5.1 have been

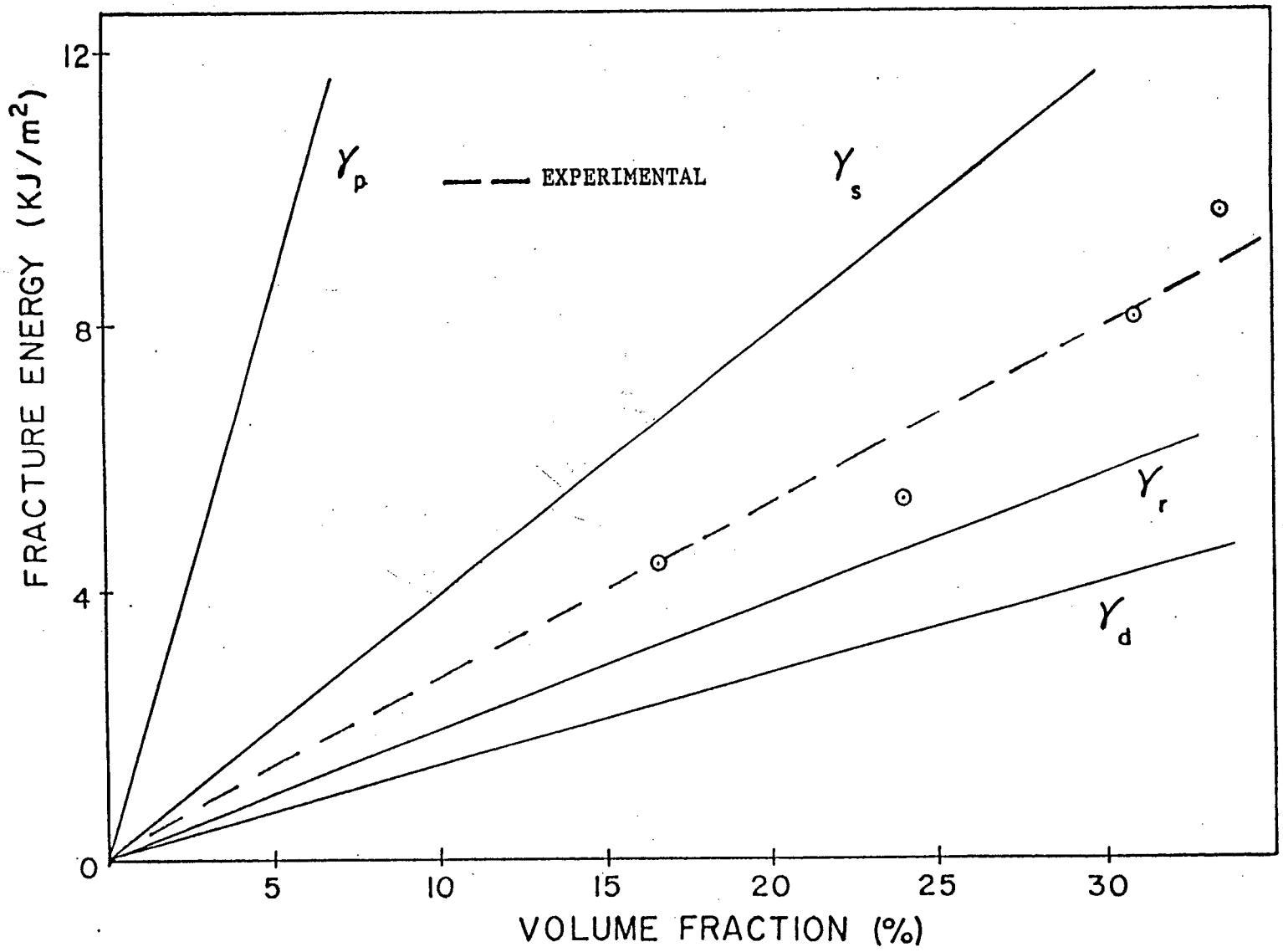

FIG. 35. A comparison of the experimental values of fracture energy of glass fibre composites with theoretical models.

The first is justifiable because in a random fibre composite, not all the fibres will contribute to toughness in a given direction. The expressions given in Table 5.1 have been developed for idealized systems of unidirectionally reinforced fibre composites. In a random fibre composite only a fraction of fibres will actually contribute to toughening through debonding and surface formation, resulting a lower effective volume fraction.

The second of the above can only be achieved through an accurate estimate of the physical parameters involved. The magnitude of the interfacial shear stress τ_i used in Equation 5.5 is dependent upon the values used for the coefficient of friction and normal stress at the fibre-matrix interface. The actual tensile strength σ_f of the fibre may also be reduced due to surface damage caused during handling and laying-up. If it is assumed that the observed pull-out length varies between 0 and $l_c/2$ the mean fibre pull-out length will approximately be equal to $l_c/4$. l_c then becomes a statistical concept and can be estimated experimentally by measuring the pull-out lengths of fibres sticking out from the fracture surfaces. Unlike in a unidirectional fibre composite, in the present composite it was difficult to make a statistical estimate of the critical transfer length due to the random nature of fibre alignment.

5.3 Fracture Toughness of Particle & Fibre Reinforced Polyester:-

The results obtained for three phase composites are self-consistent, displaying only a slight variation of critical stress intensity factor with powder volume fraction. (see Figs.8-12) The addition of metal powder to fibre reinforced composites does not in general affect the fracture toughness significantly. This is due to the relatively smaller influence of powder additions on the toughness of the matrix material. The fibre reinforcement on the other hand has a greater influence on fracture and results in an increased fracture toughness for higher contents of glass fibre.

It is thought that the particles and fibre have their individual contributions to the resulting fracture toughness. These contributions are cumulative, especially at low volume fractions of constituent components. But, as the total volume fraction of the reinforcement increases the resulting fracture toughness seems to be more influenced by other interactions.

Let us for example, consider the results of three phase composites containing nickel powder. At low glass content the composite fracture toughness is virtually unaltered by the presence of particles. But at fibre volume fractions over 30%, the addition of nickel powder tend to increase the toughness initially and then reduce it drastically. As observed earlier, a nickel powder dispersion in a matrix of polyester does not

alone constitute a composite of high fracture toughness. It can therefore be expected that the addition of nickel powder at relatively low volume fractions of fibre will not significantly alter the toughening due to fibre reinforcement. As the volume fraction of fibre increases interactions between the two reinforcement may occur and as a result a strong dependence of fracture toughness on these materials can be expected. Specifically, the addition of nickel powder may have a detrimental effect on the toughening character of fibre reinforcement. The fibres contribute to fracture toughness through the formation of new fracture surfaces which includes the processes of debonding. It is possible that, during the fracture of glass fibre-resin composites, the presence of nickel particles on fibre surfaces may affect the fibre-matrix interfacial shear stress. In Table V the expressions which include energy absorption through debonding are all based on the assumption that the fibre-matrix interfacial shear stress fall to zero on debonding. The presence of particles on the fibre surfaces may reduce the maximum interfacial shear stress prior to debonding, or decrease it not to zero but to some finite value on debonding. In any event, the result would be a reduction in energy dissipation and the resulting fracture toughness. As the volume fractions of constituent components are increased greater reductions in fracture toughness can be expected.

The mechanisms which might have led to the initial increments of fracture toughness are not very clear. However,

the resulting increase in effective volume fractions of the individual components with respect to the base matrix may also have contributed significantly to this behaviour. In fact, it is easy to reconcile this idea with the variations observed for iron powder-glass composites. The results of two phase powder composites (Section 2.2.3) indicate that the coarse iron powder has a greater influence on toughness than the fine nickel powder and 25% volume fraction of iron powder increases the fracture toughness of polyester by a factor of approximately 2.5. This may explain why there is an initial increment in fracture toughness in three phase materials due to coarse iron powder, even at lower glass contents.

The results for three phase composites containing iron powder can be analysed in the following way. At first, with increasing amounts of glass fibre or iron powder, contributions from each would tend to increase the fracture toughness. Opposing this would be the effects of fibre-particle interactions operative at high volume fractions. The net result would be an initial increase in fracture toughness prior to a subsequent reduction, with increasing amounts of iron powder. This is exactly what the series of composites containing approximately 16% volume fraction of glass fibre exhibits. Volume fractions over 30% in glass fibre result in an immediate reduction in fracture toughness when powder is added. At intermediate amounts of glass content, a relatively constant region appears before any reduction due to the additions.

VI. SUMMARY AND CONCLUSIONS

One of the important mechanical properties in modern resin matrix composites is their resistance to brittle fracture. The incorporation of reinforcing materials such as particles and/or fibres can greatly influence the resistance of these materials to fracture. An understanding of the nature and extent of this influence is an important element in engineering design, if these composites are to be utilized for optimum toughness and used to their ultimate capabilities.

Through the use of linear elastic fracture mechanics, the critical stress intensity factor can sometimes be used as a quantitative test parameter to compare and characterize the behaviour of composite materials in fracture. An attempt has been made in the present work to investigate the fracture behaviour of some composites incorporating randomly oriented chopped glass fibres and/or heavy metal powders in a polyester matrix, employing standard fracture mechanics techniques available for metallic materials. The effects of such variables as the specimen geometry, fibre and filler volume fractions, and particle size on the fracture of these composites have been evaluated.

Two phase and three phase powder composites

containing different volume fractions and particle sizes of iron and nickel powder were prepared by a simple casting method. These castings were then used to make compact tension and bending beam specimens for standard fracture toughness tests. A wet lay-up technique was employed to fabricate composites reinforced with glass fibre, with or without an additional reinforcement in metal powder. These were again used to make standard bend beam test specimens. Attempts to make bending beam specimens of short fibre reinforced composites using high pressure injection have not been very successful.

The two specimen geometries employed for powder composites resulted in different critical stress intensity factors for similar materials. The difference in fracture toughness was largest for the unfilled resin and a gradual reduction in this difference was observed with increasing amounts of particle additions. The compact tension specimens always resulted in higher toughness values, suggesting that a specimen and loading geometry dependent mechanism might be responsible for the fracture behaviour of these composites. It was found that a reasonable explanation for the observed experimental results can be advanced based on an hypothesis of stress field interaction and microcrack formation coupled with the concept of crack front interactions with dispersed particles. The effects of stress field interaction and microcrack formation would be more intense in compact tension configuration. For both geometries, and within each composite series the variation of fracture toughness with constituent

particle volume fraction is shown to be consistent with the above hypothesis, while the lower toughness of fine nickel composites has partly been attributed to clumping effects of the nickel powder.

Composites of glass fibre have shown a linearly increasing fracture toughness with increasing fibre volume fraction and the results agreed well with the surface formation model of energy absorption. This suggests that the creation of new fibre, matrix and fibre-matrix interfaces is the main contribution to fracture toughness of these composites. The resulting toughness due to fibre reinforcement however, is much higher than that due to particle dispersions in powder composites mentioned earlier.

The results obtained for three phase composites are consistent with those of two phase powder and fibre composites. Although the powder dispersions in general have relatively less influence on fracture, they seem to affect significantly the fracture toughness of three phase composites at high volume contents of reinforcing materials. This can be attributed to fibre particle interactions which may reduce the energy absorption through debonding, by affecting the fibre matrix interfacial shear stress.

The main conclusions which can be drawn from the present study are;

(1). Linear elastic fracture mechanics can successfully be applied to compare qualitatively the behaviour of resin based composites in fracture.

(2). The loading geometry and the specimen configuration are both important in establishing a suitable test specimen geometry for quantitative fracture toughness determination of resin based composites.

(3). The residual stresses due to matrix shrinkage may lead to increased fracture toughness through the formation of microcracks in particle filled composites. Crack front interactions with particles may also partly contribute to the fracture resistance of these composites.

(4). The creation of new fracture surfaces which includes debonding, is mainly responsible for the fracture behaviour of glass fibre reinforced polyester composites.

(5). The toughness of three phase particle filled, glass fibre reinforced resin composites is primarily governed by the fibre reinforcement. Heavy metal dispersions do not significantly affect the fracture toughness at low volume fractions of fibres and particles. At high volume fractions however, the

addition of metal particles may have a detrimental effect on the toughening character of fibre reinforcement.

(6). The fracture toughness of three phase composites of glass fibre and fine nickel powder is relatively independent of powder volume fraction. Particles of a dense material which tend to aggregate in the form of clumps can therefore be used to control the weight distribution, or increase the density, of a fibre reinforced composite without affecting the composite's fracture characteristics. Such composites are potentially useful for application in multirim superflywheels.

REFERENCES

1. Applications, Load bearing fibre composites, M. R. Piggott, International series on the strength and fracture of materials and structures,Pergmon Press, 1980, p 236-254.

2. Mechanical behaviour of a solid microfracture filled composite Terry G. Richard, Journal of Composite Materials, 9, April 1975, p.108-113.

3. Inorganic particle reinforced thermosetting resins, C. H. Lerchenthal and M. Brenman, Composites, April 77, p.93-99.

4. Influence of the microstructure on the fracture of materials, J. L. Chermant, A. Deschanvres, and F. Osterstock, 4th International Conference on the strength of metals and alloys, Nancy, France, Aug.-Sep. 1976, Vol.2, p 514-518.

5. Mechanical properties of Al-Mica particulate composite material, Deo Nath, R. T. Bhatt, S. R. Biswas, and P. K. Rohatgi, Transactions of the ASME, Journal of Engineering Materials and Technology, Vol.102, Jan. 1980, p 78-84.

6. Mechanical and thermal expansion properties of a particulate filled polymer G.W.Brassell, K.B.Wischman, Journal of Materials Sci., 9(1974), p 307-314.

7. R.W.Johnson, P.W.Montgomery and D.L.O'Brien, Mater.Eng. 66(1967), p 75

8. The influence of particle size on the tensile strength of particulate filled polymers, G.Landon, G.Lewis, G.F.Boden, Journal of Materials Sci., 12(1977), p 1605-1613.

9. A multirim superflywheel, H.S.Gorden, William M. Brobeck Associates, July 1975, PB-245 998.

10. The multirim superflywheel, D.W.Robenhorst, Applied Physics

Laboratory, Johns Hopkins University, Aug.1974, AD-A001 081.

11. Static and Impact behaviour of Graphite/epoxy laminates containing third phase reinforcement materials, D.F.Adams, J.F.Perry, Journal of Testing and Evaluation, Vol. 5, No. 2, March 1977, p 114-123.

12. Stiffness and strength of polyester dough moulding compounds, R.M.Ogorkiewicz, Composites, 4(1973), p 162-166.

13. Elastic moduli of randomly oriented, chopped fibre composites with filled resin, D.C.Chang, G.J.Weng, Journal of Materials Sci., 14(1979), p 2183-2190.

14 Influence of fillers on the stiffness & strength of a polyester resin, R.M.Ogorkiewicz, P.E.R.Mucci, Journal of Materials Sci., 10(1975), p 393-398.

15. The toughness of glass/resin/chalk composites, D.Cawthorne, B.Harris, Composites, May 1975, p 115-119.

16. Composite construction materials handbook, R.Nicholls, Prentice-Hall Inc., 1976.

17. Fracture energy and strength behaviour of a Sodium Borosilicate Glass-Al_2O_3 composite system, F.F.Lange Journal of American Ceram. Soc., Vol. 54(12), Dec. 1971, p 614-620.

18. Effect of alumina dispersions on Young's modulus of a glass, D.P.H.Hasselman, R.M.Fulrath, Journal of American Ceram.Soc., Vol. 48(4), p 218-219.

19. Effect of microstructure on strength of Si_3N_4-SiC composite system, F.F.Lange, Journal of American Ceram.Soc., Vol 56(9), p 445-450.

20. Measurement of particle sizes in Opaque bodies, R.L.Fullman, Trans.AIME, 197(3), 1953, p 447-452.

21. Fracture of a brittle particulate composite Part I, D.J.Green, P.S.Nicholson, J.D.Embury, Journal of Materials

Sci., 14(1979), p 1413-1420.

22. Fracture of a brittle particulate composite Part II, D.J.Green, P.S.Nicholson, J.D.Embury, Journal of Materials Sci., 14(1979), p 1657-1661.

23. Interaction of crack front with second phase dispersions, F.F.Lange, Philosophical magazine, 22(179), 1970, p 983-992.

24. The strength of brittle materials containing second phase dispersions, A.G.Evans, Philosophical magazine, 26(6), 1972, p 1327-1344.

25 A model for crack propagation in polycrystalline ceramics, A.G.Evans, L.J.Graham, ACTA Mettallurgica, Vol. 23, 1975, p 1303-1312.

26. Three dimensional finite element analysis of spherical partical composites, B.D.Agrawal, L.J.Broutman, Fibre Science and Technology, 7(1), Jan.1974, p 63-77.

27. The effect of interfacial bonding on the toughness of glass filled polymers, L.J.Broutman, S.Sahu, Mater.Sci.Eng., 8, 1971, p 98-107.

28. A deformational mechanism in particulate filled glassy polymers, R.E.Lavengood, L.Nicolais, M.Narkis, Journal of Applied Poly.Sci., Vol. 17, 1973, p 1173-1185.

29. Mechanical behaviour and Permeability of ABS/glass bead composites, L.Nicolais, E.Drioli, R.F.Landel, Polymer, Vol. 14, Jan. 1973, p 21-26.

30. Mechanical properties of glass bead filled polystrene composites, L.Nicolais, G.Guerro, C.Migliaresi, L.Nicodemo, A.J.DiBenedetto, Composites, Jan 1981, p 33-37.

31. Fracture energy of an epoxy composite system, F.F.Lange, K.C.Radford, Journal of Materials Sci., 6(1971), p 1197-1203.

32. Acoustic emission and mechanical properties of particle

reinforced composites, A.E.Godoy, M.A.Sc.Thesis, Aug.,1982.

33. Fracture behaviour of composites based on Al_2O_3-TiC, R.P.Wahi, B.Ilschner, Journal of Materials Sci., 15(1980), p 875-885.

34. Effect of size, shape and oxide content of metal particles on the formation of segregated networks in pvc composites, S.K.Bhattacharyya, S.Basu, S.K.De, Composites, July 1978, p 177-183.

35. The effect of particle shape on the mechanical properties of filled polymers, T.S.Chow, Journal of Materials Sci.,, 15(1980), p 1873-1888.

36. Fracture of a brittle composite; influence of elastic mismatch and interfacial bonding, A.K.Khaund, P.S.Nicholson, Journal of Materials Sci., 15(1980), p 177-187.

37. Influence of elastic and thermal expansion mismatch on the local crack driving force in brittle composites, A.K.Khaund, P.S.Nicholson, V.D.Krstic, Journal of Materials Sci., 12(1977), p 2269-2273.

38. Fibre reinforced plastics, L.J.Broutman, Modern composite materials, edited by L.J.Broutman, R.H.Krock, Addison-Wesley, 1967, p 337-441.

39. Fibre reinforced polymer composites, A general review, J.O.Outwater, Composites: State of the Art edited by J.W.Weeton, E.Scala, Proc.of AIME sessions 1971, p 12-21.

40. Particle and fibre reinforcement, A.Kelly, Strengthening methods in crystals edited by A.Kelly, R.Nicholson, Halsted Press, John wiley & Sons, 1971, p 433-484.

41. Load bearing fibre composites, M.R.Piggott, International series on the strength & fracture of materials & structures, Pergamon Press, 1980, p 62-140.

42. The fracture toughness of fibre composites, D.C.Phillips, A.S.Tetelman, Composites, Sept.1972, p 216-223.

43. Elements of fracture mechanics,chapter 8, Deformation and fracture mechanics of engineering materials, R.W.Hetzberg, John Wiley & sons, p 255-295.

44. Fracture toughness of composites, K.G.Kreider, L.Dardi, Failure modes in composites edited by Instvan Toth, TRW Equipment Laboratories, p 193-230.

45. Bearing pressures and cracks, H.M.Westergaard, Trans ASME, Journal of Applied Mechanics, 61, 1939, p 49-53

46. The fracture energy of a glass fibre composite, P.W.R.Beaumont, D.C.Phillps, Journal of Materials Sci., 7(1972), p 682-686.

47. Cracking and fracture in composites, G.A.Cooper, M.R.Piggott, advances in research on the strength of fracture of materials, Vol 1, edited by D.M.R.Taplin, Pergamon Press, p 557

48. Critical stress intensity factors applied to glass reinforced polyester resin, M.J.Owen, P.T.Bishop, Journal of Composite Materials., Vol 7, Apr 1974, p 146-159.

49. Macroscopic fracture mechanics of glass reinforced polyester resin laminates, A.W.Holdsworth, M.J.Owen, Journal of Composite Materials., Vol 8, April 1974, p 117-129.

50. The development of a damage zone at the tip of a crack in a glass reinforced polyester resin, S.Gaggar, L.J.Broutman, International journal on fracture, 10(1974), p 606-616.

51. Effect of reinforcement geometry on stress intensity factor calibrations in composites, H.Harel, G.Marom, S.Fischer, I.Roman, Composites, April 1980, p 69-72.

52. Preliminary development of a fudamental analysis model crack growth in a fibre reinforced composite material, M.F.Kanninen, E.F.Rybicki, W.L.Griffth, ASTM STP 617, 1977.

53. The fracture toughness of composites reinforced with weakened fibres, G.A.Cooper, Journal of Materials Sci., 5(1970), p 645-654.

54. Interfacial fracture energy and the toughness of composites, T.U.Marston, A.G.Atkins, D.K.Felbeck, Journal of Materials Sci., 9(1974), p 447-455

55. Tensile stregth of notched carbon fibre and glass fibre composites, Journal of Composite Materials., Vol. 6, Jan.1972, p 32-46.

56. Fracture mechanisms in glass reinforced plastics, B.Harris, J.Morley, D.C.Phillips, Journal of Materials Sci., 10(1975), p 2050-2061.

57. fracture toughness and mechanical properties of glass fibre epoxy composites, B.Gershon, G.marom, Journal of Materials Sci., 10(1975), p 1549-1556.

58. Fracture toughness and crack growth measurements in GRP, M.J.Owen, R.J.Cann, Journal of Materials Sci., 14(1979), 1982-1996.

59. Dynamic elastic moduli and toughness of dough moulding compounds, D.Cawthorne, B.Harris, Composites, Jan.1975, p 25-29.

60. Fracture toughness testing methods, J.E.Srawley, W.F.Brown, ASTM special publication, 381(1965), p 133-196.

61. A note on the fracture of polyester resin, B.Harris, F.E.de Moncunill, Journal of Materials Sci., 4(1969), p 1023-1026.

62. Theory of elasticity, S.Timoshenko, J.N.Goodier, 2nd ed., McGraw-Hill, New York, 1951.

63. Influence of microstructure on fracture propagation in rocks, R.G.Hoagland, G.T.Hann, A.R.Rosenfeld, Rock Mechanics, 5(1973), p 77.

64. Fracture mechanics of ceramics, D.J.Green, P.S.Nicholson, J.D.Embury, Vol. 2, edited by R.C.Bradt, Plenum Press, New York, 1974, p 541.

65. Theoretical estimation of fracture toughness of fibrous composites, M.R.Piggott, Journal of Materials Sci.,

5(1970), p 669-675.

66. Composite flywheel stress analysis and materials study, G.F.Morganthaler, S.P.Bonk, Advances in structural composites, 12th annual symposium, Soc. of Aerospace Material & Process Engineers, 1967.

67. Kinetic energy storage of off-peak electricity, L.A.Simpson, I.E.Oldaker, J.Stermscheg, Assesment report-Atomic energy of Canada Ltd., AECL-5116, sep. 1973.

68. Flywheels, R.F.Post, S.F.Post, Scientific American, Vol 229, No 6, Dec. 1973, p 17-23.

APPENDIX A.

High Energy Density Flywheels.

Flywheels have traditionally been made of conventional materials, particularly high strength steel. The amount of energy that can be stored in such a flywheel, per unit weight of flywheel material, is significantly limited due to the high density of steel. However, recent progress in materials technology has led to the design of flywheels that are capable of storing very large amounts of energy per unit of mass.

It has been shown that the maximum amount of kinetic energy that can be stored per unit weight of flywheel material is proportional to the materials strength divided by its density. As reviewed at the end of this Appendix, a different constant of proportionality, often referred to as the shape factor is associated with each flywheel configuration. In view of this, it appears that the materials with high strength and low densities are mostly suited for high energy density flywheels. Many fibre composites, being several times lower in density than steel

and some even exhibiting strengths higher than those of the strongest steels, have exactly the properties required.

In order to take advantage of these properties in designing composite flywheels several flywheel configurations, that are appropriate to composites, have been studied during the past decade.[9 10 66 67] Of these, the concentric multi-ring flywheel, originally suggested by Rabenhorst[10] and Post[68] is of particular interest. It comes closer to effective utilization of a fibre composite representing a practical configuration of a high volume efficiency, ie; nearly all of the swept volume stores energy. This comprises a set of concentric rings, coupled with bonded bands of rubber-like material placed in the gaps between the rings. Flywheels incorporating several rings of circumferentially wound fibres in resin have been constructed.[9] The design minimizes the radial stresses preventing radial delamination and distributes the circumferential stresses more evenly across the thickness. The magnitudes of these stresses, at a radius r, in a ring of inner radius a and outer radius b are given by,[62]

$$\sigma_r = \frac{3+\nu}{8}\rho\omega^2\left(a^2 + b^2 - \frac{a^2b^2}{r^2} - r^2\right) \qquad \text{(A1)}$$

$$\sigma_\theta = \frac{3+\nu}{8}\rho\omega^2\left(a^2 + b^2 + \frac{a^2b^2}{r^2} - \frac{1+3\nu}{3+\nu}r^2\right) \qquad \text{(A2)}$$

where,

σ_r = radial stress

σ_θ = circumferential stress

ν = Poisson's ratio

ω = angular velocity

ρ = density of the flywheel material

The distribution of these biaxial stresses are plotted in Fig.36[67] for different values of a, after normalizing by dividing by $\rho\omega^2 r^2$ It is evident from these expressions that as the thickness of the rim is reduced, the radial stresses become very small and the stress distribution approaches a uniaxial situation. The problem of radial delamination of a unidirectional fibre composite can thus be avoided by making the individual rings thin enough to minimize the internal radial stresses.

However, since all the rims must be constrained to the maximum allowable angular velocity of the outer one, the inner rings are now less stressed with respect to the outer ones and so, do not utilize their full capacity of energy storage. The multirim flywheel does not therefore achieve the optimum unless this problem is overcome by suitable material design. Rabenhorst[10] has suggested adding increasing amounts of a dense loading material, such as lead powder, to the inner rings to increase the loading (and stored energy). The main purpose would be to distribute the stresses more evenly from ring to ring as

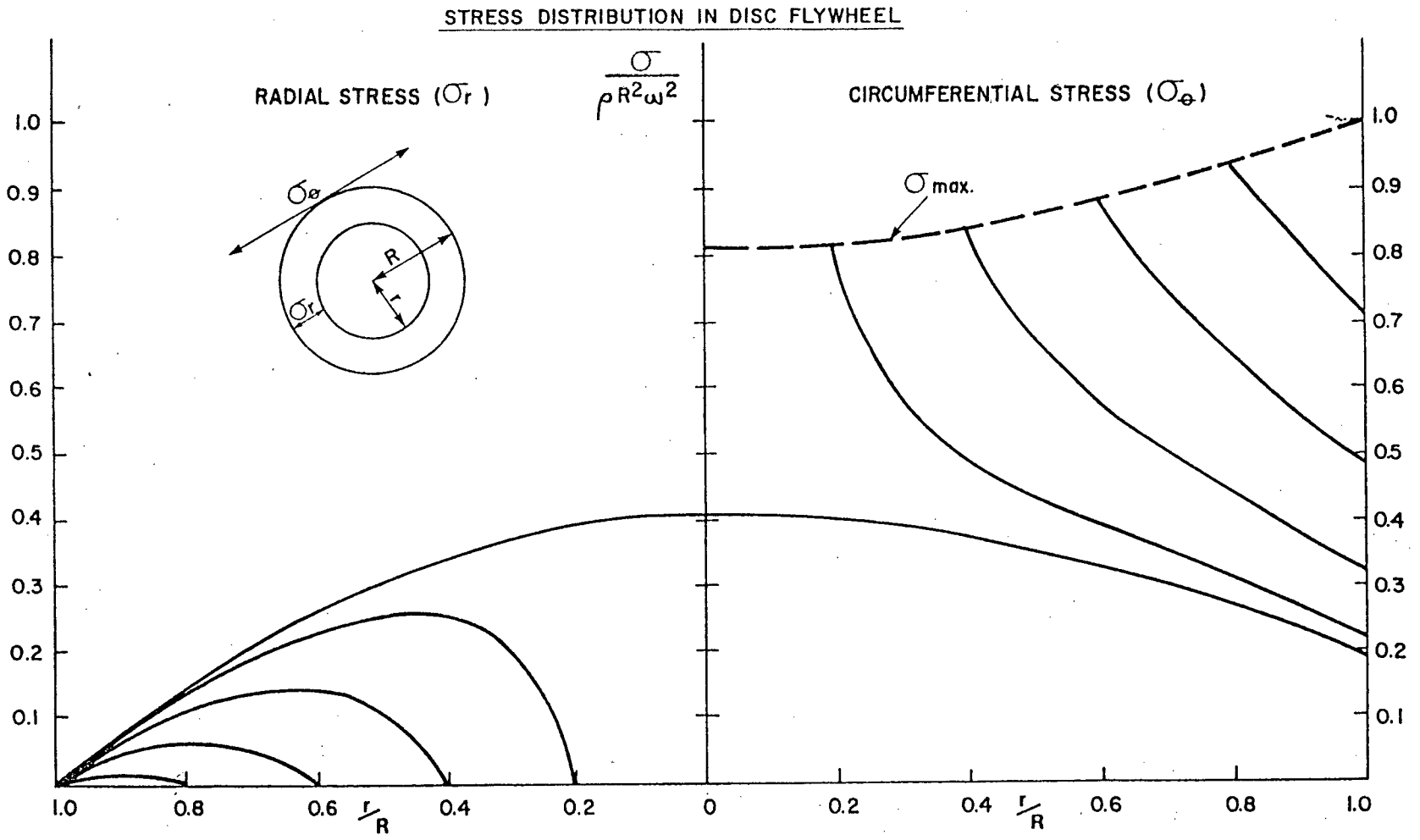

FIG. 36. RADIAL AND CIRCUMFERENTIAL STRESS DISTRIBUTIONS IN A DISC FLYWHEEL VS RATIO OF INNER TO OUTER RADII. STRESSES ARE NORMALIZED BY DIVIDING BY $\rho R^2 \omega^2$, THE CIRCUMFERENTIAL STRESS IN A THIN RIM.

well as within the individual rings, and maximize the total amount of energy stored in the flywheel.

Physics of Flywheels:-

The moment of inertia about the axis of rotation of a solid disc of radius r, thickness t and density ρ is given by,

$$I = \int_0^r r^2 \rho t . 2\pi r \, dr$$

$$= \frac{1}{2} \rho t . \pi r^4$$

$$= \frac{1}{2} m r^2$$

where,

m = total mass of the disc.

The kinetic energy stored in the disc when it rotates at an angular velocity ω is

$$K.E. = \frac{1}{2} I \omega^2$$

$$= \frac{1}{4} m \omega^2 r^2 \qquad (A3)$$

The maximum hoop stress at the centre of the disc is

$$\sigma_{max} = \frac{3 + \nu}{8} \rho \omega^2 r^2 \qquad (A4)$$

where,

ν = Poisson's ratio

From (A3) and (A4) it is found that,

$$K.E. / m \propto \sigma_{max} / \rho$$

and kinetic energy per unit mass can now be expressed as;

$$K.E. / m = S. \frac{\sigma_{max}}{\rho} \qquad (A5)$$

where,

S = shape factor associated with the flywheel geometry.

Kinetic energy per unit volume is;

$$K.E. / V = S. \sigma_{max} \qquad (A6)$$

For the solid disc configuration the shape factor S, is found to be

$$S = \frac{2}{3 + \nu}$$

$$= 0.606 \quad \text{for} \quad \nu = 0.3$$

It can be shown that for rod and thin rim configurations the value of the shape factor is 1/3 and 1/2 respectively.

APPENDIX B.

Volume Fraction Determination.

An initial estimate of the volume fraction of each constituent component was made before the actual fabrication of the composite. These initial estimates were based on the requirement of a final set of data points that extend over the whole range of interest. At the same time physical limitations to these workable ranges were set by certain parameters that were inherent in the particular fabrication technique used. For instance, the thickness or the viscosity of a resin powder mixture increased with increasing amounts of powder additions, until it became too thick for proper infiltration of glass mats or to be used in a simple casting process without much porosity being introduced.

The weight proportions of powder(s) and the liquid resin to be mixed were determined for the intended volume fraction(s) of powder(s) using a simple relationship of the form;

$$W_P = W_R \frac{D_P}{D_R} \cdot \frac{V_P}{V_R} \qquad \text{(B1)}$$

where,

W_P = Weight of powder in gms.

W_R = Weight of resin in gms.

V_P = Volume fraction of powder.

V_R = Volume fraction of resin matrix.

D_P = Density of powder in gms/cc

D_R = Density of the cured resin in gms/cc

The resin was catalysed (3 drops per oz. of resin) before the addition of powders and it was assumed that the catalyst does not make any significant difference in the volume fraction(s) of powder(s) present. Nevertheless it was thought that the volume fraction of the constituent powder(s) may have been altered slightly by segregation effects and weight losses in polyester due to evolved gasses, during the curing reactions. Hence a correction to the initial estimates of volume fractions was thought to be appropriate and done accordingly, as explained later in this section. The results showed a less than 5% drop in the initial estimates of volume fractions for 20% V.F. and 2% for 1% V.F. in single powder polyester composites. This was considered to be too small a correction to be applied with any practical significance to

actual functional behaviour discussed here. Hence for composites containing only powders, the initial estimates of volume fractions were assumed to be true volume fractions. In other words Equation (B1) was used with sufficient accuracy to determine the quantities of powder and resin that had to be mixed in order to achieve any desired volume fraction.

The same equation was used to calculate the quantities by weight of powder and resin to arrive at different volume fractions of powder in composites, containing both glass fibres and metal powders. But here the incorporation of glass fibre mats significantly changed the initial values of powder volume fractions used in Equation (B1) for computing the weight proportions of powder and resin. Besides no prior estimate of the glass fibre volume fraction could be made and different volume fractions in glass were obtained simply by incorporating different number of layers in the layup. An alternative method of estimating both the powder and the glass fibre volume fractions was therefore required for these composites.

The method used was to burn a small sample of composite at a temperature of 600°. It was left in an oven overnight and the weight loss noted. Although the polyester that was burnt off reduced the overall weight of the sample, oxidation of the metal powders resulted in a slight

gain in weight. An allowance for the weight gain due to oxidation was made by estimating the fractional gain in weight of a small sample of powder, placed inside the oven for the same period of time. If the fractional weight gain thus determined is given by C and the original ratio by weight of powder and resin mixed together is given by R, an expression for the total weight loss dW can be written as follows.

$$dW = W_R - W_R.RC$$

hence,

$$W_R = dW / 1 - RC$$

$$W_P = W_R.R = dW.R / 1 - RC \qquad \text{(B2)}$$

$$W_F = W - (W_R + W_P)$$

where,

W_R, W_P, W_F are the weights of resin, powder and fibre present in the sample. These weights together with corresponding densities were then used to calculate the individual volume fractions of constituent components. These are the true approximate volume fractions used for composites containing both glass fibres and metal powders. For composites containing only glass fibres the calculations were futher simplified, and the above expressions would become;

$$dW = W_R \text{ and } W_F = W - W_R. \qquad \text{(B3)}$$

APPENDIX C.

FRACTURE TOUGHNESS TEST RESULTS OF THREE-POINT BENDING BEAMS:-

The following nomenclature has been used:-

VOL%= Particle or fibre volume fraction

B = Specimen thickness

A = Crack length

W = Specimen width

PM = Maximum load at fracture

PQ = 5% offset load at fracture

KM = Critical stress intensity factor calculated using PM in units of $MPa.m^{0.5}$

KQ = Critical stress intensity factor calculated using PQ in units of $Mpa.m^{0.5}$

Coarse Iron in Polyester:-

CODE NO	VOL %	B (CM)	A (CM)	W (CM)	PM (LB)	KM (MPA)
21	3.0	0.690	1.027	1.400	4.2	0.641
22	3.0	0.685	0.635	1.395	20.0	1.024
31	5.0	0.695	0.935	1.400	6.8	0.737
32	5.0	0.700	0.630	1.390	19.3	0.967
41	8.0	0.690	0.627	1.395	24.0	1.200
42	8.0	0.695	0.623	1.385	15.6	0.784
51	12.0	0.690	0.630	1.390	28.6	1.454
52	12.0	0.700	0.640	1.400	27.1	1.359
61	13.0	0.700	0.635	1.395	28.5	1.429
62	13.0	0.705	0.643	1.400	27.5	1.378
71	16.0	0.705	0.633	1.395	31.8	1.576
72	16.0	0.700	0.627	1.390	28.5	1.419
81	25.0	0.700	0.640	1.400	36.0	1.805
82	25.0	0.700	0.643	1.400	36.2	1.827

Coarse Nickel in Polyester:-

CODE NO	VOL %	B (CM)	A (CM)	W (CM)	PM (LB)	KM (MPA)
111	1.0	0.695	0.718	1.390	10.2	0.626
112	1.0	0.700	0.598	1.355	20.5	1.031
113	1.0	0.695	0.637	1.400	21.8	1.094
114	1.0	0.695	0.615	1.380	20.0	0.998
121	3.0	0.695	0.635	1.400	19.9	0.994
122	3.0	0.700	0.638	1.400	19.5	0.974
123	3.0	0.695	0.640	1.400	21.6	1.091
124	3.0	0.690	0.630	1.400	20.6	1.026
131	5.0	0.700	0.630	1.395	20.0	0.992
132	5.0	0.695	0.633	1.395	20.0	1.005
133	5.0	0.690	0.638	1.400	21.2	1.074
134	5.0	0.700	0.630	1.395	15.6	0.774
141	10.0	0.685	0.632	1.400	22.6	1.139
142	10.0	0.700	0.626	1.390	22.6	1.123
143	10.0	0.690	0.637	1.400	22.0	1.112
144	10.0	0.695	0.605	1.360	20.1	1.023

Continued.,

CODE NO	VOL %	B (CM)	A (CM)	W (CM)	PM (LB)	KM (MPA)
151	15.0	0.680	0.630	1.392	22.2	1.140
152	15.0	0.695	0.628	1.382	23.5	1.200
153	15.0	0.695	0.630	1.392	24.2	1.216
154	15.0	0.700	0.635	1.390	21.4	1.084
161	20.0	0.680	0.628	1.382	28.0	1.462
162	20.0	0.695	0.626	1.380	31.0	1.583
163	20.0	0.695	0.557	1.315	24.9	1.253
164	20.0	0.690	0.638	1.400	28.2	1.428

Fine Nickel in Polyester:-

CODE NO	VOL %	B (CM)	A (CM)	W (CM)	PM (LB)	KM (MPA)
211	1.0	0.695	0.611	1.380	19.0	0.940
212	1.0	0.700	0.637	1.400	13.0	0.648
213	1.0	0.685	0.727	1.400	9.4	0.585
214	1.0	0.700	0.690	1.396	11.1	0.626
221	5.0	0.695	0.648	1.400	19.5	1.002
222	5.0	0.695	0.628	1.382	18.2	0.930
223	5.0	0.700	0.640	1.400	12.2	0.612
224	5.0	0.695	0.635	1.395	13.4	0.676
231	16.0	0.690	0.630	1.395	14.0	0.704
232	16.0	0.695	0.635	1.392	19.9	1.011
233	16.0	0.695	0.630	1.395	18.8	0.939
234	16.0	0.680	0.640	1.400	20.0	1.032
241	20.0	0.695	0.623	1.390	18.7	0.930
242	20.0	0.690	0.622	1.398	17.2	0.846
243	20.0	0.700	0.638	1.400	18.2	0.909
244	20.0	0.695	0.638	1.400	18.5	0.930

Coarse Iron plus Fine Nickel in Polyester:-

CODE NO	VOL %	B (CM)	A (CM)	W (CM)	PM (LB)	KM (MPA)
261	5.0	0.695	0.621	1.383	23.8	1.195
262	5.0	0.700	0.623	1.386	21.7	1.080
263	5.0	0.695	0.597	1.363	19.2	0.954
264	5.0	0.700	0.503	1.255	14.3	0.719
271	12.0	0.700	0.633	1.393	26.3	1.318
272	12.0	0.700	0.621	1.388	25.9	1.278
273	12.0	0.700	0.625	1.392	26.6	1.313
274	12.0	0.700	0.624	1.395	27.8	1.361
281	20.0	0.695	0.610	1.380	27.8	1.372
282	20.0	0.700	0.606	1.380	31.0	1.507
283	20.0	0.695	0.628	1.392	28.4	1.421
284	20.0	0.695	0.622	1.388	29.3	1.460

Glass Fibre in Polyester:-

CODE NO	VOL %	B (CM)	A (CM)	W (CM)	PQ (LB)	PM (LB)	KQ (MPA)	KM (MPA)
311	16.8	0.700	0.630	1.395	137.5	160.5	6.819	7.960
312	16.8	0.700	0.635	1.396	125.0	151.2	6.253	7.563
313	16.8	0.700	0.638	1.398	125.0	156.5	6.267	7.846
314	16.8	0.700	0.631	1.395	136.3	153.4	6.774	7.624
321	24.2	0.700	0.635	1.398	160.0	226.0	7.971	11.259
322	24.2	0.695	0.625	1.390	153.6	235.8	7.669	11.773
323	24.2	0.700	0.633	1.398	168.8	225.3	8.374	11.176
324	24.2	0.692	0.627	1.388	180.0	213.8	9.102	10.811
331	31.1	0.690	0.625	1.392	230.0	247.5	11.520	12.397
332	31.1	0.695	0.625	1.393	231.2	276.0	11.474	13.697
333	31.1	0.695	0.630	1.393	236.8	281.2	11.877	14.104
334	31.1	0.700	0.646	1.398	208.8	277.2	10.648	14.137
341	33.7	0.692	0.632	1.395	280.2	309.2	14.117	15.578
342	33.7	0.692	0.618	1.385	257.6	302.4	12.858	15.094
343	33.7	0.700	0.635	1.395	272.5	302.8	13.659	15.177
344	33.7	0.685	0.631	1.395	280.8	328.0	14.261	16.658

Fine Nickel in Polyester Containing 24.2 Vol% Glass:-

CODE NO	VOL %	B (CM)	A (CM)	W (CM)	PQ (LB)	PM (LB)	KQ (MPA)	KM (MPA)
361	0.4	0.700	0.638	1.397	209.2	227.0	10.510	11.404
362	0.4	0.690	0.625	1.392	169.2	190.5	8.475	9.542
363	0.4	0.700	0.627	1.390	168.4	188.0	8.384	9.359
364	0.4	0.700	0.629	1.370	168.8	180.0	8.796	9.379
371	0.8	0.700	0.635	1.400	172.4	215.2	8.554	10.677
372	0.8	0.680	0.635	1.400	180.0	205.6	9.193	10.501
373	0.8	0.698	0.625	1.390	224.0	240.4	11.136	11.952
374	0.8	0.700	0.667	1.397	160.8	185.2	8.600	9.905
381	2.5	0.695	0.638	1.400	167.6	188.0	8.429	9.455
382	2.5	0.698	0.618	1.380	170.8	188.0	8.538	9.398
383	2.5	0.700	0.637	1.390	177.0	203.0	9.002	10.324
384	2.5	0.690	0.622	1.375	180.0	199.0	9.275	10.254
391	6.6	0.700	0.644	1.389	174.0	178.8	9.002	9.250
392	6.6	0.696	0.637	1.385	160.4	184.0	8.290	9.509
393	6.6	0.700	0.640	1.378	178.8	189.0	9.384	9.919
394	6.6	0.690	0.643	1.395	156.3	164.7	8.085	8.519

Continued.,

CODE NO	VOL %	B (CM)	A (CM)	W (CM)	PQ (LB)	PM (LB)	KQ (MPA)	KM (MPA)
401	14.1	0.695	0.641	1.390	157.8	177.0	8.153	9.145
402	14.1	0.700	0.640	1.393	161.0	179.4	8.190	9.126
403	14.1	0.700	0.646	1.398	169.2	185.6	8.629	9.465
404	14.1	0.690	0.635	1.388	159.0	186.0	8.202	9.595

Coarse Iron in Polyester Containing 24.2 Vol% Glass:-

CODE NO	VOL %	B (CM)	A (CM)	W (CM)	PQ (LB)	PM (LB)	KQ (MPA)	KM (MPA)
511	0.8	0.690	0.636	1.384	163.2	174.6	8.507	9.101
512	0.8	0.690	0.640	1.390	183.4	207.0	9.523	10.749
513	0.8	0.695	0.645	1.395	182.5	202.0	9.412	10.418
514	0.8	0.695	0.642	1.395	148.6	181.0	7.615	9.275
521	2.5	0.695	0.643	1.396	187.5	206.5	9.609	10.583
522	2.5	0.700	0.636	1.392	151.5	176.0	7.657	8.895
523	2.5	0.680	0.644	1.392	161.6	188.3	8.553	9.966
524	2.5	0.695	0.648	1.398	162.8	186.4	8.398	9.616
531	6.5	0.700	0.639	1.390	195.3	206.4	9.975	10.542
532	6.5	0.690	0.642	1.392	135.3	185.4	7.027	9.629
533	6.5	0.695	0.636	1.395	189.0	221.4	9.562	11.201
534	6.5	0.695	0.638	1.390	202.2	216.0	10.379	11.088
541	13.9	0.690	0.640	1.393	106.5	185.1	5.496	9.552
542	13.9	0.690	0.642	1.390	135.3	178.2	7.056	9.293
543	13.9	0.695	0.647	1.395	131.7	195.0	6.822	10.100
544	13.9	0.700	0.645	1.392	96.0	176.4	4.946	9.089

Fine Nickel in Polyester Containing 16.8 Vol% Glass:-

CODE NO	VOL %	B (CM)	A (CM)	W (CM)	PQ (LB)	PM (LB)	KQ (MPA)	KM (MPA)
561	2.6	0.700	0.665	1.385	123.0	132.0	6.720	7.211
562	2.6	0.697	0.698	1.392	99.0	122.0	5.762	7.101
563	2.6	0.690	0.695	1.400	126.3	138.0	7.246	7.917
564	2.6	0.695	0.689	1.383	126.5	139.6	7.379	8.144
571	14.2	0.696	0.672	1.387	114.5	143.0	6.362	7.946
572	14.2	0.695	0.696	1.387	109.0	132.0	6.404	7.755
573	14.2	0.695	0.675	1.395	118.5	158.0	6.525	8.700
574	14.2	0.690	0.687	1.383	105.5	126.2	6.171	7.382

Coarse Iron in Polyester Containing 16.8 Vol% Glass:-

CODE NO	VOL %	B (CM)	A (CM)	W (CM)	PQ (LB)	PM (LB)	KQ (MPA)	KM (MPA)
581	2.7	0.695	0.698	1.394	145.7	160.0	8.467	9.298
582	2.7	0.695	0.696	1.387	161.0	180.0	9.459	10.576
583	2.7	0.695	0.685	1.385	142.4	168.0	8.195	9.669
584	2.7	0.692	0.715	1.394	157.5	175.5	9.559	10.651
591	14.3	0.695	0.685	1.388	115.7	149.0	6.615	8.519
592	14.3	0.700	0.679	1.391	150.2	167.8	8.357	9.336
593	14.3	0.695	0.688	1.400	135.6	179.0	7.603	10.037
594	14.3	0.695	0.685	1.400	122.0	171.8	6.795	9.569

Fine Nickel in Polyester Containing 31.1 Vol% Glass:-

CODE NO	VOL %	B (CM)	A (CM)	W (CM)	PQ (LB)	PM (LB)	KQ (MPA)	KM (MPA)
611	0.7	0.695	0.628	1.390	235.2	271.6	11.818	13.648
612	0.7	0.700	0.640	1.400	266.0	282.0	13.338	14.141
613	0.7	0.695	0.642	1.400	244.8	270.8	12.416	13.735
614	0.7	0.695	0.632	1.386	255.2	266.5	13.040	13.617
621	9.8	0.695	0.698	1.388	200.0	233.0	11.778	13.722
622	9.8	0.690	0.705	1.393	178.4	211.0	10.634	12.578
623	9.8	0.695	0.707	1.395	166.0	204.0	9.825	12.074
624	9.8	0.690	0.698	1.398	177.4	197.2	10.292	11.441

Coarse Iron in Polyester Containing 31.1 Vol% Glass:-

CODE NO	VOL %	B (CM)	A (CM)	W (CM)	PQ (LB)	PM (LB)	KQ (MPA)	KM (MPA)
631	2.4	0.695	0.691	1.393	209.3	249.6	11.997	14.307
632	2.4	0.695	0.690	1.395	187.4	238.0	10.671	13.552
633	2.4	0.686	0.687	1.394	192.6	243.6	11.060	13.989
634	2.4	0.695	0.685	1.393	192.0	240.0	10.858	13.572
642	13.2	0.688	0.670	1.387	156.0	194.6	8.730	10.890
643	13.2	0.695	0.698	1.397	144.8	171.6	8.359	9.906
644	13.2	0.695	0.651	1.381	155.2	189.6	8.351	10.202
646	13.2	0.890	0.685	1.420	196.0	258.0	8.169	10.753
647	13.2	0.885	0.702	1.420	210.0	244.0	9.136	10.615

APPENDIX D.

COMPUTER PROGRAMS:-

The following programs were used to calculate various parameters involved, and to produce the plots using the UBC computing facility. A brief description of each program is given in appropriate comment fields.

```
C     ****************************************************
C
C     THIS IS A PROGRAM  TO CALCULATE THE  CRITICAL STRESS
C     INTENSITY FACTOR OF BRITTLE POLYMER COMPOSITES USING
C     A  BENDING  BEAM  SPECIMEN  CONFIGURATION.  STANDARD
C     EQUATIONS  FOR  PLANE STRAIN  FRACTURE  TOUGHNESS  OF
C     METALLIC MATERIALS GIVEN IN ASTM E399-78A ARE USED.
C
C     ****************************************************
C
C     DEFINE VARIABLES.
C
C           VF = VOLUME FRACTION (%)
C            B = SPECIMEN THICKNESS (CM)
C            A = CRACK LENGTH (CM)
C            W = SPECIMEN WIDTH (CM)
C           PM = MAXIMUM LOAD AT FRACTURE (LBS)
C           PQ = 5% OFFSET LOAD AT FRACTURE (LBS)
C
    1 READ(5,2)N
    2 FORMAT(I2)
      IF(N.EQ.0)GOTO 7
      WRITE(6,5)
    5 FORMAT(/////,2X,'CODE',8X,'VOL',4X,'B',6X,'A',6X,'W',
     16X,'PM',8X,'KM',6X,'A/W')
      WRITE(6,6)
    6 FORMAT(/,3X,'NO',10X,'%',4X,'(CM)',3X,'(CM)',3X,'(CM)'
     1,3X,'(LB)',5X,'(MPA)',/)
      GOTO 10
```

```
C
    7 WRITE(6,8)
    8 FORMAT(/////,2X,'CODE',8X,'VOL',4X,'B',6X,'A',6X,'W',
     16X,'PQ',4X,'PM',6X,'KQ',5X,'KM',5X,'PM/PQ',6X,'A/W')
      WRITE(6,9)
    9 FORMAT(/,3X,'NO',10X,'%',4X,'(CM)',3X,'(CM)',3X,'(CM)'
     1,3X,'(LB)',2X,'(LB)',3X,'(MPA)',2X,'(MPA)',/)
C
   10 READ(5,12,END=120)I,J,VF,B,A,W,PM,PQ
   12 FORMAT(I2,I3,F5.1,3F6.3,2F6.1)
      REAL KQ,KM
C
C     ASSIGN THE VALUE OF SPAN S IN CM
C
      S=5.6
C
      C=S/(B*W**1.5)
      CQ=PQ*C*4.448E-3
      CM=PM*C*4.448E-3
C
      F1=(3*SQRT(A/W))*(1.99-(A/W)*(1-A/W)*(2.15-3.93*(A/W)
     1+2.7*(A/W)**2.0))
      F2=2*(1+2*(A/W))*(1-(A/W))**1.5
      F=F1/F2
      Z=A/W
      IF(PQ.EQ.0)GOTO 18
      KQ=CQ*F
      KM=CM*F
      R=PM/PQ
      GOTO 28
C
   18 KM=CM*F
      WRITE(7,19)VF,KM
   19 FORMAT(F8.1,F14.3)
      IF(I.LE.0)GOTO 21
      WRITE(6,20)J,VF,B,A,W,PM,KM,Z
   20 FORMAT(//,I5,F12.1,3F7.3,F7.1,F10.3,F9.3)
      IF(I)1,10,10
   21 WRITE(6,22)J,VF,B,A,W,PM,KM,Z
   22 FORMAT(/,I5,F12.1,3F7.3,F7.1,F10.3,F9.3)
      IF(I)1,10,10
C
   28 WRITE(7,29)VF,KQ,KM
   29 FORMAT(F8.1,2F7.3)
      IF(I.LE.0)GOTO 31
      WRITE(6,30)J,VF,B,A,W,PQ,PM,KQ,KM,R,Z
   30 FORMAT(//,I5,F12.1,3F7.3,F7.1,F6.1,F8.3,F7.3,F8.1,F11.3)
      IF(I)1,10,10
   31 WRITE(6,32)J,VF,B,A,W,PQ,PM,KQ,KM,R,Z
   32 FORMAT(/,I5,F12.1,3F7.3,F7.1,F6.1,F8.3,F7.3,F8.1,F11.3)
      IF(I)1,10,10
  120 STOP
      END
```

```
C     ****************************************************
C
C     THIS IS  A PROGRAM  TO PLOT  THE  EXPERIMENTAL  VALUES
C     OF  CRITICAL   STRESS   INTENSITY  FACTOR AGAINST  THE
C     VOLUME  FRACTION  OF A SECOND PHASE FILLER MATERIAL IN
C     POLYMER COMPOSITES.THIS PROGRAMME PLOTS A SMOOTH CURVE
C     THROUGH THE AVERAGE VALUES OF STRESS INTENSITY FACTORS
C     USING A PARABOLIC  CURVE FITTING ROUTINE. THIS PROGRAM
C     HAS THE FLEXIBILITY OF COMBINING NUMBER OF PLOTS
C     TOGETHER OR PLOTTING AT A PRE-CHOSEN SCALE.
C
C     ****************************************************
C
C
      DIMENSION X(300),Y(300),Z(300),AVEX(100),AVEY(100)
    1 READ(5,2)M
    2 FORMAT(I2)
      IF(M.EQ.0)GOTO 300
C
   10 N=0
C
C     READ THE CALCULATED VALUES OF CRITICAL STRESS
C     INTENSITY FACTORS AND THE EXPERIMENTALLY
C     DETERMINED VOLUME FRACTIONS
C
      DO 100 I=1,300
      READ(5,50,END=200)L,X(I),Y(I),Z(I)
   50 FORMAT(I2,F6.1,2F7.3)
      N=I
      K=2*N
C
      IF(L.NE.0)GOTO 200
  100 CONTINUE
  200 IF(N.EQ.0)GOTO 300
      DO 250 I=1,100
      AVEX(I)=0.0
  250 AVEY(I)=0.0
      INP=0
      CALL XNUM(X,N,INP)
C
C     START PLOTTING A CURVE THROUGH N DATA POINTS
C
      CALL GRAPH(X,Y,Z,N,K,L,AVEX,AVEY,INP)
      IF(M.NE.1)GOTO 1
  300 CONTINUE
      CALL PLOTND
      STOP
      END
      SUBROUTINE GRAPH(X,Y,Z,N,K,L,AVEX,AVEY,INP)
      DIMENSION X(N),Y(N),Z(N),W(300),AVEX(INP),AVEY(INP)
C
      NTEST=0
      DO 2 I=1,N
```

```
      IF(Y(I).EQ.0)NTEST=1
    2 CONTINUE
C
      IF(L.LT.10)GOTO 3
      IF(L.EQ.11)GOTO 30
      IF(L.EQ.21)GOTO 30
      GOTO 40
C
C     SET THE SCALES FOR THE PLOT
C
   30 XMI=0.0
      DDX=2.5
      YMI=0.4
      DDY=0.2
      CALL AXIS(0.0,1.0,'VOLUME FRACTION(%)', -18,10.0
     1,0.0,XMI,DDX)
      CALL AXIS(0.0,1.0,'CRITICAL STRESS INTENSITY(MPA.M1/2)'
     1,35,8.0,90.0,YMI,DDY)
   40 J=2
      LL=0
      IF(L.LT.20)GOTO 41
      LL=L
      L=L-10
   41 IF(L.EQ.16)J=0
      IF(L.EQ.17)J=1
      IF(L.EQ.18)J=3
      IF(L.EQ.19)J=11
      JJ=J+1
      DO 42 I=1,N
   42 X(I)=(X(I)-XMI)/DDX
      IF(NTEST.EQ.1)GOTO 60
      DO 52 I=1,N
   52 Y(I)=(Y(I)-YMI)/DDY+1.0
   60 DO 62 I=1,N
   62 Z(I)=(Z(I)-YMI)/DDY+1.0
      IF(NTEST.EQ.1)GOTO 80
      DO 72 I=1,N
   72 CALL SYMBOL(X(I),Y(I),0.07,JJ,0.0,-1)
      CALL CURVE(X,Y,N,AVEX,AVEY,INP)
   80 DO 82 I=1,N
   82 CALL SYMBOL(X(I),Z(I),0.07,J,0.0,-1)
      CALL CURVE(X,Z,N,AVEX,AVEY,INP)
      IF(LL.LT.20)GOTO 90
      CALL PLOT(12.0,0.0,-3)
   90 RETURN
C
    3 IF(NTEST.EQ.1)GOTO 10
C
      DO 4 I=1,N
      W(I)=Y(I)
    4 W(N+I)=Z(I)
C
      CALL SCALE(W,K,8.0,YMIN,DY,1)
      CALL AXIS(0.0,1.0,'CRITICAL STRESS INTENSITY(MPA.M1/2)'
```

```
     1,35,8.0,90.0,YMIN,DY)
      DO 6 I=1,N
      Y(I)=W(I)
    6 Z(I)=W(N+I)
      GOTO 11
C
   10 CALL SCALE(Z,N,8.0,YMIN,DY,1)
      CALL AXIS(0.0,1.0,'CRITICAL STRESS INTENSITY(MPA.M1/2)'
     1,35,8.0,90.0,YMIN,DY)
   11 CALL SCALE(X,N,10.0,XMIN,DX,1)
      CALL AXIS(0.0,1.0,'VOLUME FRACTION(%)',-18,10.0,
     10.0,XMIN,DX)
      J=1
      IF(L.EQ.6)J=0
      IF(L.EQ.7)J=1
      IF(L.EQ.8)J=3
      IF(L.EQ.9)J=11
C
      IF(NTEST.EQ.1)GOTO 19
      DO 18 I=1,N
      Y(I)=Y(I)+1.0
   18 CALL SYMBOL(X(I),Y(I),0.07,J,0.0,-1)
      CALL CURVE(X,Y,N,AVEX,AVEY,INP)
   19 DO 20 I=1,N
      Z(I)=Z(I)+1.0
   20 CALL SYMBOL(X(I),Z(I),0.07,4,0.0,-1)
      CALL CURVE(X,Z,N,AVEX,AVEY,INP)
      CALL PLOT(12.0,0.0,-3)
      RETURN
      END
      SUBROUTINE CURVE(X,Y,N,AVEX,AVEY,INP)
      DIMENSION X(N),Y(N),AVEX(INP),AVEY(INP)
      EXTERNAL PARAB
      IND=0
      IN=0
C
      DO 100 J=1,INP
      IND=IND+IN
      XX=X(IND+1)
C
      NN=N-IND
      DO 1 I=1,NN
      IF(X(IND+I).NE.XX)GOTO 2
    1 IN=I
    2 SUMY=0.0
      DO 4 I=1,IN
    4 SUMY=SUMY+Y(IND+I)
      AVEX(J)=XX
      AVEY(J)=SUMY/IN
  100 CONTINUE
C
  200 CALL SKETCH(AVEX,AVEY,INP,25,1,1.5,PARAB)
      RETURN
      END
```

```
      SUBROUTINE XNUM(X,N,INP)
      DIMENSION X(N)
      IND=0
      IN=0
  300 IND=IND+IN
      IF(IND.GE.N)GOTO 500
      NN=N-IND
      DO 350 I=1,NN
      IF(X(IND+I).NE.X(IND+1))GOTO 360
      IN=I
  350 CONTINUE
  360 INP=INP+1
  400 GOTO 300
  500 RETURN
      END
```

```
C     ******************************************************
C
C     THIS  IS A  PROGRAM  TO CALCULATE  THE CRITICAL STRESS
C     INTENSITY   FACTORS  OF  POLYMER  COMPOSITES  USING  A
C     COMPLIANCE  METHOD. A  LEAST  SQUARE POLYNOMIAL  CURVE
C     FITTING ROUTINE IS USED TO FIT THE COMPLIANCE DATA.
C
C     ******************************************************
C
C
      IMPLICIT REAL*4 (A-H,O-Z)
      DIMENSION X(50),Y(50),YF(50),YD(50),WT(50),S(11),
     1SIGMA(11),A(10),B(10),P(11),XX(25),YY(25),YYD(25)
      DIMENSION XXP(600),YYP(650),YYDP(600)J(25),VF(25),
     1BB(25),PM(25),GC(25),TC(25),TIC3(25),TIC5(25)
      LOGICAL LK
C
    1 READ(5,5)K,N,BBS
    5 FORMAT(/,2I2,F6.3)
      IF(N.EQ.0)GOTO 100
C
C     READ THE COMPLIANCE VALUES AND THE CORRESPONDING
C     CRACK LENGTHS
C
      DO 21 I=1,N
      READ(5,20,END=21)X(I),Y(I)
   20 FORMAT(2X,2F8.3)
   21 CONTINUE
      READ(5,25)M,E
   25 FORMAT(I4,E11.3)
      DO 41 I=1,M
      READ(5,40,END=41)J(I),VF(I),BB(I),XX(I),PM(I)
   40 FORMAT(2X,I3,F5.1,2F6.3,6X,F6.1)
   41 CONTINUE
C
      NWT=0
      LK=.FALSE.
C
C     CHOOSE THE BEST FITTING CURVE OF POLYNOMIAL OF DEGREE
C     LESS THAN OR EQUAL TO K
C
      CALL OLSF(K,N,X,Y,YF,YD,WT,NWT,S,SIGMA,A,B,SS,LK,P)
      CALL OLINT(XX,YY,YYD,M)
C
C     SEE THE PLOT ON THE SCREEN
C
      CALL SEE(X,Y,XXP,YYP,YYDP,N)
      C=2.54E-6
C
      WRITE(6,70)K
   70 FORMAT(////,2X,'TOUGHNESS USING COMPLIANCE METHOD',3X,
     1'K=',I2,/)
      DO 90 I=1,M
```

```
      GC(I)=(PM(I)**2./(2.*BB(I)**2.))*YYD(I)*BBS
      TC(I)=SQRT(GC(I)*E*C)*1.099E-3
      TIC3(I)=TC(I)/SQRT(0.91)
      TIC5(I)=TC(I)/SQRT(0.75)
      WRITE(6,80)J(I),TC(I),TIC3(I),TIC5(I)
   80 FORMAT(/,I5,3X,3F10.3)
      WRITE(7,81)VF(I),TIC3(I)
   81 FORMAT(F8.1,F14.3)
   90 CONTINUE
      GOTO 1
  100 STOP
      END
      SUBROUTINE SEE(X,Y,XXP,YYP,YYDP,N)
      DIMENSION X(N),Y(N),XXP(600),YYP(650),YYDP(600)
      CALL PLCTRL('SCAL',0.7)
      CALL AXCTRL('YORI',1.0)
      CALL AXCTRL('LABE',1)
      CALL AXCTRL('SYMS',0.118)
C
      DDX=(X(N)-X(1))/599
      DO 200 I=1,600
  200 XXP(I)=X(1)+DDX*(I-1)
      CALL OLINT(XXP,YYP,YYDP,600)
      DO 201 I=1,N
  201 YYP(I+600)=Y(I)
      NN=600+N
C
      CALL SCALE(XXP,600,10.0,XMIN,DX,1)
      CALL SCALE(YYP,NN,7.5,YMIN,DY,1)
      CALL AXPLOT('CRACK LENGTH (cm);',0.0,10.0,XMIN,DX)
      CALL AXPLOT('COMPLIANCE (cm/lbf);',90.0,7.5,YMIN,DY)
C
      DO 208 I=1,N
      X(I)=(X(I)-XMIN)/DX
      YYP(I+600)=YYP(I+600)+1.0
  208 CALL SYMBOL(X(I),YYP(I+600),0.1,4,0.,-1)
C
      DO 210 I=1,600
      YYP(I)=YYP(I)+1.0
      IF(I.GT.1)GOTO 209
      CALL PLOT(XXP(I),YYP(I),+3)
      GOTO 210
  209 CALL PLOT(XXP(I),YYP(I),+2)
  210 CONTINUE
      CALL PLOT(10.0,0.0,-3)
      RETURN
      END
```

APPENDIX E.

STRAIN ENERGY RELEASE RATE ANALYSIS.

The strain energy release rate for a linear elastic isotropic specimen of unit thickness is given by;[43]

$$G_{IC} = \frac{P^2}{2} \left(dC/da \right) \qquad (C1)$$

where,

G_{IC} = Critical strain energy release rate

P = Load to fracture a specimen of unit thickness

C = Compliance for unit thickness

a = Crack length

If a specimen of thickness B^* is used for the compliance calibration, and the compliance of this specimen is found to be C_B^* , then

$$dC/da = \frac{d(C_B^* . B^*)}{da}$$

$$= B^* (dC_B^* / da) \qquad (C2)$$

where,

C_B^* = Compliance of a specimen of thickness B^*

If a load P_B is required to fracture a specimen of thickness B, the load P required for a unit specimen thickness is given by;

$$P = \frac{P_B}{B} \qquad (C3)$$

Substituting (C2) and (C3) in (C1),

$$G_{IC} = \frac{(P_B/B)^2}{2} B^* (dC_B^* / da)$$

$$= \frac{P_B^2}{2B^2} . B^* (dC_B^* / da)$$

APPENDIX F.

INJECTION MOULDING UNIT.

The injection moulding unit shown in Figs.21 and 37 which was built to make rectangular beam specimens of chopped fibre reinforced composites, mainly consisted of;

a. A cylindrical hopper that holds the catalysed liquid resin mixture and delivers it to the system.
b. A pressure gauge connected to the inlet of the injecting cylinder.
c. An injector consisting of a piston and a cylinder.
d. The mould consisting of a main specimen chamber and a top chamber to accumulate the excess resin, plus a slider-clamp arrangement to ram the fibres in.

A flat bottom cylindrical hopper was made out of mild steel, and through a small hole at the centre of the bottom, a delivery tube was provided. This passed through an inlet valve and was connected at the end to the inlet of

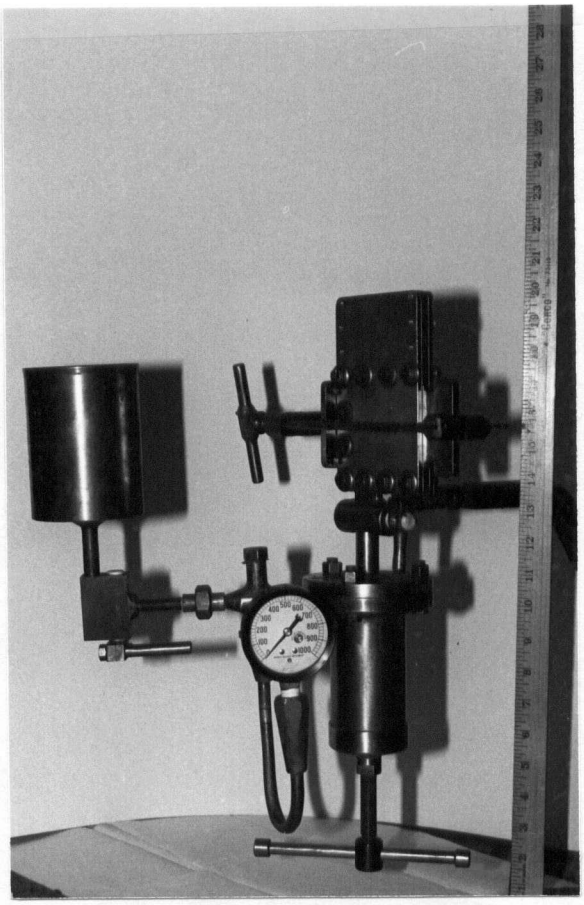

FIG. 37. Injection Moulding Unit.

the injector system. The inlet of the injector was again a short segment of steel tubing with connections to a pressure gauge through its sides. The pressure gauge was connected through a copper U-tube, that was permanently attached to the pressure gauge. The gauge could read pressures up to 1000 lbf/in^2

The injector consisted mainly of a piston and a cylinder. The bearing surfaces of these were machined very accurately and a circular groove was provided on the piston for an O-ring. The piston was connected to a cranking device by means of a threaded piston rod. This rod passed through a set of threads made in the cylinder cap and provided the necessary piston movements when it was cranked in the proper direction. The piston end of the rod was made to rotate freely on its bearing surfaces. This allowed for straight piston movements without any rotation. The piston cap which screwed on to the cylinder and carried the piston rod, facilitated the removal of the piston, piston rod and crank assembly for cleaning purposes. The cylinder was open on both sides and had threads on the outside surface of one end for the fastening of the cap. The other end had a thick circular rib surrounding the cylinder. This provided room for 3 equally spaced holes, drilled parallel to the cylinder axis and another circular groove, machined on the flat edge and inside of the 3 holes. A set of bolts passing through these holes secured the mould in position and a good sealing between the base of the mould and the cylinder

was achieved by an O-ring placed in the circular groove. The inlet to the cylinder was through a steel tube, connected to the rib, which also had provisions for pressure gauge connections. The other end of the inlet tube was connected to the hopper as explained earlier.

The mould, a 3-piece assembly consisting of a central plate and two side plates, was supported on a circular base plate which had 3 holes that match with those in the circular rib of the cylinder. These holes were used to assemble the mould and cylinder together, as mentioned earlier. A short segment of a 3/4 in. diameter steel rod, located at the centre with its axis perpendicular to the plane of the circular base plate, was welded on to the base plate. This structure was used to support the mould and provide an inlet to the main specimen chamber. In addition it also provided room for another control valve between the cylinder and the mould. The centre plate of the mould was welded on to this support structure and the mould inlet, a 1/8 in. diameter hole, was drilled through.

The mould contained the main specimen chamber and another top chamber to collect the excess resin. These were milled on the central plate with the planar dimensions of the specimen chamber being accurate to within ±0.005 cm. The thickness of the centre plate was the same as the required specimen thickness and the width of the specimen chamber was made equal to the length of the final specimen.

It was also made deep enough to pack the fibres loosely at the beginning before being pressed tight by means of a slider-clamp mechanism. The central plate was covered on the sides with two flat plates that were bolted on to the central plate. The two chambers were connected through a small hole of about 0.01 in. in diameter which was drilled parallel to the inlet hole, across the centre arm, separating the two chambers. This was the outlet of the main specimen chamber through which all excess resin flowed under pressure, leaving behind the glass fibres. The fibres were packed inside the specimen chamber and pressed in to position using a slider and a clamping device. The slider, a plate of steel of the same thickness as the centre plate of the mould, was machined accurately along the two edges which would be in contact with the surfaces of the specimen chamber, to obtain a perfect sliding fit. The dimensions of the slider were such that, when slid in until its shoulders sat against the outer edge of centre plate, it formed the mould cavity. No clearance was left between the contact surfaces of the slider and the mould plates, in order to prevent any leakage of excess resin through these under the injection pressure. The clamp was used to push the slider in through the specimen chamber, pushing the loosely packed fibres into a cavity of known dimensions.

As the parts of the injection moulding set up were subjected to periodical disassembly as well as a high service pressure, a type of fitting that would withstand

repeated tight reconnections had to be employed. A 3-piece steel tube fitting consisting of body, nut and sleeve was used to join the end of the delivery tube of the hopper to the inlet of the injector system. The end of the U-tube of the pressure gauge was also connected to the inlet of the injector through a 45° flare type two piece fitting. Pipe threads were furnished on the connecting end of the injector inlet and the U-tube end was flared and clamped between the former and a short length union nut. The mould was mounted on top of the cylinder and the base plate of the mould was bolted on to the circular rib of the cylinder. A good radial sealing was achieved by means of a standard O-ring of Buna-N (Nitrile), which was placed in the circular groove of the rib surface, as explained earlier. A standard O-ring of Buna-N (Nitrile) was also used on the bearing surfaces of the piston.

The copper U-tube connected to the pressure gauge was designed to prevent the catalysed resin flowing in to the gauge. This was done by evacuating air from inside the gauge and U-tube and filling it with water. The less compressible water provided a medium to transmit the hydrostatic pressure of the liquid resin into the gauge, without the column of water being significantly compressed, preventing the flow of resin into the U-tube.

The sleeves of the inlet and outlet valves were thick walled steel cylinders of about 1/2 in. inner

diameter, which were welded in position with their axes lying perpendicular to the respective delivery holes. The delivery holes were extended into and across the valve sleeves. A short length of a 1/2 in. diameter teflon rod was pushed into each of these sleeves and a diametrical hole drilled across the teflon, was brought in line with the delivery holes. This left the valve in its open position and a handle attached to one end of the teflon rod was used to rotate and bring it in to a closed position.